University of Bergen

Master Thesis

The Effect of Fluid Viscosity and Geometry on Hydrocyclone Performance

Author:
Arman Salimi

Supervisors:
Alex Hoffmann

A thesis submitted in fulfilment of the requirements for the degree of Master of Science

in

Process Technology
Department of Physics and Technology

February 2015

Abstract

Hydrocyclones have been widely used throughout industries for separating sand particles of various sizes and shape from fluids. Producing petroleum resources includes amounts of water, which contain different amounts of dispersed and dissolved oil and sand that make the process control more difficult. These components can create various problems for the equipment during separation and production and are harmful to the environment. Therefore it is necessary to remove them from the liquids. For these reasons, our knowledge about separation processes as well as equipment has to be improved. Additionally, we have to know which equipment should be used at which stage.

The main objective of this project is to advance that work by studying the "removal of particles from highly viscous liquids by using hydrocyclones". To identify an optimal configuration for hydrocyclone performance, the choice was made to modify the hydrocyclone to make it appropriate for highly viscous liquids. The influence of governing geometric variables such as the overflow diameter as well as the conical part length on the separation performance and pressure drop are investigated. On this basis, an experimental rig was built, based on an existing rig, to study the effects of the conical part length and the overflow diameter. Some modifications were made during assembly and after testing the rig. In this thesis, an Eulerian-Eulerian CFD, Reynold Stress Model (RSM) simulation of a solid-liquid hydrocyclone has been performed.

The CFD simulation and experimental investigation the separation performance and pressure drop of a hydrocyclone for solid-liquid separation with variations in body dimensions show that the results obtained from the simulation are somewhat different probably due to the CFD model utilized in this thesis. The results from this thesis show that when the viscosity of the liquid is increased, the separation efficiency and the pressure drop decrease and the situation is the same for the tangential and axial velocity. Investigations illustrate that an increase in the conical part length leads to a rise in separation performance, while the pressure drop decreases. The results obtained from the methods indicate that the reduction in overflow diameters result in an increase in the separation efficiency, while this leads to an increase in pressure loss across the hydrocyclone.

Acknowledgements

First of all, I would like to thank my supervisor Professor Alex C. Hoffmann for his guidance and cooperation throughout this Master's Project. Professor Alex C. Hoffmann, with his significant knowledge in this field, has given me different tasks that gradually developed my knowledge in order to complete this project. I would like to express my gratitude for his generous support and scientific advice. The way he always found time to answer my questions, and the instructive discussions we had, made this project both interesting and a great learning experience for me.

Sincere thanks to the Chief Engineer, Rachid Maad, for his support with the experimental work, and the way he found time in spite of his busy schedule. Thanks to Professor Tanja Barth in the Department of Chemistry for her guidance in the proper use of chemicals. Thanks to Chief Engineer, Egil Nodland, for his help in chemometrics. I also want to thank Leif Egil Sandnes at the Mechanical Workshop at the University of Bergen, who provided excellent help with the experimental set-up. Many thanks to Endress+Hauser AS, for allowing me to borrow one device , a Coriolis flow meter, without any charge for a year.

Many thanks and acknowledgements go to my fellow students for the valuable and instructive discussions, as well as the appreciated breaks. I would also like to thank my good friend Suzanne C. LIoyd for her support and encouragement. Finally, I would like to express my deepest thanks to my wife, Shirin Dalir, for her understanding, patience, help and support throughout my work on this thesis.

Contents

Abstract ii

Acknowledgements iii

List of Figures ix

List of Tables xi

Symbols xiii

1 Introduction 1
- 1.1 Relevance . . . 1
- 1.2 Background . . . 2
- 1.3 Application in the industry . . . 3
- 1.4 History of hydrocyclone . . . 4
- 1.5 Previous work and objective . . . 4

2 Theory 7
- 2.1 Hydrocyclone . . . 7
- 2.2 Swirling flow . . . 7
- 2.3 Forces in swirling flow . . . 9
  - 2.3.1 Centripetal force . . . 9
  - 2.3.2 Centrifugal force . . . 10
- 2.4 How hydrocyclones work . . . 11
  - 2.4.1 Merits and disadvantages . . . 12
- 2.5 Liquid flow pattern and velocity . . . 13
  - 2.5.1 Tangential velocity . . . 14
  - 2.5.2 Axial velocity . . . 15
  - 2.5.3 Radial velocity . . . 16
  - 2.5.4 Eddy flow . . . 16
  - 2.5.5 The air core . . . 17
  - 2.5.6 Locus of zero vertical velocity and mantle . . . 17
- 2.6 Cyclone pressure drop . . . 18
- 2.7 Particle motion . . . 21

2.7.1 Particle size . . . 22
2.8 Separation efficiency . . . 23
2.8.1 Total efficiency . . . 23
2.8.2 Reduced total efficiency . . . 24
2.8.3 Grade-efficiency . . . 24
2.8.4 Reduced grade-efficiency . . . 25
2.8.5 Cut size . . . 26
2.9 Design aspects . . . 26
2.9.1 Cone angle . . . 27
2.9.2 Hydrocyclone inlet design . . . 27
2.9.3 Vortex finder . . . 28
2.9.4 Apex design . . . 29
2.10 Hydrocyclone models . . . 29
2.10.1 The simple, fundamental theories . . . 29
2.10.2 The crowding theory . . . 33
2.10.3 Hybrid models . . . 33
2.10.4 The regression models . . . 34
2.10.5 The dimensionless group model . . . 34
2.10.6 Numerical simulation of the flow . . . 34
2.11 Liquid viscosity . . . 34
2.12 Computational fluid dynamic . . . 36
2.12.1 Numerical solution . . . 36
2.12.2 Turbulence models . . . 36
2.12.3 Eulerian and Lagrangian models . . . 39
2.13 Bivariate plots . . . 39
2.14 Principal component analysis (PCA) . . . 39

3 Literature study **41**
3.1 The effect of viscosity on cut size . . . 41
3.2 The effect of viscosity on the pressure drop . . . 42
3.3 The effect of geometry on separation efficiency . . . 43
3.4 Computation studies of hydrocyclone separators . . . 44

4 Design and experimental set-up **45**
4.1 The hydrocyclone . . . 45
4.2 Previous design of the rig . . . 46
4.3 The new design of the rig . . . 47
4.3.1 Pump . . . 49
4.3.2 Coriolis flow meter . . . 49
4.3.3 Electromagnetic flow meter . . . 49
4.3.4 Pressure sensors . . . 50
4.3.5 Equipment and materials . . . 51
4.4 Analytical and precision balance and density determination kit . . . 51

5 Experimental Methods **53**

5.1 Particle size distribution analysis . . . 53
5.1.1 Sedimentation method . . . 53
5.2 Principal component method . . . 58
5.3 Viscosity of glycerol-water mixture . . . 59
5.4 Experimental procedure . . . 60
5.4.1 Measuring process . . . 60
5.4.2 Overall separation efficiency . . . 61

6 Numerical methods and set-up 63
6.1 Software . . . 63
6.2 Mesh . . . 64
6.3 Multiphase flow model . . . 65
6.4 Developed numerical model . . . 66

7 Results and discussion 69
7.1 Numerical results . . . 71
7.1.1 The effect of liquid viscosity on separation efficiency, pressure drop and distributions of particles . . . 71
7.1.2 The effect of different conical part length on separation efficiency and pressure drop . . . 74
7.1.3 The effect of different overflow diameters on separation efficiency and pressure drop . . . 78
7.1.4 Distribution of velocities within the hydrocyclone . . . 81
7.2 Experimental results . . . 86
7.3 Further discussion . . . 93
7.3.1 Principal components analysis (PCA) . . . 93
7.3.2 Interpreting the principal component model . . . 94

8 Conclusions 97

9 Suggestions for further work 99
9.1 Simulations . . . 99
9.2 Improving the experimental set-up . . . 99
9.3 Analyzing the new geometry of hydrocyclone . . . 100

A An estimate of errors 103

B Calculation of flow meters 105
B.1 The Coriolis flow meter . . . 105
B.2 The electromagnetic flow meter . . . 106

C Processing of simulation raw data 109

D Efficiency calculations from experiments 111

List of Figures

2.1 Sketch showing the two ideal vortex flow 9
2.2 Sketch showing the tangential distribution in a real vortex. 10
2.3 Forces acting on a rotating fluid element 11
2.4 Sketch of a hydrocyclone with tangential-inlet and the flow pattern is indicated 12
2.5 Tangential velocity distribution in a hydrocyclone. 14
2.6 Vertical (axial) velocity distribution in a hydrocyclone. LZVV, . . . 15
2.7 Radial velocity distribution in a hydrocyclone. 16
2.8 Schematic representation of the short circuit and eddy flows. 17
2.9 Static and dynamic pressure within a hydrocyclone. 20
2.10 Grade-efficiency curve for a hydrocyclone (full line), ... 26
2.11 Schematic representation of Narrow-angle and wide-angle configuration 27
2.12 Schematic representation of side and top views of the three most used inlet configurations. 28
2.13 Sketch showing the concept behind the 'equilibrium-orbit' model. . 30
2.14 Schematic representation of the inlet flow pattern in a cyclone with a 'slot' type of rectangular inlet. 32
2.15 Schematic representation of the structure of glycerol. 35

4.1 Schematic drawing of cyclone. 46
4.2 Schematic drawing of previous rig before the rig was modified to fit its new purpose. 47
4.3 Illustration of the experimental set up of the cyclone rig in the circulating system. 48
4.4 Photo of experimental rig. 48
4.5 Shows maximum measured error in % reading. 50

5.1 Sedimentation model to illustrate the incremental model, (a) sedimentation model, (b) temporal change of the accumulated mass. . . 56
5.2 Graphical determination of mass fraction and slope from data using a sedimentation balance. 57
5.3 Photo of magnetic stirrer 58

6.1 Shows an illustration of the grid used for simulation. 67

7.1 Bivariate plot of diameter (D) versus conical part length (CL) . . . 70

7.2 The effect of viscosity on grade-efficiency. 72
7.3 The effect of viscosity on pressure drop. 72
7.4 Distribution of volume faction of particles in the hydrocyclones . . 73
7.5 Distribution of absolute pressure drop in the hydrocyclones with different viscosity. 74
7.6 The effect of conical length on grade-efficiency. 75
7.7 The effect of conical length on pressure drop. 76
7.8 Distribution of volume fraction in the hydrocyclones with different conical length. 77
7.9 Distribution of pressure in the hydrocyclones with different conical length. 77
7.10 The effect of overflow diameter on grade-efficiency. 79
7.11 The effect of overflow diameter on pressure drop 79
7.12 Distribution of volume fraction of particles with different overflow diameter. 80
7.13 Distribution of pressure in the hydrocyclones with different overflow diameter. 81
7.14 Tangential velocity profiles for 1 and 15.1 [cP] in viscosity at axial position Z=350 [mm] and the particle dimensions of D_p=20 [μm] within the hydrocyclones. 82
7.15 Tangential velocity distributions of hydrocyclones in the position of Z=350 mm and for particle dimensions of D_p. 83
7.16 Tangential liquid velocity profiles for 1 and 15.1 [cP] in viscosity along radius position at Z=100 [mm] and the particle dimensions of D_p=20 [μm] within the hydrocyclones. 84
7.17 View of the annular 84
7.18 Axial velocity profiles for 1 and 15.1 [cP] in viscosity at axial position Z=350 [mm] and the particle dimensions of D_p=20 [μm] within the hydrocyclones. 85
7.19 Axial velocity distributions for 1 and 15.1 [cP] in viscosity at axial position Z=350 [mm] and the particle dimensions of D_p=20 [μm]within the hydrocyclones. 85
7.20 Axial velocity profiles for 1 and 15.1 [cP] in viscosity at axial position Z=100 [mm] and the particle dimensions of D_p=20 [μm] within the hydrocyclones. 86
7.21 The effect of conical length on separation efficiency. 90
7.22 The reduced grade-efficiency 90
7.23 The effect of conical length on separation efficiency. 91
7.24 The reduced grade-efficiency 91
7.25 The effect of vortex finder diameter on separation efficiency. 92
7.26 The reduced grade-efficiency 92
7.27 Loadings plot of variables. 93
7.28 Biplot plot. 95

List of Tables

2.1 Viscosity of some common liquids at 20° 35

4.1 Size characteristics for the hydrocyclone. 46

6.1 Results from the grid dependency test. 67

7.1 Overview of the experiments 70
7.2 The measured values of parameters which 87
7.3 Overview of the experiments 88
7.4 The calculated data 88
7.5 The calculated data 89

9.1 Experimental design 101
9.2 Coding of data. 101

B.1 Calibration of the Coriolis flow meter versus manual measured outlet flow. 106
B.2 Calibration of the Electromagnetic flow meter versus manual measured outlet flow. 107

C.1 Schematic drawing of the cyclone. 109

D.1 Raw and processed data from experiment for experiment B. 111

Symbols

a	Acceleration vector	ms^{-2}
a	Height of tangential inlet	m
b	Width of tangential inlet	m
cl	Conical length	m
C	Constant	Dimensionless
CS	Control-surface	m
D	Diameter	m
D_i	Inlet diameter for cylindrical cyclone inlet	m
D_x	Overflow diameter/vortex finder diameter	m
D_o	Overflow diameter/vortex finder diameter	m
D_p	Particle diameter	m
D_u	Underflow diameter/apex diameter	m
d_{50}	Cut size	m
D_c	Diameter of cyclone	m
E_u	Euler number, $\Delta p/(1/2\rho v_z^2)$	Dimensionless
F_C	Centrifugal force	N
F_D	Drag force vector	N
f	Friction factor	Dimensionless
$f(.)$	Differential density distribution function	m^{-1}
g	Gravitational acceleration (abs. value g)	ms^{-2}
h	Height	m
H	Height, distance below surface of suspension	m
H_{CS}	Height of control-surface CS	m
I	Length of cylindrical section of cyclone body	m
I, I_0	Transmitted, incident light intensity	Wm^{-2}
J	Length of vortex finder	m
K_1	Constant	Dimensionless

K_x	Length of cone section of cyclone body	m
L	Length of cyclone body	m
m	Mass	kg
$M_{pyc,p}$	Mass of particles in pycnometer	kg
$M_{pyc,liq+p}$	Mass of liquid and particles in pycnometer	kg
M_c	Mass flow rate of captured particles	kgs^{-1}
M_e	Mass flow rate of emitted particles	kgs^{-1}
M_f	Mass flow rate of feed	kgs^{-1}
$\bar{M}$	Mean mass flow rate	kgs^{-1}
$\dot{M}_{calib}$	Manually measured mass flow rate of liquid	kgs^{-1}
$\bar{\dot{M}}_{calib}$	Average manually measured mass flow rate of liquid	kgs^{-1}
$\dot{M}_{p,o}$	Mass flow rate of particles in overflow	kgs^{-1}
$\dot{M}_{p,u}$	Mass flow rate of particles in underflow	kgs^{-1}
N	Number of measurements	Dimensionless
p	Pressure	Pa
p_f	Pressure of feed	Pa
p_o	Pressure of overflow	Pa
p_u	Pressure of underflow	Pa
ΔP	Hydrocyclonee's pressure drop	Pa
Q	Volumetric flow rate	$\mathrm{m}^3\mathrm{s}^{-1}$
Q_f	Volumetric flow rate of feed	$\mathrm{m}^3\mathrm{s}^{-1}$
Q_o	Volumetric flow rate of overflow	$\mathrm{m}^3\mathrm{s}^{-1}$
Q_u	Volumetric flow rate of underflow	$\mathrm{m}^3\mathrm{s}^{-1}$
Q_{calib}	Measured volumetric flow rate of Coriolis flow meter	$\mathrm{m}^3\mathrm{s}^{-1}$
$Q_{coriolis}$	Volumetric flow rate of Coriolis flow meter	$\mathrm{m}^3\mathrm{s}^{-1}$
r	Radial coordinate	m
r	Radius	m
R_f	Underflow-to-throughput ratio	Dimensionless
R_e	Particle Reynolds number	Dimensionless
S	Length of vortex finder within cyclone	m
S	Empirical standard deviation	Varies
S^2	Empirical variance	Varies
Stk	Stokes number $(\Delta\rho x^2 v_{ch})/(18\mu D)$	-
t	Time	s
T	Temperature	°C
U	Underflow rate	$\mathrm{m}^3\mathrm{s}^{-1}$

V	Volume	m^3
$V_{pyc,liq}$	Volume of liquid in pycnometer	m^3
$V_{pyc,p}$	Volume of particles in pycnometer	m^3
υ	Velocity of particles	ms^{-1}
υ_θ	Tangential velocity	ms^{-1}
υ_t	Terminal velocity	ms^{-1}
υ_z	Axial velocity	ms^{-1}
υ_r	Radial velocity	ms^{-1}
$\upsilon_{\theta w}$	Wall velocity just after inlet	ms^{-1}
$\upsilon_{\theta CS}$	Tangential velocity at CS	ms^{-1}
W	Length of apex section of cyclone body	m
x	Particle diameter	m
x_{50}	Cut size	m
$\bar{y}$	Mean value of y	Varies
z	Axial coordinate	m
α	Entrance constriction coefficient	Dimensionless
ρ	Fluid density	kgm^{-3}
ρ_f	Density of feed	kgm^{-3}
ρ_l	liquid density	kgm^{-3}
ρ_o	Density of overflow	kgm^{-3}
ρ_p	Particle density	kgm^{-3}
ρ_u	Density of underflow	kgm^{-3}
η	Overall fractional separation efficiency	Dimensionless
$\eta(.)$	Grade-efficiency	Dimensionless
$\eta'(.)$	Reduced grade-efficiency	Dimensionless
μ	Viscosity	$kgm^{-1}s^{-1}$
Ω	Angular velocity	s^{-1}
θ	Tangential coordinate	Dimensionless
λ	Particle size,diameter	m
$\| \, . \, \|$	Absolute value	-

Chapter 1

Introduction

This chapter briefly gives the background and relevance for this master thesis, the application in industry, history of hydrocyclones, as well as the previous work.

1.1 Relevance

Producing petroleum resources includes co-producing amounts of water, which is called produced water. The produced water contains different amounts of dispersed and dissolved oil, chemical residues and solids. It is necessary to treat the water and remove the components that are harmful to the environment before discharging it to the sea. In the oil and gas industry, there are big challenges due to the abundance of sand and other solid components in produced oil and gas. Additionally, preserving the environment has been very important in recent years. This leads to strict policies for the waste discharge to the sea. In terms of preserving the environment, the rules will become stricter in future years. The separation of solid components from liquid is therefore very important. We have to improve our knowledge about the separation process as well as the equipment, and we have to know which equipment should be used at which stage.

In this thesis, the influence of liquid viscosity and hydrocyclone geometry on separation efficiency in a hydrocyclone has been investigated. Knowledge about the hydrocyclone geometry and the separation performance for solids, e.g. sand from viscous medias, such as mono-ethylene glycerol, is important to investigate.

1.2 Background

Sand and solid components have created many problems in the oil and gas industry. These problems can occur in production, separation and processing equipment. Consequently, it is important to separate the solids from the carried fluids. Hydrocyclones are among the types of equipment that have been applied to separate the sand from oil and get sufficient oil quality. Cyclones are relevant in in the cases where components of different densities are to be separated. This is achieved with the aid of a strong centrifugal force created by a swirling flow. The reasons for the popularity of the hydrocyclone lie in the simplicity of its design and operation, high capacity, and low maintenance and operating costs. It has no moving parts and is only driven by a external pump. These have made cyclones favourable in comparison to other separators [1].

As mentioned earlier in this section, sand and other solid components can create many problems for the equipment during separation and production. Moreover, they have created problems for the environment. Some examples for such problems are as following:

- Erosion can be caused by solid particles in the processing equipment, which reduces the lifetime of the equipment.

- Solid particles can interfere with control instruments, which may reduce reliability and safety in the process.

- The operational capability, safety and reliability can be reduced due to clogging of valves.

- Solid components can create problems with walls and pump injection.

- Separation tanks may be filled with solid particles. This will probably require manual removal of the solids.

1.3 Application in the industry

Hydrocyclones are very widely used throughout industry. The hydrocyclones are flexible in their application and we can use them for various degrees of separation by changing the loading conditions or geometric proportions. As mentioned earlier they have simple design, operation and maintenance. Therefore they have been used in different types of industries such as [2]:

- Oil and gas industry
- Power generation
- Iron and steel industry
- Sand plants
- Food processing plants
- Catalyst manufacturing plants
- Food industry

Each application has its specific requirements. The design and operation of the cyclone should be changed to make the cyclone most suitable for each case. According to Svarovsky [3] in principle, hydrocyclones separate particles (solids, droplets and bubbles) of the dispersed phase from a liquid (continuous phase) on the basis of density difference between the phases. Furthermore, the separation is either very depending on particle size or depends on the density if the system is not uniform. Svarovsky stated that hydrocyclones have also been used to produce thick underflow, thickening, i.e. the total mass recovery of the mass feed solids. Solid-solid classification by particle size is another application of the hydrocyclone. In this case one can use the grade-efficiency (see later) to split the feed solids into fine and coarse fractions. They have also been used for washing of solids by setting up several stages in a counter-current arrangement [3].

1.4 History of hydrocyclone

Cyclones have been used in many technical applications such as physical separation processes and chemical reactions for more than 100 years. The first patent for a cyclone was granted to John M. Finch in 1985. The cyclone from that time and today's hydrocyclones have the same principles except the outlet was on the side, i.e. the particles were discharged on the side of the cylindrical body instead of the conical section. In 1891, the first hydrocyclone was patented by Bretney [4]. It was used for the purification of water. The idea of using the centrifugal force rather than the force of gravity to separate particles from fluid was a new idea until in the late 1800's. The centrifugal force is created from its tangential inlet which forces the liquid into a circular motion. The hydrocyclone design has been improved over the years and the conical cyclones appeared for the first time in the early 1900's as we use them today. As mentioned earlier, hydrocyclones have been widely used in different applications for their advantages such as simple structures, robust separation devices with no moving parts, small physical size of unit, and low installation and maintenance costs.

Recently, hydrocyclones have been applied in environmental, food, mineral processing, petrochemical, electro-chemical and other industries [5]. The design and performance of hydrocyclones have been investigated for several decades. We know that the hydrocyclone separation performance is influenced by the structure of the hydrocyclone and the separation parameters. The structure of the hydrocyclone is the determinant factor for the established solid-liquid separation system. There have been many investigations with respect to the structure and geometric dimension scale of hydrocyclones to achieve satisfactory separation performance.

1.5 Previous work and objective

The purpose of this project is to extend the work performed by Marthinussen et al. namely, studying the "removal of particles from highly viscous liquids with hydrocyclones" [6]. In their work, they studied how the fluid viscosity will influence the hydrocyclone's performance. The viscosity of the liquid was gradually increased by adding sugar to the feed tank. Three pressure gauges were installed close to the inlet and outlets. The pressure loss over the hydrocyclone was measured by subtracting the pressure loss of the overflow from the pressure loss of the inlet.

To measure the flow rates, the ultrasonic flow meters didn't handle the situation when the particles were added to the system, therefore the flow rate was checked by sampling a volume over a specific period of time. The flow split is defined as the fraction of flow rate at the under and overflow, and the amount of flow fraction at the outlets could be determined by flow split [6].

The experimental equipment which was needed was built by the workshop at the Physics and Technology department at the University of Bergen. The hydrocyclone was tested in both the primary stage and while under operation. Thus, some modifications were made to the experimental rig in the previous work.

Chapter 2

Theory

The essence of the theoretical investigation is an understanding of the important phenomena inside the hydrocyclone and how it physically works. In this chapter, the cyclone is investigated in more detail. The forces acting on fluid elements in swirling flow are discussed. The pressure drop and separation efficiency are also discussed in detail.

2.1 Hydrocyclone

A hydrocyclone is a very simple piece of equipment to make. It has moving parts and consists of a conical section joined to a cylindrical portion. It has one entrance (feed) and two exits; the smaller one is on the bottom (underflow) and a larger one is at the top (overflow). The underflow is generally the denser or coarser fraction, while the overflow is the lighter or finer fraction. The hydrocyclones are efficient when promoting solid-liquid, gas-liquid, gas-solid and liquid-liquid separations. The most important feature in the separation procedure is the density difference between the two phases.

2.2 Swirling flow

"Swirling flow, or vortex flow, occurs in different types of equipment, such as a cyclone, hydrocyclones, spray dryers and vortex burners." [2] It plays a central

role in the operation of foam-braking or 'defoaming' separators that have received significant industrial attention in recent years. According of Hoffmann [2], here are two types of ideal swirling flows:

1. Forced vortex flow, i.e. swirling flow with the same tangential velocity distribution as a rotating solid body. The motion of particle and its separation in a cyclone, depends on its size, density and tangential velocity. Since the particle size is one of the significant factors for separation, therefore it is important to know more about the size of particles and what we mean by the size of particles. Normally, by the term size, one means the diameter of a particle. One can define the diameter in different ways. Which definition is used, depends on the given context. The volume equivalent, i.e. is the diameter of the sphere with the same volume as the actual particle. The surface diameter is defined as the diameter of a sphere with the same surface area as the actual particle. The surface/volume, i.e. is the diameter of a particle with the same surface-to-volume ratio as the actual particle.

2. It is the way in which the fluid without friction would swirl, i.e. free vortex flow. In this case, the tangential velocity is such that the moment-of-momentum of fluid elements is the same at all radii.

In the first situation, one can assume that the swirling fluid has an infinite viscosity. This means that there is no shearing motion between fluid layers at different radii and the fluid has the same angular velocity, Ω , at all radii and behaves like a solid body. The swirl with constant ,Ω, has been called forced vortex flow or solid body rotation. The tangential velocity is given by Eq. 2.1, where v_θ is the tangential velocity measured in m/s, Ω is the angular velocity which is measured in radius per unit of time s^{-1} and r is the radius.

$$v_\theta = \Omega_r \tag{2.1}$$

In the second situation, one can assume that the swirling fluid has no viscosity. This means that the motion of a given fluid element is not influenced by the neighboring elements. In this case, the tangential velocity will increase if the element is moved to a smaller radius. This is because the momentum-of-momentum (mass times tangential velocity times radius of rotation: mv_θr) is conserved. A vortex

where momentum-of-momentum is conserved in this way is called 'loss free', or 'frictionless'. The tangential velocity in such a flow is given by Eq. 2.2, where C is a constant.

$$v_\theta = \frac{C}{r} \tag{2.2}$$

Since the amounts of v_θ ,r and Ω have both magnitude and direction, they are vectors. Here, we are only interested in their magnitudes and we dispense with the vectorial notation.

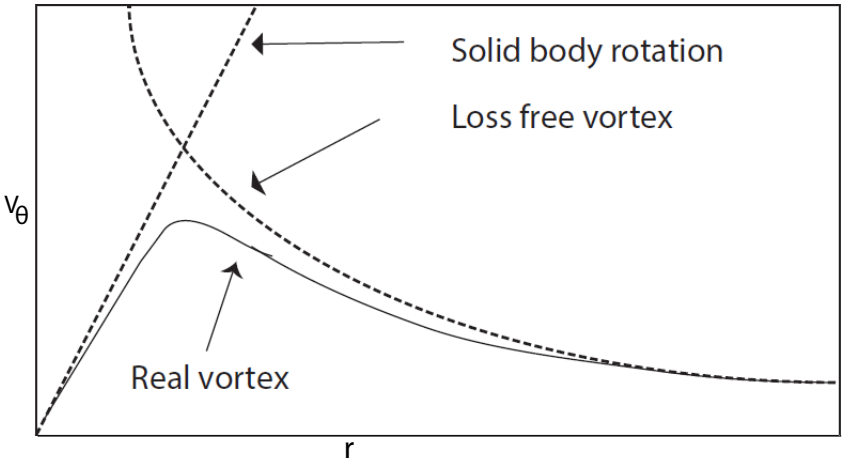

FIGURE 2.1: Sketch showing the two ideal vortex flow and the tangential velocity distribution in a real vortex. Redrawn from [2].

A real swirling fluid has some finite viscosity. This will cause the transfer of moment-of-momentum between layers at different radii. In addition, there is also some turbulence and this presence will also cause the transfer of moment-of-momentum. This is because of the exchange of fluid elements between the layers. In a real swirling flow, there is a core of near solid-body rotation surrounded by a region of near loss-free rotation as sketched in Fig. 2.1. A vortex with such properties, is called a Rankine vortex [2].

2.3 Forces in swirling flow

2.3.1 Centripetal force

To describe the forces acting on a fluid element in a swirling flow, we use a cylindrical coordinate system (r,θ,z) fixed in space with the z-axis of rotation, pointing

off of the paper. The element accelerates toward the center as it rotates. The acceleration towards the center of rotation is known as the centripetal acceleration and it is shown in Fig. 2.2. The element would continue in a linear path tangent to the orbit towards the axis of rotation if it did not accelerate. This means that there are velocity changes due to the acceleration, and it indicates that there is a force acting towards the center. This force is known as centripetal force [2].

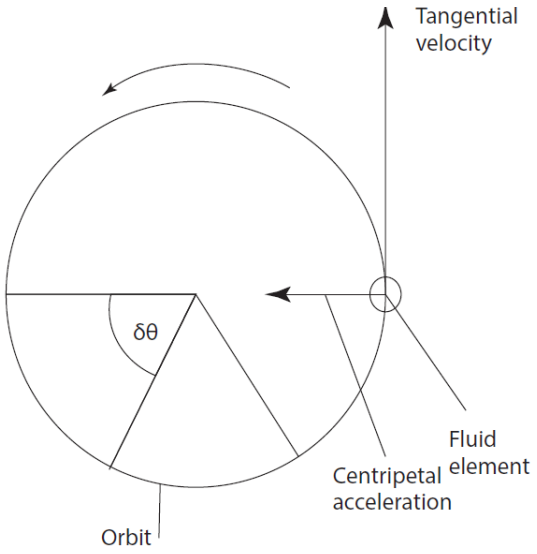

FIGURE 2.2: Sketch showing the tangential distribution in a real vortex. Redrawn form [2].

2.3.2 Centrifugal force

If the element we mentioned above will be considered from a coordinate system, which is not fixed in space by rotating, the centripetal acceleration will not longer be observed. It will appear as an apparent force directed away from the axis of rotation which is known as the centrifugal acceleration. The centrifugal acceleration acts away from the axes of rotation and it is similar in nature to the gravitational force. The magnitude of the force is equal to the mass of the element times the centripetal acceleration. The magnitude of the force is given by Eq. 2.3, where m is the mass of the particle, v_θ is the tangential velocity and r is the radius [2].

$$F_c = \frac{mv_\theta^2}{r} \tag{2.3}$$

Newtons equations of motion apply only in a coordinate system that is not accelerating. So, the centrifugal force is strictly speaking, not a real force. However,

it is often used as an accelerating coordinate system for mathematical simplicity and by scientists in order to apply or preserve the equation of motion. One is talking of a none-physical or pseudo force (a rotating one, for instance) because, it is not possible to identify a physical object in a rotating coordinate system which produces the force needed to satisfy Newtons laws of motion. Real forces always occur in pairs. For a fluid element, the centrifugal force is balanced by a force created by a gradient in the static pressure. This pressure gradient is pointing towards the center of rotation and keeps the liquid element in its path as shown in Fig. 2.3.

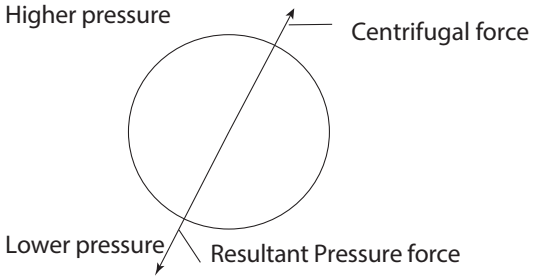

FIGURE 2.3: Forces acting on a rotating fluid element in a rotating coordinate system. Redrawn from [2].

2.4 How hydrocyclones work

The main hydrocyclone is divided in two parts, the cylindrical section and the conical part. The cylindrical section is placed on the top of the conical part. This is called a cylinder on cone cyclone. There is an overflow pipe coming out at the top of the cylindrical section, which is called the vortex finder. The end of the vortex finder is inserted into the cyclone's body and it stabilizes the inner vortex. The underflow is lead out of the cyclone and into the underflow box through the bottom of the cyclone. The inlet section is a rectangular shape and is located on the upper level of the cylindrical section, as shown in Fig. 2.4. The swirling flow is produced by leading the flow into the cyclone tangentially to the cyclone body. The fluid moves axially downwards in the outer vortex in the cylindrical section of the cyclone. When the fluid moves into the lower part of the conical section it is forced into the inner vortex which is moved axially upwards. As can be seen in the figure, the particles in the fluid are flung out on the wall in the cylindrical section until they exit through the underflow. The suspended particles are separated because of the size and gravity. The vortex flow in the cyclone

consists of a downward flow which is located in the outer region and one which is located in the inner upward region. According to Stokes law, the heavy settling particles move to the wall of the cyclone and flow out through the underflow. The lighter settling particles move to the low pressure zone in the center of the cyclone [3].

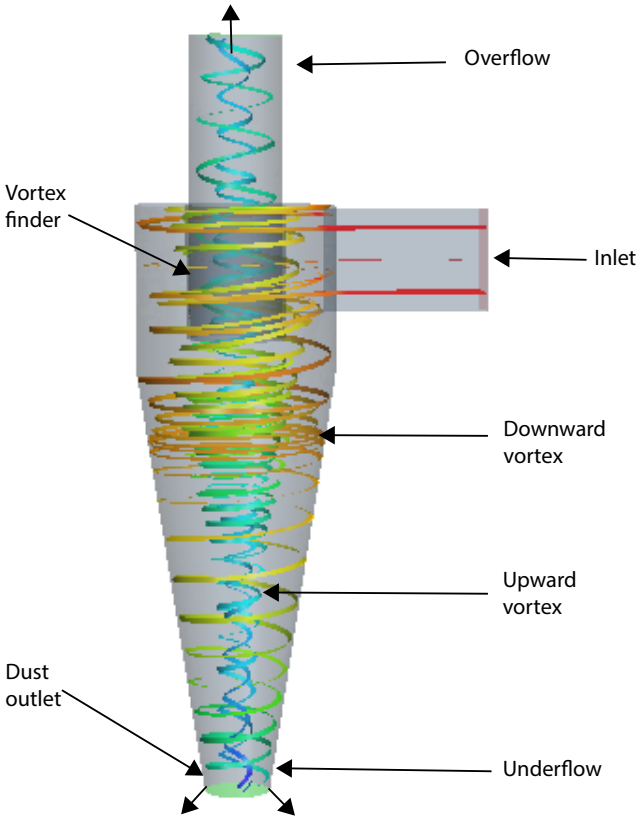

FIGURE 2.4: Sketch of a hydrocyclone with tangential-inlet and the flow pattern is indicated, as well as the exit for dust and lighter settling particles.

2.4.1 Merits and disadvantages

Every apparatus has its pros and cons. "The relative merits of the hydrocyclone sums up as follows according to Svarovsky [3].

1. They are extremely versatile in application in that they can be used to clarify liquids, concentrate slurries, classify solids, wash solids, separate two immiscible liquids, degas liquids or sort according to density or shape;

2. They are simple, cheap to purchase, install, and run, and require little maintenance and support structures;

3. They are relatively small compared to the other separators, thus saving space and also giving low residence time, which gives them an advantage in terms of the speed of control over the sedimentation classifiers for example;

4. The existence of high shear forces in the flow is an advantage in classification of solids because it breaks any agglomerates, and also in the treatment of thixotropic and Bingham plastic slurries.

The disadvantages of the hydrocyclone are:

1. They are somewhat inflexible once installed and operated, giving low turn-down ratios due to the strong dependence of their separation performance on flow rate and feed concentration; they are also inflexible due to their general sensitivity to instabilities in feed flow rate and solids concentration;

2. There are limitations on their separations performance in term of the sharpness of the cut, the range of operating cut size, de-watering performance or the clarification power; some of the these characteristics may be improved in the multi-stage arrangements, but at additional costs of power and investment.

3. They are susceptible to abrasion but steps can be taken to reduce abrasive effects;

4. The existence of shear may sometimes turn into a disadvantage because flocculation cannot be used to enhance the separation as in the case of gravity thickeners (as most flocs do not survive the shear)."

2.5 Liquid flow pattern and velocity

The flow pattern in a hydrocyclone is set out in the radial, tangential and axial velocity. The flow pattern has been reviewed many times and in many places. According to Bradley [7], the flow pattern in a normal design of a hydrocyclone is a spiral within a spiral. On the entry, the fluid starts a downward flow in the outer regions of the cyclone body. The combination of the downward flow with the rotating motion creates the outer spiral. Chang et al. [8] stated that the mixture enters the upper cylinder of the hydrocyclone in a direction causing the mixture

to swirl along the inner wall toward the outlet at the other end of the separation space which is the underflow outlet. The denser phase of the mixture is flung onto the wall and transported to the underflow outlet during the swirling motion [2].

2.5.1 Tangential velocity

The tangential velocity v_t at lower level below the rim of the vortex finder increases considerably with decreasing radius, which is smaller than the exit radius of the vortex finder. This is shown in Fig. 2.5. The relationship between the tangential velocity and radius can be described by Eq. 2.4.

$$v_t r^n = constant (0.6 \leqslant n \leqslant 0.9) \tag{2.4}$$

From Eq. 2.4, one can see that the tangential velocity decreases and it is proportional to r when the radius is further increased. This relationship holds as long as the cylindrical air column (which normally forms in a hydrocyclone discharging at atmospheric pressure) is reached. As it cab be seen from Fig. 2.5, the break in the rise of tangential velocity occurs at a larger radius at levels higher than the rim of the vortex finder. Apart from this phenomenon and the wall effects, the tangential velocity is independent. This leads to envelope of constant tangential velocity as it is cylindered coaxial with the cyclone.

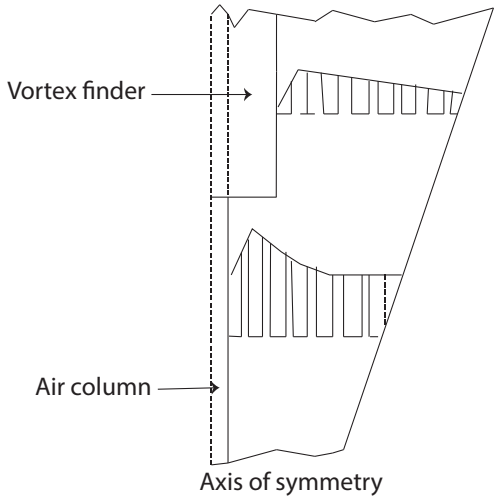

FIGURE 2.5: Tangential velocity distribution in a hydrocyclone. Redrawn from [3].

2.5.2 Axial velocity

From Fig. 2.6, you can notice that there is a strong downward flow along the outer walls of both the cylindrical and conical portions. The axial velocity is significant for cyclone operation because it removes the particles that have been separated into the underflow orifice. As a result it is not necessary to build cyclones with the apex pointing downwards. Regarding the gravity field, the cyclone efficiency is influenced very little by its position. Depending on the underflow-to-throughput ratio, the downward current is partially counterbalanced by an upward flow in the core region. As can be seen from Fig. 2.6, there is a well defined locus of zero vertical velocity (LZVV) which follows the profile of the cyclone. At a higher level than the rim of the vortex finder, the largest downward velocities are located near the cyclone wall. The axial velocity goes upward at radii between the cyclone wall and the vortex finder. One can see a strong downward flow around the vortex finder. This is because of wall-induced flow which runs inward along the top of the cyclone [3].

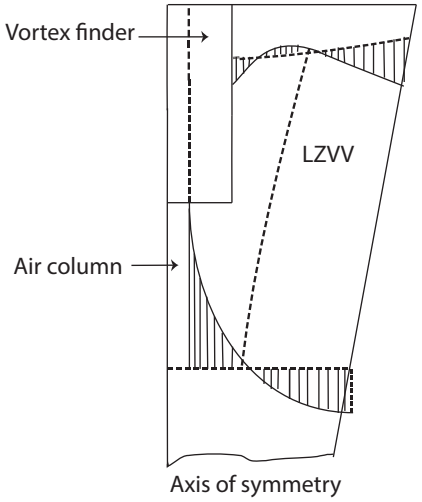

FIGURE 2.6: Vertical (axial) velocity distribution in a hydrocyclone. LZVV, the locus of zero vertical velocity. Redrawn from [3].

2.5.3 Radial velocity

Normally, the radial velocity components are hard to measure accurately as they are much smaller than tangential and axial velocity components. Fig. 2.7 indicates that the radial velocity is inward and decreases with decreasing radius. The radial location of zero radial velocity is unknown. Hoffmann and Stein [2] stated that the radial velocity is mostly inwardly directed below the lip of the vortex tube, but it is not uniform with height. The greatest inward flow is located below the vortex tube opening.

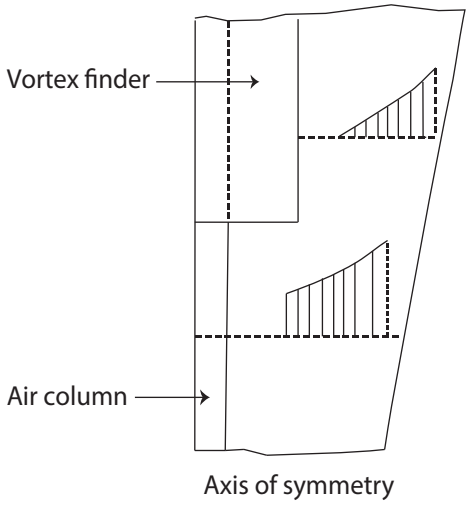

FIGURE 2.7: Radial velocity distribution in a hydrocyclone. Redrawn from [3].

2.5.4 Eddy flow

One can divide the flow inside the hydrocyclone into the inner and outer vortex. This part has been discussed in detail in section 2.4. Some of the vertical flow can exist in the region outside of the radius of the outer wall of the vortex finder. The vertical flow outside of the outer wall exists in the form of the recirculating eddy or eddies. This occurs due to the inability of the normal overflow opening to handle the natural upflow in the vortex. Fig. 2.8 shows an illustration of eddy flows [7].

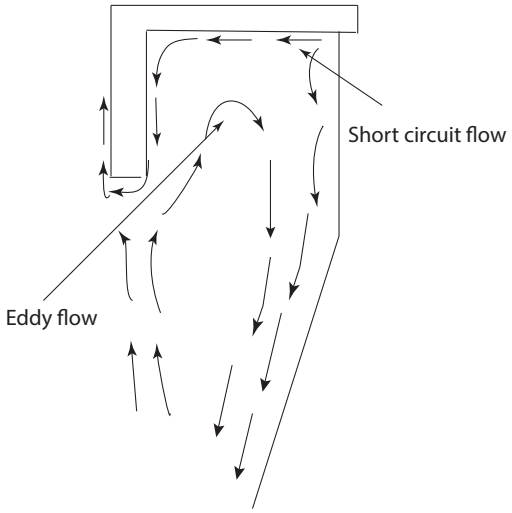

FIGURE 2.8: Schematic representation of the short circuit and eddy flows. Redrawn from [7].

2.5.5 The air core

It creates a low pressure axial core due to the rotation of fluid, which in the case of a hydrocyclone, normally results in free liquid surface. The core in a cyclone has direct contact with the atmosphere at either one outlet or the other, so it becomes air-filled. In the case when there is no communication, it can still exist filled with vapour and gases from the solution in the liquid. Since the air core has a generally constant diameter throughout the cyclone length, it can show if there are other irregularities in it. Formation of the air core in a cyclone indicates the stability of a vortex. According to Bradley [7], observations of air core formation have represented that the minimum pressure drop in normal designs of cyclones is about 5 Psi.

2.5.6 Locus of zero vertical velocity and mantle

According to Bradley [7], there are two different flow regions in the hydrocyclone. The existence of an outer region of downward flow and an inner region upward flow that leads to a position where there is no vertical velocity. This comes throughout the majority of the cyclone body. A locus of zero vertical velocity can traced. The centres of the eddy flow are around this locus. An illustration of locus of zero vertical velocity has been given in Fig. 2.6.

2.6 Cyclone pressure drop

In the process industry, the method which being is used for determining a pressure drop is to measure the static pressure drop at the wall in the upstream and downstream piping or duct. Due to the swirling flow in the exiting liquid, this method is complicated for a hydrocyclone. Because of the swirling pattern, the static pressure at the wall would be higher than the cross-sectional average. We have to think about what to do with the dynamic pressure stored in the swirling motion. To understand the pressure distribution within hydrocyclones, we have to know the relationship between the static and dynamic pressures [2]. One can find out this relationship by using the well-known Bernoulli equation for steady flow of a frictionless fluid. This equation can be derived from the Navier-Stokes Eq. 2.5 [9].

$$\frac{p}{\rho} + gh + \frac{1}{2}v^2 = c \tag{2.5}$$

In this equation, the first and third terms on the left-hand side are respectively the static and dynamic pressures and the latter is often called the velocity head. One obtains the pressures by multiplying the Eq. 2.5 by fluid density. Consequently, the static pressure is p and the dynamic pressure becomes $\frac{1}{2}\rho v^2$. Eq. 2.5 shows that the static and dynamic pressures can be interchanged in the flow field. In the areas where the static pressure is low, the velocity i.e. the dynamic pressure, will be high and vice versa. Due to the swirl in cyclones and swirl tubes, the static and dynamic contributions to the total pressure vary strongly throughout the equipment. The static pressure is therefore difficult to measure at any given position. The pressure drop means the drop in total pressure, i.e.dynamic plus static. We can say that the drop in total pressure is the same as to dissipative loss of mechanical energy per unit volume in the flowing liquid.

The liquid moves inward from the outer to the inner part of the vortex in the cyclone body. It is also accelerated simultaneously in order to the principle of conservation of momentum-of-momentum or as someone would call it, conservation of angular momentum. This causes a decrease in the static pressure, while the dynamic pressure increases. It means that the vortex transforms static pressure to dynamic pressure. For a given velocity at the wall, the vortex becomes more intense for a smaller frictional loss. The conversion of static to dynamic pressure is more efficient if the vortex is more intense. This leads to a lower central static pressure

with which the liquid enters the vortex finder. Therefore smooth-walled and clean cyclones produce the highest spin in the vortex and greatest decrease in static pressure within the core. It is a dissipation of mechanical energy because of friction at the walls and in the vortex core. The permanent pressure drop over the cyclone rises just like in normal pipe flow because of the dissipation of mechanical energy. The energy is stored as dynamic pressure in the tangential velocity component in the liquid entering the vortex finder. This energy is dissipated in the vortex finder and downstream piping without much recovery of static pressure. Normally, the pressure drop over a hydrocyclone is subdivided into three contributions:

1. Losses in the entry.
2. Losses in the separation space (the main cyclone body).
3. Losses in the vortex finder.

For a hydrocylone with tangential velocity, the losses in the entry are often negligible compared to the other contributions. The pressure drop in the cyclone body is higher, but their main significance is in limiting the intensity of the swirl in the separation place. The vortex gets less intensive with more frictional losses at the walls. The general pressure drop is not dominated by such wall losses. The losses in the vortex finder are therefore the largest. But there are however some exceptions, e.g. when there are highly loaded solids or rough-cut cyclones. In this case the frictional drag at the walls dominates and will become an important contribution to the overall pressure loss at the expense of losses in the vortex core and the vortex finder. From our experience with pipe flow we expect that hydrocyclone pressure drop increases with increasing solid load, wall roughness and cyclone body length. But despite the pipe flow, cyclone pressure drop decreases with increasing solid body, wall roughness or cyclone body length. But with the ideas as mentioned above the natural cause of the hydrocyclone pressure drop, we can expect a decrease in the hydrocyclone pressure drop. To describe why an increasing wall friction leads to a decreased cyclone pressure drop, we will study two extremes for the flow pattern in the cyclone body:

1. An intense swirl with very low wall loss, and
2. Almost complete attenuation of the swirling motion by wall friction in the body.

In the first case, a large amount of static pressure is transformed into dynamic pressure. This creates a high dynamic pressure that dissipates in the vortex finder and downstream piping per unit volume of liquid. For the other case, wall friction takes a lot of dynamic pressure and with extremely rough walls the spin is reduced to almost zero. The dissipation in the vortex finder is less here in comparison with the first case. One can conclude that the dissipation and consequently the pressure drop is lower for the second case than for the first case. This means that the rougher the walls are, the less pressure loss we observe. With respect to this, it should not be problem for someone to understand that the wall solids where the solid loading is high, reduces the overall pressure loss relative to the same cyclone operating with negligible solids loading. In this case, when the liquid contains a lot of solids, drag between solids and the liquid robs the fluid of much of its energy. This leads to a reduction in the core velocity and a reduction in static pressure drop [2].

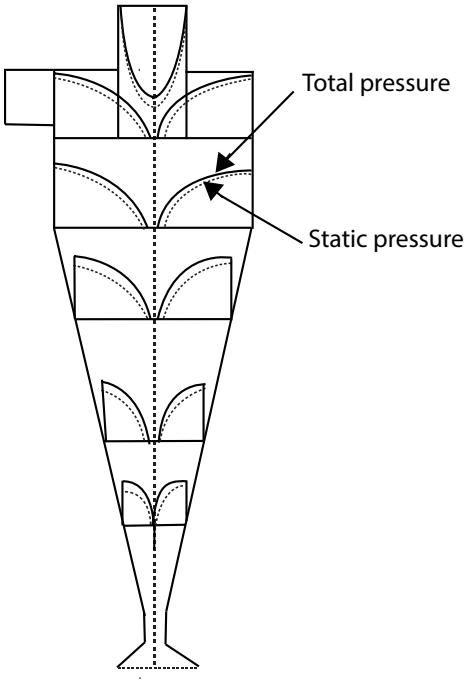

FIGURE 2.9: Static and dynamic pressure within a hydrocyclone. Redrawn from [2].

Now we will take a look at the interpretation of cyclone pressure drop measurements. Since the static pressure is uniform at the inlet of a cyclone and there is no swirl there, we can measure the pressure with a standard pressure tapping on the wall. On the other hand, there are still some swirls in the outlet of the cyclone which makes the interpretation of the pressure measurement difficult. Here, a significant dynamic pressure is stored in the swirling motion, and the static pressure

is not uniform over the cross section. "One way out of these difficulties is the observation that the static pressure at the wall is close to the cross-sectional mean of the static pressure plus the dynamic pressure stored in the swirl." according to Hoffmann and Stein [2]. It means that the pressure measured at the wall is nearby to the static pressure that would be measured after a correct flow and it would convert all the static pressure to the dynamic pressure. As a result, in the absence of pressure recovery devices, one can say that the pressure at the wall of the outlet tube minus the static pressure at the inlet gives the correct dissipative loss in the cyclone body.

2.7 Particle motion

In a fluid cyclone, the particles are always moving at their terminal velocity relative to the fluid. The terminal velocity of a particle decides if it will be captured or lost. The terminal velocity is exactly equivalent to that of a particle settling in the earth's gravitational field under steady-state conditions, and in a cyclone the radially directed centrifugal force mv_θ^2/r is replaced by the gravitational force. Therefore one is interested to calculate the particle velocity in the swirling flow. Newtons law to a particle moving in a fluid equals the mass times acceleration to the sum of the forces acting on it [2].

$$\begin{pmatrix} mass \\ times \\ acceleration \end{pmatrix} = \begin{pmatrix} body \\ forcedrag \end{pmatrix} + \begin{pmatrix} fluid \\ drag \end{pmatrix} + \begin{pmatrix} unsteady \\ force \\ terms \end{pmatrix}$$

Where, the body force is normally because of a gravitational field or a centrifugal force. The centrifugal force as mentioned earlier is not a real force. So, the above force balance is performed in a reference coordinate system rotating with the particle. The fluid drag is the drag acting on the particle when the particle moves with a steady velocity relative to the fluid. The unsteady terms account for the effects of acceleration of the particles relative to the fluid. Due to high turbulent velocity in the inlet of the hydrocylone, the particles which are close to the wall by the entrance can be dispersed inwards.

According to Bradley [7], the main separation is carried out in the conical section and the information on the flow pattern in the cylindrical section is therefore limited. When a particle enters the inlet of a hydrocyclone, it is influenced by

an inwardly directed drag force and outwardly directed centrifugal force. At the point where the incoming fluid first experiences a centrifugal force acting radially outward, the separation space starts. The separation space varies with inlet design. The centrifugal force is proportional to particle mass and therefore the cube of particle diameter (see later). Consequently, the largest particles are easier to separate than the smaller particles. How the particles will be influenced by the rotational flow depends on the particle's dimension, so the size of particles is very important.

$$m = \rho_p \times \frac{\pi}{6} \times x^3 \tag{2.6}$$

According to Stokes law, the drag force is proportional to the particle diameter, which is due to the flow of fluid from the outer to the inner part of the vortex. Since the study of the particle flow pattern inside a hydrocyclone is not easy experimentally, one uses the CFD simulations to examine the particle's trajectory inside a hydrocyclone.

2.7.1 Particle size

The motion of a particle and its separation in a cyclone, depends on its size, density and tangential velocity. Since the particle size is one of the significant factors for separation, therefore it is important to know more about the size of particles and what we mean by the size of particles. Normally, by the term size, one means the diameter of a particle. You can define the diameter in different ways, and therefore one should be aware of which one has been used in a given context. The volume equivalent, i.e. is the diameter of a sphere with the same volume as the actual particle. The surface diameter is defined as the diameter of a sphere with the same surface area as the actual particle. The surface/volume, i.e. is the diameter of a particle with the same surface-to-volume ratio as the actual particle. The dynamically equivalent particle diameter is very important to cyclone technology. This kind of diameter is the diameter of an equi-dense sphere that has the same terminal velocity as the actual particle. One can have difficulties calculating this in terms of intermediate Reynolds number, or when the Cunningham correction is significant [2].

2.8 Separation efficiency

When one uses a hydrocylone to separate a mixture of two phases in which the liquid phase is the most abundant, this is generally operated with a certain underflow. This means that if one operates a certain hydrocyclone with a given suspension or emulsion, there are still two variables. One is throughput and the other one is the ratio underflow to throughput. The pressure increases with the increasing of the throughput, and this leads to improving separation when the separation curve shifts to smaller particle sizes. The separation efficiency is influenced by the ratio of underflow to throughput due to two reasons. If the ratio is very small and the concentration of the solids in the feed is high, the capacity of underflow can be too small to remove all the solids. The concentration of solids in the hydrocyclone increases in this case and the solids are entrained partly with the overflow [10].

In a cyclone body, the highest separation efficiency is located in the outer vortex. Because of the high swirling motion, the large particles will be flung out to the wall and out through the underflow, but the small particles will be thrown into any part of the vortex in the flow. The inner vortex has lower rotation movements in comparison with the outer vortex, and therefore the separation power is lower here. The particles that enter in this location will follow the fluid out through the overflow [11].

2.8.1 Total efficiency

In cyclone operation, there are three particle fractions that we are interested in, namely the feed, the captured(or collected) and the overflow(or emitted or lost) fractions. Their masses are represented by symbols M_f, M_c and M_e respectively. The mass balance for solids over the cyclone is given by Eq. 2.7.

$$M_f = M_c + Me \tag{2.7}$$

The ratio of total mass collected in the underflow to the total particle mass in the feed is the total separation efficiency in the hydrocyclone. This relationship is given by Eq. 2.8.

$$\eta = \frac{M_c}{M_f} = 1 - \frac{M_e}{M_f} = \frac{M_c}{M_c + M_e} \tag{2.8}$$

We calculate the efficiency by collecting samples and weighing two of the fractions. The total efficiency, is what counts the most in the context of an industrial process. The total efficiency is not a good measure for characterizing the intrinsic separation performance of a particle cyclone, because the efficiency is depending on both the cyclone and the size and density of the solids [2].

2.8.2 Reduced total efficiency

If one wants to look at the net separation effect alone, he/she can use the reduced efficiency concept. In the case of a hydrocyclone, the total flow is split into underflow and overflow and the efficiency is always achieved as a result of this split. According to Svarovsky [3] the best and most widely used definition for reduced efficiency is Eq. 2.9.

$$\eta' = \frac{\eta - R_f}{1 - R_f} \tag{2.9}$$

Where R_f is the volumetric ratio of underflow to throughput. This is given by Eq. 2.10

$$R_f = \frac{Q_{underflow}}{Q_{feed}} \tag{2.10}$$

2.8.3 Grade-efficiency

The total separation efficiency does not consider the particle size in the feed and therefore it is not a good way to find the separation efficiency for a cyclone. The separation characteristics efficiency is best described by the grade-efficincy curve (GEC). This means various sizes are separated with different efficiency and the total efficiency η defined in Eq. 2.8 depends on the size distribution of the feed solids [2] [3]. The grade-efficiency cure can be obtained by feeding the separator with mono sized solids in several batches, or one batch containing particles in the required size range is fed into the cyclone. The latter method is the easiest, quickest

and cheapest way. Both of these methods are depending on the measurement of the total efficiency. For the latter method, the size distribution for two of the material streams (feed, underflow and overflow) has to be analysed. According to Svarovsky [3] the grade efficiency is a kind of transfer function which is derived from the effect the separator has on the particle size distribution of the feed solids as they pass from the feed to the underflow. The curve of the grade-efficiency tells the probability that the particles of different sizes have to separate into the underflow. The grade-efficiency curves are usually S-shaped in devices that use particle dynamics in which the body forces are acting on the particles. In the hydrocyclone case, this force of gravity or centrifugal forces are opposed by drag forces. The grade efficiency curve is shown in figure Fig. 2.10. The grade-efficiency curves can be obtained by using this formula:

$$\eta_x = \eta\frac{f_u(x)}{f_f(x)} = 1 - (1-\eta)\frac{f_o(x)}{f_f(x)} = 1 - (1-\eta)\frac{dF_o(x)}{dF_f(x)} \tag{2.11}$$

Where, f and F are differential and cumulative mass and $f_f(x)$, $f_u(x)$ and $f_o(x)$ are the mass distributions of the feed, the under and overflow fractions, respectively.

2.8.4 Reduced grade-efficiency

For a hydrocyclone as a separator with a size-dependent performance, the grade-efficiency varies with the particle size. A graphical representation of this is called the grade-efficiency curve. The grade-efficiency curve is influenced by the effect of flow splitting. In the case for a hydrocyclone, this makes the performance seem better than it actually is. The curve has an intercept and does not start from the origin. The value of the intercept is equal to the underflow-to-throughput ratio (R_f), as already stated under section 2.10.2. This is due to very fine particles easily following the flow and are being split between the underflow and the overflow in the same ratio as the fluid. By removing the effect of flow splitting from the efficiency definition, this describes only total efficiency. Fig. 2.10 shows a typical grade-efficiency cure [12].

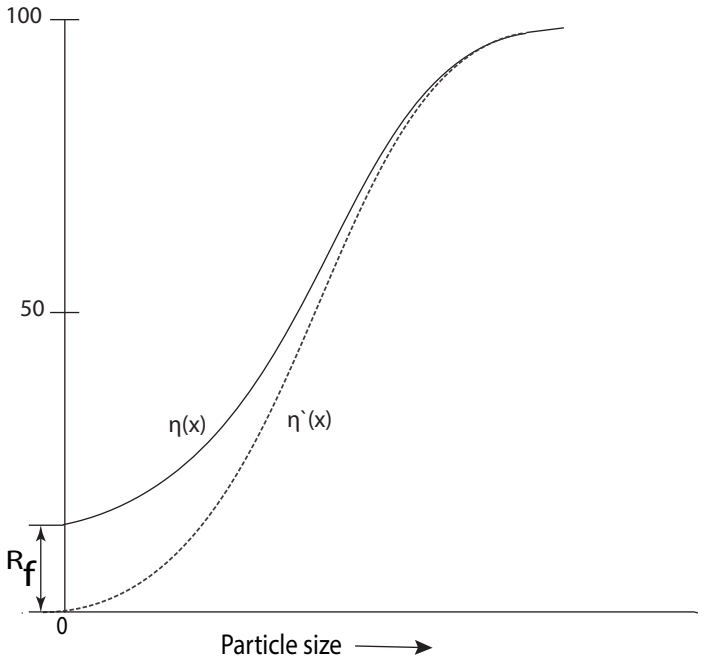

FIGURE 2.10: Grade-efficiency curve for a hydrocyclone (full line), and the reduced grade-efficiency (dashed line). Redrawn from [3].

2.8.5 Cut size

The size corresponding to a 50% probability collection efficiency is called the equiprobable size. One may describe the collection efficiency of a cyclone in terms of the cut-size or critical particle diameter, which represents the particle size that corresponds to a 50% collection efficiency. We have to estimate the tangential velocity,v_θ, of the air flow at the edge of the cyclone core, and the length ,L, of the cyclone core to calculate the cut-size of a specific cyclone geometry. This means that we have to take into account the geometrical dimensions of the cyclone when calculating the cut-size. A particle at the cut-size has a 50% chance of exiting through the overflow or the underflow [13].

2.9 Design aspects

There are many different designs of cyclone geometries, styles and fittings we can choose. The hydrocyclone is used in many different industries in different contexts. One of the factors that affects the performance, is the design of the hydrocyclone. Here, the focus will be on the main design variables which are cone angle, the inlet configuration and the vortex finder design [2] [14].

2.9.1 Cone angle

There are two basic shapes for the conventional hydrocyclone with tangential entry inlet. This is depending on the angle of the cone. The narrow-angle design, i.e. with an angle of up to about 25° is more used than the wide-angle design with angles about from 25° to 180°, as shown in Fig. 2.11. The cone angle has a significant effect on the existence of circulating flows in the cone. At narrow angles, flows are decreased and this makes the cyclone efficient for separation of fine particles. The required cut size is relatively low for such cyclones [3]. In the hydrocyclone with large angle, the small particles aggregate around the air core and there are some large particles in the vortex finder along the axis line. The separating space becomes small with a large cone [15].

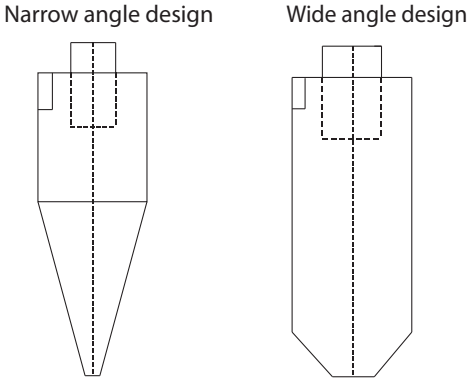

FIGURE 2.11: Schematic representation of Narrow-angle and wide-angle configuration of a conventional hydrocyclone. Redrawn from [3].

2.9.2 Hydrocyclone inlet design

The cross section of a tangential inlet is often rectangular. For small sampling cyclones, one uses inlets with circular cross sections. A cyclone with small inlet and outlet openings gives higher mass recovery but will offer higher resistance to flow and therefore have a lower capacity. Most pipes are circular in industry. This leads to a need for a circular or rectangular transition piece. This piece is often situated quite close to the cyclone. The flow transition occurs rather abruptly. This type of transition leads to the boundary layer therefore it is not ideal [2]. Svarovsky [3] stated that a single tangential inlet is most common:" There is little advantage in using multiple entries which would complicate the design of the manifolding." He stated also that a dual inlet is used in the designs developed

for liquid-liquid separation. The shape of the cross-section of the inlet according to Svarovsky [3] might be either circular or rectangular. The latter one is better because it brings the particles slightly closer to the wall on entry. Some different types of single inlet configurations are shown in Fig. 2.12.

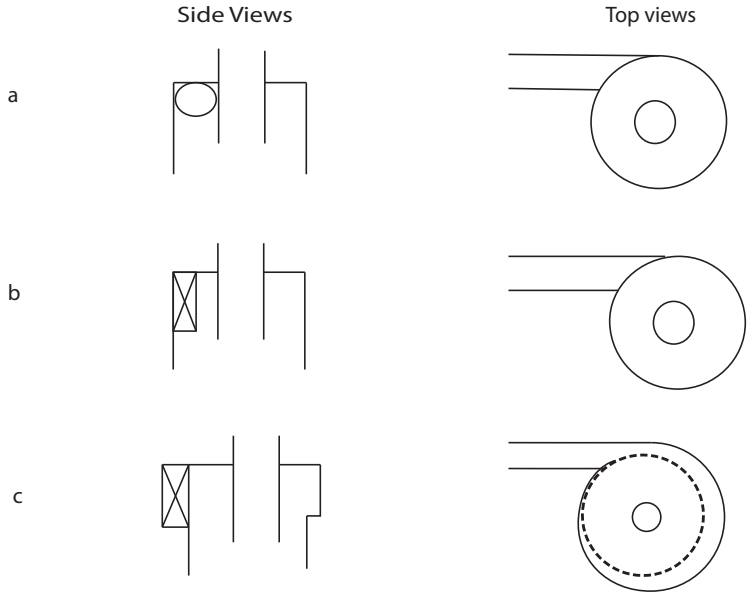

FIGURE 2.12: Schematic representation of side and top views of the three most used inlet configurations. a. Circular or 'pipe' inlet, b. 'slot' also called 'tangential' inlet, and c. 'wrap-around' inlet. Redrawn from [2].

2.9.3 Vortex finder

Basically, one takes the inside diameter of the vortex finder to check the capacity and cut size of the hydrocyclone. Hoffmann and Stein [2] stated that both separation cut-point diameter and pressure drop are strongly dependent upon the diameter of the vortex finder. Due to its importance, it is often regarded as the "heart" of the cyclone. Depending on design objectives, the vortex finder will be in a variety of shapes and sizes. According to Hoffmann et al. [16], the position of the vortex is one of the most important parameters to take into account in practical cyclone design. The sharpness of the separation of the hydrocyclone is related to the end of the vortex. The sharpness of cut can be manipulated by designing the cyclone with this in mind.

2.9.4 Apex design

Apex design and location has an important influence on the performance of hydrocyclones. Svarovsky [3] stated the size of the underflow orifice directly influences the underflow-to-throughput ratio, the underflow concentration and the cut size. One should adjust the underflow orifice during operation whenever any operating conditions change. There are several possible designs which are available, namely replaceable nozzles, mechanically adjustable openings, hydraulically controlled orifices and self-adjusting devices which maintain a constant underflow density or concentration. The orifice should always be kept circular because the underflow is still rotating when it comes out. With an orifice of another shape, blocking would be more likely. Obermair et al. [17] proposed using a long connection tube to the dust bin, because this prevents re-entrainment of already separated dust and affects the efficiency. He states that the apex diameter should be 1.2 to 1.4 times the vortex finder diameter. An optimal separation efficiency can be achieved by located 90° apex cone underneath the apex.

2.10 Hydrocyclone models

A various number of models and theories have been presented in this section. It is important to emphasize that these models and theories are not meant to be a complete solution or a substitute for real test results, but they have been used in design and construction of the hydrocyclones.

2.10.1 The simple, fundamental theories

There are essentially two models, namely equilibrium-orbit theory and the residence-time theory for cyclone separation efficiency. Fig. 2.13 illustrates the concept behind the equilibrium-orbit model. The equilibrium orbit theory is based on the concept of the equilibrium radius. This concept states that the particles of a given size achieve an equilibrium radial orbit position in the cyclone. In this position, the particles terminal settling velocity is the same as the radial velocity of the liquid. According to the balance of the centrifugal and centripetal forces, particles are therefore separated by the inward radial flow. These models are based on a particle that is rotating in cylindrical surface(CS) at radius $R_x = \frac{1}{2}D_x$. Hoffmann

and Stein [2] stated that in this balance, the outwardly directed centrifugal force is balanced against the inward drag caused by the fluid flowing through. The forces are normal to the surface CS and into the inner part of the vortex.

The centrifugal force is proportional to particle mass and therefore to x^3 and the drag force is proportional to x. Therefore, the large particles are centrifuged out to the cyclone wall, while the small particles are dragged in and escape out the vortex finder. The coarse particles will stay on large radii in the downward flow, while the fine particles reach equilibrium on small radii in the upwards flow. The dividing surface is the locus of zero vertical velocity(LZVV). The particle size for which the two forces balance or the size that orbits in equilibrium is taken is called the cyclone's x_{50}, or cut size. The particles have an equal chance to go to either overflow or underflow [3].

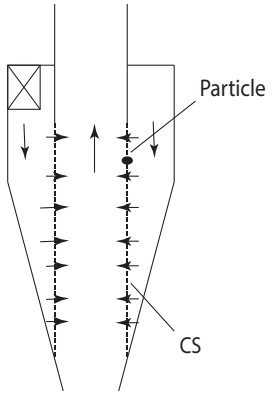

FIGURE 2.13: Sketch showing the concept behind the 'equilibrium-orbit' model. Redrawn from [2].

According to Hoffmann and Stein [2] there are two forces acting on a particle in cylindrical surface(CS):

• The centrifugal force(F_c) acting outward with magnitude of:

$$F_c = m_p \frac{v_{\theta CS}^2}{R_x} \tag{2.12}$$

The relationship between the particle mass, volume and density is shown by Eq. 2.13. The centrifugal force is proportional to the particle mass and therefore to x^3. The centrifugal force can therefore be shown by Eq. 2.14.

$$m_p = v_p \rho_p = \frac{\pi}{6} x^3 \rho_p \tag{2.13}$$

$$F_c = \frac{\pi x^3}{6} \rho_p \frac{v_{\theta CS}^2}{R_x} \tag{2.14}$$

• The drag is acting inward, and can be shown by Eq. 2.15.

$$F_d = 3\pi x \mu v_{rCS} \tag{2.15}$$

Here, $\|v_r(R_x)\| \equiv v_{rCS}$ is the average radial velocity in CS, and the absolute value for this is called v_{rCS}. The radial velocity near the wall is neglected, and in the surface CS it is assumed to be uniform. This is given by Eq. 2.16.

$$\|v_r(R_x)\| \equiv v_{rCS} = \frac{Q}{\pi D_x H_{CS}} \tag{2.16}$$

Where, Q is the volumetric flowrate through the cyclone, D_x is the diameter of the vortex finder and also CS, f is the wall friction factor i Eq. 2.17 and H_{CS} is the hight of the surface CS.

To calculate the tangential velocity at CS, $v_{\theta CS}$, one should first calculate the wall velocity $v_{\theta w}$ from the inlet velocity v_{in}. You can calculate the tangential velocity by following expression Eq. 2.17.

$$v_{\theta CS} = \frac{v_{\theta w}\frac{R}{R_x}}{1 + \frac{H_{CS}R\pi f v_{CS}}{Q}} \tag{2.17}$$

We need to calculate the wall velocity $v_{\theta w}$ to compute the tangential velocity at CS. The wall velocity can be calculated by Eq. 2.18.

$$\alpha \equiv \frac{v_{in}R_{in}}{v_{\theta w}R} \tag{2.18}$$

Where R_{in} is the radial position of the center of the inlet, and R is the radius of the inside wall of the cyclone's upper body or 'barrel' section. Fig. 2.14 illustrates the inlet flow pattern in a cyclone with a slot type of rectangular inlet.

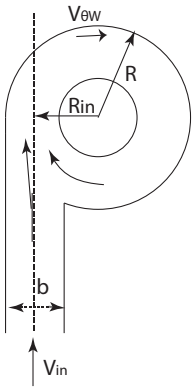

FIGURE 2.14: Schematic representation of the inlet flow pattern in a cyclone with a 'slot' type of rectangular inlet. Redrawn from [2].

For a slot inlet $R_{in} = (R - \frac{b}{2})$. Here, alpha ($\alpha$) is taken for a wrap-around inlet. Alpha (α) is calculated by algebraic relations by following Eq. 2.19.

$$\alpha = 1 - 0.4\left(\frac{b}{R}\right)^{0,5} \tag{2.19}$$

Eq. 2.19 is valid for slot type inlets with the ratio of inlet to outlet cross-sectional areas in the range of 0.9 to 1.8. Where b is the width of the inlet chute.

The cut size (x_{50}) has been calculated by equating the centrifugal force from Eq. 2.14 and the drag force from Eq. 2.15. In Eq. 2.20, ρ_p and ρ_l are the density of particles and liquid, respectively.

$$x_{50} = \sqrt{\frac{v_{rCS}9\mu D_x}{(\rho_p - \rho_l)v_{\theta CS}^2}} \tag{2.20}$$

One can fit the grade-efficiency cure through the cut size when the cut size has been calculated. A functional form to grade-efficiency curve following by Eq. 2.21, and the equation represents one functional form for representing the grade efficiency curve (GEC).

$$\eta_x = \frac{1}{1 + \left(\frac{x_{50}}{x}\right)^{6.4}} \tag{2.21}$$

The residence time theory was first proposed by Rietema. He assumed homogeneous distribution of all particles across the inlet. One assumes non-equilibrium conditions and considers that a particle will reach the cyclone wall in the residence time available in the residence-time theory. The cut size will then be the size of the particle which whether entering precisely in the centre of the inlet pipe will just reach the wall in residence time T. One does not take into account the radial fluid flow in Rietema's theory. This theory neglects any effects of inertia and does not take into account hindered settling at higher concentration. It also assumes any influence of turbulence to be negligible [3].

2.10.2 The crowding theory

This theory was first suggested by Fahlstrom. According to him, the cut size is primarily a function of the capacity of the underflow orifice and the particle size analysis of the feed. A hinder discharge through the apex or the crowding effect, can swamp the primary interaction to the extent that the cut size can be estimated from the mass recovery to the underflow [3].

2.10.3 Hybrid models

In these types of models, one takes into account both particle interchange between the outer and the inner vortices across CS (cylindrical surface) and particle migration to the wall. Therefore it can be said that these kinds of models are hybrids between the other two types, namely the equilibrium-orbit and the time-of- flight models. In practice, the x_{50} calculated by these models is often close to the x_{50} predicted by the equilibrium-orbit models [2].

2.10.4 The regression models

This is a group of mathematical models which are in fact based on regression analysis of test data. They are concerned with the capacity (or pressure drop) of hydrocyclones and the separation efficiency of the hydrocyclones in the form of the cut size [3].

2.10.5 The dimensionless group model

This model is based on fundamental theory combined with dimensional analysis to produce the necessary correlations. The required constants are derived from tests rather than from theory [3].

2.10.6 Numerical simulation of the flow

The methods of computational fluid mechanics have been used to develop numerical simulations of the flow. Nowadays, the numerical simulations are a common way to design and predict the performance of a hydrocyclone. Today, there are many types commercial software that provide computational fluid dynamics(CFD) for performing numerical simulations of the flow inside the hydsocyclone [3].

2.11 Liquid viscosity

Chang [18] defined the viscosity as following: "viscosity is a measure of fluid's resistance to flow". The liquid flows more slowly, the greater the viscosity is. The viscosity generally increases with molecular weight and decreases with increasing temperature. At the same temperature, the viscosity of liquids are much higher than those of gases. The main effect of temperature change is because liquid expands as temperature increases [19]. One of the factors that influences the liquid viscosity is intermolecular forces. Liquids that have strong intermolecular forces have higher viscosities than those that have weak intermolecular forces. Water has a high viscosity due to its ability to form hydrogen bonds. The viscosity of glycerol is remarkably higher than that of all the other liquids listed in Table 2.1. Each glycerol molecule has three OH-groups which participate in hydrogen

TABLE 2.1: Viscosity of some common liquids at 20°, redrawn from [18]

.

Liquid	Vicosity($N\frac{s}{m^2}$)
Acetone (C_3H_6O)	3.16×10^{-4}
Benzene (C_6H_6)	6.25×10^{-4}
Blood	4×10^{-3}
Carbon tetrachloride (CC_{l4})	9.69×10^{-4}
Diethyl ether ($C_2H_5OC_2H_5$)	2.23×10^{-4}
Ethanol (C_3H_5OH)	1.20×10^{-3}
Glycerol ($C_3H_8O_3$)	1.49
Mercury (Hg)	1.55×10^{-3}
Water (H_2O)	1.01×10^{-3}

bonding with other glycerol molecules as it has been displayed in Fig. 2.15. The molecule has a special shape and due to that, the molecules have a great tendency to become entangled rather than to slip past one another as the molecules of less viscous liquids do. These kinds of interactions contribute to the increased viscosity of glycerol [18].

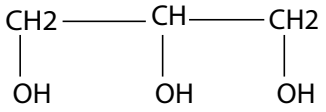

FIGURE 2.15: Schematic representation of the structure of glycerol. Redrawn from [18].

Bradley [7] states that an increase in viscosity decreases the separation efficiency (see later). The pressure drop decreases due to an increase in viscosity for the same flow rate. The results from some experiments with sugar solutions have showed that an increase in viscosity suppresses the tangential velocity to the extent of preventing air core formation and preventing the formation of intensive spiral movement. The absence of an air core under high viscous conditions, i.e. the character of underflow is changed and the amount of the feed which goes to the underflow increases. This means, the volume split or flow ratio increases as a result of an increase in viscosity.

2.12 Computational fluid dynamic

Computational fluid dynamic, or CFD for short, is undergoing important expansion in terms of the number of courses offered at the universities. There are some software packages available which solve fluid flow problems. The equations governing the flow of the gas in CFD, namely Navier-Stocks equations, are written in a finite difference form. The program has solved the equations with the aid of a computer on a grid of points that cover the body of the separator [2].

The CFD programs appeared in the 1950s, and since then, they have been developed continually. This is due to development of hardware and software. One needs a solid background in both fluid mechanics and numerical analysis to work in CFD. People have made significant errors due to a lack of knowledge in one way or another. Therefore, it is important to obtain a working knowledge of these subjects before using the program [20].

2.12.1 Numerical solution

Numerical solution is the study of methods of computing of numerical data and using a computer to calculate the answer. By using CFD, a program solves the Navier-Stocks equations for all the grid points. The grid is essentially a discrete representative of the geometric domain on which the problem is to be solved. The position of any grid point within the domain is identified by a set of two (in 2D) or three (in 3D) indices, e.g.(i,j,k). People who employ this method for solving the problems are worried about some issues, namely the rate of convergence, i.e. how long does it take for the method to find an answer, the validity of the answer and, are there any other solutions in addition to the one found [20]?

2.12.2 Turbulence models

Most flows that we meet in practical engineering are turbulent. Turbulence therefore requires special treatment. Hoffmann and Stein [2] stated that direct turbulence modeling such CFD simulations are carried out in small geometries. This field is advancing as the computational power increases. The number of grid points

and the time steps needed are to high. Consequently, turbulence models are required. In this thesis, there will be a brief description of some of the different models.

Direct numerical simulation

In direct numerical simulation, the Navier-Stokes equations are solved without averaging or approximation other than numerical discretizations and the errors can be estimated and controlled. In the DNS model, all of the motions included in the flow are solved. The domain on which the computation is performed must be at least as large as the physical domain to be considered or the largest turbulent eddy. This is because to be sure that all of the significant structures of the turbulence have been captured. All of the kinetic energy must be captured in a valid simulation. This can happen on the smallest scales, the ones on which viscosity is active. Therefore the size of the grid should not be larger than a viscous determination scale that is called the Kolmogoroff scale(η).

Ferzinger [20] announced that the number of grid points that can be used in a computation are limited by the processing speed and memory of the machine on which it is carried out. For this reason, DNS is possible only for flows at relatively low Reynolds numbers up to a few hundred. By using DNS, one can get detailed useful information about the flow. You obtain detailed information about the velocity, pressure and any other variable of interest at a large number of grid points. It is far more information than any engineer needs. Furthermore, DNS is to expensive to be employed and can not be used as a design tool.

Large eddy simulation (LED)

According to Ferziger [20], turbulent flows include a range of eddy sizes. The large scale eddies contain much more energy than the smaller scale ones. Their size and strength make them the most effective transporters of the conserved properties, but the smaller ones are much weaker and provide little transport of these properties. Even if DNS is generally more expensive in comparison to LES, but it is more accurate. By using large eddy simulation, the largest eddies in the flow can be solved and the smaller eddies will be modelled. Breuer [21] said that Reynolds-averaged Navier-Stokes equations combined with the statistical turbulence models, and an appropriate description using it is difficult to achieve.

The large eddy simulation(LES) offers a suitable method for solving such flow problems. The large eddies in LES are depending strongly on the special flow configuration and are resolved numerically, whereas the fine scale turbulence has to be modeled by a subgrid scale model. It is important that before LES can be used for applications of practical relevance, the influence on the quality of LES solutions must be understood. This includes numerical aspects such as resolution requirements, and modelling aspects such as subgrid scale models.

K-Epsilon model

The K-epsilon model is a two equation model, i.e. it contains two transport equations to represent the turbulent properties of the flow. It is one of the most common turbulent models. The first transport variable is turbulent kinetic(K) and the second transport variable is the turbulent dissipation(ϵ). The first variable determines the energy in the turbulence, whereas the second variable determines the scale of the turbulence. This model has been useful for free shear layer flows with relatively small pressure gradients [22].

Reynolds Stress Transport Models(RSM)

Reynolds stress models which are based on dynamic equations stress tensors are the most complex models that are used today. These equations can be derived from Navier-Stokes equations. This is the most complex model. Reynolds stress models have greater potential to represent turbulent flow phenomena more accurately. The use of this model has provided excellent results for some flows, namely swirling flows, and flows with strong curvature and with separation from the curved surface [20]. Since they are anisotropic turbulence models, the turbulence properties depend on the direction of the flow which works with swirling flows, flows with strong curvature, etc.

2.12.3 Eulerian and Lagrangian models

There are two ways of simulating the particle flow. When both the particles and fluid are treated as a continuous phase , it corresponds to the Eulerian approach. In this case, the continuum equations are solved for both phases with an appropriate interaction [22]. In the Lagrangian approach, the fluid is still treated as continuum, but the particles phase is treated as single particles. This approach involves the tracking of a single particle through the fluid flow field . This method is good for mechanisms of disperse phase behaviour, such as particle-particle and particle-wall interactions. Eulerian is less computer intensive and is good to utilize on a large scale, but Lagrangian is very computer intensive, and can therefore be used on very small systems [23].

2.13 Bivariate plots

Bivariate plots are used for bivariate data of two quantities which are related to one object. When you make graph of bivariate data, you do this on a scatter plot or scatter graph. Visualization of the distributed points in two dimensions can be performed by scatter plots. These methods are used to find patterns e.g. relation between two variables [24].

2.14 Principal component analysis (PCA)

Principal component analysis is a significant mathematical method that is used to squeeze a large number of data in chemistry. By this method, one transforms orthogonal correlated data into a set of linearly uncorrelated variables. Therefore this method is regarded by many as the most important change of data analysis within chemistry. The aim of this method is to achieve an explanation of a data table which are uncorrelated with respect to the new variables that is called principal component (PC). Compressing of data is important, because one can only relate to a restricted amount of dimensions at a time. The number of PCs are equal or less than the number of original variables. They are given as loading or scores vectors, where the score vectors are a basis for the object space, while the

loading vectors are a basis for the variable space. A combination of the variable and object space into one plot is called a biplot [25]. The principal components :

• Are located such that they can describe most of the variation in the data table.

• Are orthogonal in relation to each other as well as to residual matrix, i.e. the angle between them is 90°.

Chapter 3

Literature study

Hydrocyclones have been getting more and more interest from various industries. This is due to their obvious advantages such as simple structure, large capacity, low cost and small volume. Cyclones have found wide applications in various fields of technology. This chapter contains a review of the present research including some of the same process variables as reviewed in this chapter.

3.1 The effect of viscosity on cut size

As mentioned earlier in the section 2.11, the effect of viscosity on the cut size of a hydrocyclone is predicted by Equilibrium-orbit 'the Model of Barth'. The cut size has been calculated by using the Eq. 2.20. As mentioned earlier, this equation is the result of force balance on a particle rotating in the cylindrical surface(CS). The centrifugal force is acting outward and the drag force is acting from the outer part of the hydrocyclone to the inner part. Equation Eq. 2.20 shows that the cut size increases with the square root of the viscosity. In the same equation, the tangential velocity($v_{\theta CS}$) will be decreased by increasing viscosity, consequently the cut size x_{50} decreases [2]. Marthinussen et al. [6] stated that there is limited experimental information about the influence of the liquid viscosity on the literature since most applications of hydrocyclones are involving water as the liquid.

Van Rossum [26] studied the effect of viscosity on a cyclone. By applying Stoke's law for the viscous drag, in equilibrium, it can be seen that the size of drops at a given radius is proportional to the square root of the oil viscosity and inversely proportional to the square root of the tangential velocity at the same

radius. As a consequence, it is also proportional to the square root of the inlet velocity.

Guo et al. [27] performed some experiments to study the separation of sand particles from crude oil. The gravitational sedimentation technique is applied most widely in oil fields. They found that the present sand removal by sedimentation due to gravity has failed to meet the requirements of removing very fine particles. In their research, they applied the motion of sand particles of various diameters within liquids of different viscosities. They concluded that the rotational separation is a very useful way to improve the efficiency of oil/sand separation, where the centrifugal force is the key to decide the efficiency of small-diameter sand particles.

Kawara et al. [28] studied the effect of slurry viscosity on the cut size of a hydrocyclone. In their study, they modified the hydrocyclone model to predict the cut size due to changes in slurry viscosity. They claimed that besides the solids content, there are some other factors, namely temperature and chemical environment which affect viscosity.

Marthinussen et al. [6] as quoted from Agar and Herbst [29], they did research on the effect of the fluid viscosity on the hydrocyclone efficiency. In their study, they measured hydrocyclone efficiency by adding a wide range of various concentrations of sucrose for varying the viscosity of aqueous liquids. The density of solutions had also been varied because of high concentrations of sucrose. They found that the cut size can be calculated by using Eq. 3.1.

$$d_{50} = K_1 \frac{D_c^{1.4}}{Q^{0.55}} \frac{\mu^{0.58}}{(\rho_p - \rho_l)^{0.5}} \tag{3.1}$$

Where, d_{50} is the cut size, K_1 is a constant which is dimensional, D_c is the diameter of the hydrocyclone, and ρ_p and ρ_l are the density of particles and liquid, respectively. They determined that the viscosity should be raised to a power of 0.58 to reflect its influence on the cut size.

3.2 The effect of viscosity on the pressure drop

According to Hoffmann and Stein [2], the swirling motion in a hydrocyclone can complicate the understanding of cyclone pressure drop. The effect of roughening the cyclone walls is an example which, in contrast, in pipe flow leads to less pressure drop. Bradley [7] investigated the influence of viscosity on pressure and

has concluded that an increase in viscosity causes a decrease in pressure drop for the same flow rate.

According to Marthinussen et al. [6] the work done by Agar and Herbst as mentioned earlier in this chapter, shows that an increase in viscosity leads to a decrease in pressure drop.

3.3 The effect of geometry on separation efficiency

Hydrocyclones have ordinarily been designed on the basis of empirical equations to determine their geometric and operating parameters. Mossavian and Najafi [15] studied the influence of geometry on separation efficiency in a hydrocyclone. Their study was mainly directed to identify an optimal method used to study effective parameters. They investigated the inlet flow variations and body dimension variations on the separation performance. The results from their work indicate that the flow fields in the hydrocyclones of different sizes and lengths are different which makes different performance.

Jiang et al. [30] did some research studies for hydrocyclones with different structures and have analysed their effect and operating parameters on pressure drop and Oil-Water separation performance by hydrocyclones. They found that a hydrocyclone with a longer small conical section can reduce the pressure drop and enhance separation efficiency at the same time. One of the important operating parameters for a hydrocyclone, is flowrate. They also found that when the flowrate is lower than 50% of its optimum flowrate, oil-water mixed fluid can not be well separated, and then the ideal separation efficiency can not be obtained. This is due to the fact that a strong enough revolving flow field can not be formed inside the hydrocyclone. The conclusion from their work showed that, to obtain better separation effect, different geometric parameters of hydrocyclones should be selected under different conditions.

Yang et al. [5] presented a study concerning the effects of hydrocyclone cone combinations on the separation performance for solid-liquid separation. In their work, they had a two cone angle and they used the Computational Fluid Dynamic (CFD) method to simulate the flow fields inside hydrocyclones, and compared that with those that have been experimentally studied. The results from their work showed that the larger the two cone changes, the smaller the high separation

efficiency area is. The change of the cone angle leads to the change of fluid flow. As a consequent, this leads to the change of high separation efficiency area.

3.4 Computation studies of hydrocyclone separators

Hydrodynamic Fluid Dynamics (CFD) is a common tool which has been used to investigate the hydrodynamics in different process dynamics. In this section, some of the works that are related to CFD are presented.

Mousavian and Najafi [15] studied a numerical study on the influence of geometry on separation efficiency in a hydrocyclone. In their study, they used three models of turbulence, namely the RNG $k-\varepsilon$ model, the Reynolds stress model and Large eddy simulation. Their presentation was mainly aimed at identifying an optimal method to study the effective parameters which have influenced the separation performance and pressure drop. They utilised the three models to simulate air core and compared those to predict the flow split and axial and tangential velocities. In their research, they found that the large eddy simulation model was clearly closer in predicting the experimental data than the other two models. The effects of hydrocyclone geometries and operation variation indicate that the flow fields in the hydrocyclones of different sizes and lengths are different, which provide different performance.

Swain and Mohanty [31] examined an Eulerian-Eulerian multiphase model of solid-liquid hydrocyclone, which contains two solid phases and one liquid phase, to study the flow behaviour liquid-solid hydrocyclone. In their examination, they used two types of turbulence models, namely the $k-\epsilon$ and RSM models to predict the separation efficiency. They found small differences for the separation efficiency which was carried out by each model. The largest differences between the models were for larger particle size particles and was near the wall. They stated that the $k-\epsilon$ model can be preferred over the RSM model for a small diameter hydrocyclone operation at low velocity due to less computational time for the $k-\epsilon$ model [31].

Chapter 4

Design and experimental set-up

In this chapter, the previous design is presented together with the modifications that were needed to get the system up and running. The modifications have been made during assembly and after testing the rig. The rig was built by the workshop at the Physics and Technology department at the University of Bergen.

4.1 The hydrocyclone

The cyclone that was used for this project is identical to the one used in the previous project. The cyclone was made of steel with three different sizes of cone sections and also three different sizes of vortex finder diameters. The hydrocyclone body was made of steel, and the inlet, overflow and underflow pipes are made of steel material in the first part, and the rest were made of PVC. A plastic dust bin was connected to the apex cone to prevent any overestimates of the pressure drop and cut-off diameter. The specific design with all the size characteristics is given in Fig. 4.1 and Table 4.1.

TABLE 4.1: Size characteristics for the hydrocyclone.

Symbols	a	b	D_x	D_u	J	L	D	W	K_x
Cyclone [mm]	29	9	10,15,20	15	35	445	40	25	120,240,360

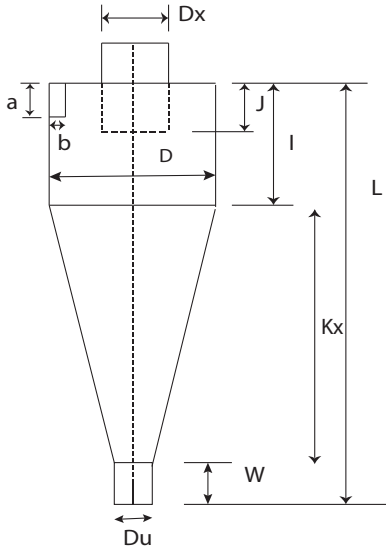

FIGURE 4.1: Schematic drawing of cyclone.

4.2 Previous design of the rig

As mentioned earlier, the rig was used in a previous thesis. The design of the hydrocyclone was done in respect to high efficiency design with some modifications done for the purpose of de-sanding. The hydrocyclone was made of glass fibre and the inlet and overflow pipes were made of PVC material. The rig consisted of a feed tank which was connected to a centrifugal pump. The media from the hydrocyclone, discharged back to the feed tank via overflow and underflow through the separate pipes. Two ultrasonic flow meters were connected to the overflow and underflow pipes to measure the flow rate, as illustrated in the figure below. Since the ultrasonic flow meters did not work due to increasing viscosity which influenced the signals in the flow meters, thus they were not used in the previous work. With such a configuration, one could make a continuous process independent of time. The original rig design is shown as Fig. 4.2.

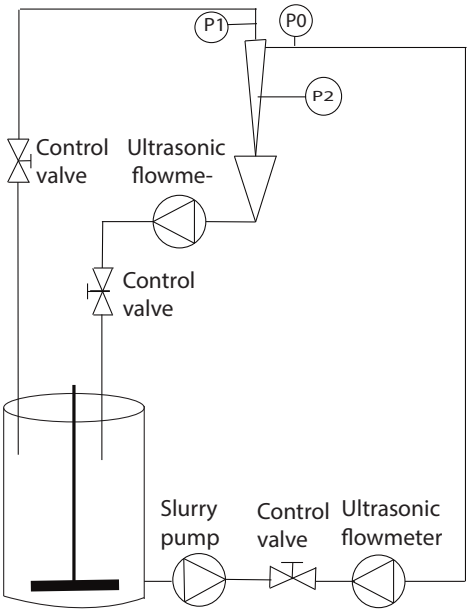

FIGURE 4.2: Schematic drawing of previous rig before the rig was modified to fit its new purpose.

4.3 The new design of the rig

As depicted in Fig. 4.3, some changes were made in the rig set-up during the installation of the new separator. The ultrasonic flow meters used to measure the total flow rate failed to get a signal when the viscosity is increased. Consequently, they were removed and replaced by a Coriolis flow meter and an Electromagnetic flow meter to measure the amount of the flow rate from the feed tank to the hydrocyclone and from overflow, respectively. Two outlets from the hydrocyclone were then connected to the feed tank by hoses.

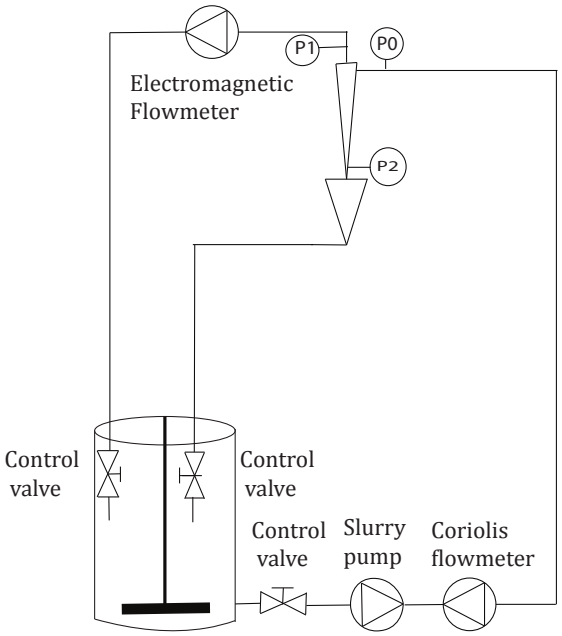

FIGURE 4.3: Illustration of the experimental set up of the cyclone rig in the circulating system.

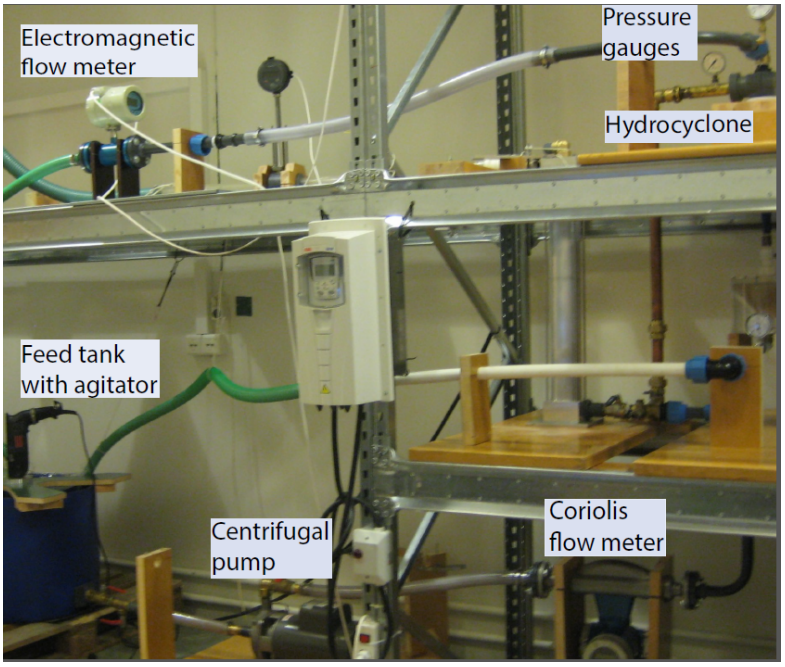

FIGURE 4.4: Photo of modified experimental rig set-up that was used for experiments.

4.3.1 Pump

The fluid was transported to the hydrocyclone by a centrifugal pump. The pump has a 1-phase electrical engine, high rotational speed (2850 RPM) and was running at 230 V. A valve was connected to the pipe after the centrifugal pump to control the flow rate. The maximum flow rate was 6.8 m^3/h, and the amount of flow rate was decided to be 4.7 m^3/h, which corresponding 5 m/s. So, by using the valve after the pump, it was possible to reduce and achieve the desired flow rate.

4.3.2 Coriolis flow meter

In order to measure the volumetric flow rate to the hydrocyclone, a Coriolis flow meter was installed. In the case of the Coriolis meter, the measured object flows through measuring tubes which are brought into oscillation. The Coriolis force generates a phase shift in these oscillations and is created in the tubes. The volume rate from the registered tube oscillations is calculated by the sensors which are located at the inlet and the outlet of the flow meter [32].

The fluid, i.e. both liquids and gases can be measured simultaneously by using the Coriolis flow meter. In addition to volume flow rate, these flow meters have the ability to measure several process variables, e.g. density and temperature. These pieces of equipment are known for their accurate measurement. By using this device, there is no obstruction placed in the fluid path due to turbulent motion. Due to these advantages, this flow meter has been concluded to be the most appropriate for the inlet flow conditions of the hydrocyclone. This flow meter is relatively expensive in comparison to other flow meters, but after contacting Endress+Hauser AS, one device was borrowed without any charge for a year [32].

4.3.3 Electromagnetic flow meter

The electromagnetic flow mater was installed at the overflow to measure the volumetric flow rate. The choice of flow meter installation on either underflow or overflow outlet was arbitrary since the inlet (total) volumetric flow rate could be measured by the Coriolis flow meter and the electromagnetic flow meter could be used to measure the flow rate from arbitrary outlets. Since it was desirable to have 5% (= 0.25 m^3/h)of total flow rate in the underflow outlet and the flow meter did

not handle the situation with 5%, it was determined to connect the flow meter to overflow. Fig. 4.5 illustrates maximum measuring error with respect on flow meter sizes.

The electromagnetic flow meter is designed with the intention of meeting all the demands of a modern water management system. The flow meter is suitable for measuring and billing in the civil, industrial and agriculture sectors since it supports extended functions which make it suitable to use in different contexts. Furthermore, it has been developed to measure small flow rates with maximum accuracy. The flow meter design concept offers flexibility, cost-savings and reliability. It provides a long service life and very little maintenance. The new generation of electromagnetic flow meters are allowing better control of flows in every point of installation [33].

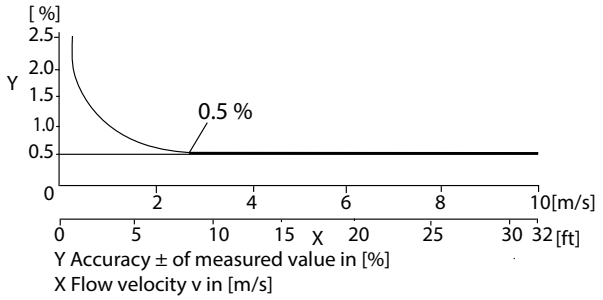

FIGURE 4.5: Shows maximum measured error in % reading. Redrawn from [33].

4.3.4 Pressure sensors

To measure the pressure loss over the hydrocyclone, there are three pressure gauges installed close to the inlet and the two outlets of the hydrocyclone. The inlet pressure gauge had a measuring range area from 0 to 2 bar, whereas the two outlets pressure gauges had a range area much lower than 1 bar. In a normal situation when the feed tank was approximately one meter lower than the separator, the overflow pressure gauge measured just 0. The problem was fixed by reducing the amount of flow rate from the underflow by the valve which were connected at the end of the hose of the overflow outlet.

4.3.5 Equipment and materials

As mentioned earlier in this section, the cyclone was made of steel by the workshop at the University of Bergen. It was made with three different sizes for the cone section as well as three different sizes for the vortex finder used in this project. A part of the inlet pipe was made of steel and the rest was made of PVC. This is due to cost and furthermore, the PVC piping was evaluated to withstand the pressure.

The tank that was used for this project had a capacity of 120 litres. The agitator from the previous work was utilized to mix the particles in the water and glycerol contents. The impeller agitator was a pitched-blade turbine, with a four-blade propeller and an angle 60° transversal. The agitator with such properties was powerful, so the number of blades was reduced to three and the transversal angle was reduced to 10°. The agitator with this condition provided sufficient overall circulation of fluid. The impeller was connected to a drill and then fixed and located on the tank.

The particles that were used in this project were Arizona Test Dust. The particles have a density of 2650 kg/m^3 and a size distribution in the range of 0-50 μm.

4.4 Analytical and precision balance and density determination kit

An analytical scale from Sartorius with a density determination kit was used for the sedimentation of particles. The equipment was installed and calibrated before being used. By calibration, one could determine the differences between the weight readout and the true weight of a sample. It does not impact any change within balance. We have to adjust the equipment to correct any differences between the measured value displayed and the true weight (mass) of the sample. Consequently, one must implement the internal calibration before using the balance as a legal measuring instrument. The density of a solid or liquid can be measured by the density determination Kit. The results reached from the density determination are not entirely certain because the results of measurements may be affected by various factors that cause errors. The several factors that can impact the accuracy of a density are: buoyancy of air, temperature of liquid, etc. The sample, liquid, and

the ambient temperature should have the same temperature to improve measuring accuracy. Density, referred to as the total amount of the mass of a sample per unit volume, is calculated by Eq. 4.1. When a body is immersed in a liquid, it will impact an upward force (i.e. buoyancy) that is equal to the weight of the liquid it displaced. The liquid surface position rises if a solid sample which is immersed in a liquid, is placed on the density pan for a density measurement. The measurement error caused by the buoyancy can be minimized by adjusting the sample size so that the liquid surface is not raised too much [34].

$$\rho = \frac{M}{V} \tag{4.1}$$

Where ρ is density, M is the mass and V is the volume of a sample.

Chapter 5

Experimental Methods

This chapter gives the methods used for obtaining the particle size distributions and a brief introduction of the method that was used to measure the viscosity of the liquid used in the experiments.

5.1 Particle size distribution analysis

The size distribution of the particles in the feed and overflow was needed to obtain the grade-efficiency for different cases. The sedimentation method was tested in the primary stage before the executing of experiments. This method was chosen because of simple configuration, low cost and reliability.

5.1.1 Sedimentation method

The sedimentation method is based on recording the sedimentation of particles dispersed phase in a liquid. From the record data, the particle size distribution is derived from the measured temporal change of the particle concentration. A free-fall or Stokes diameter should be determined since the sedimentation process is determined by the free-fall velocity of the particles. There are two methods that one can apply to introduce the particle into the liquid. One is with a two-layer method, a thin layer of particles is introduced at the top of the liquid column. In the other one, the particles are uniformly dispersed in the liquid by shaking the sedimentation column or by ultrasonic agitation before measurement. The

two approaches for sedimentation method that are used to decide the particle size distribution are the incremental method and cumulative method [23].

- Incremental method

In the incremental method, the rate of change of particle density or concentration is measured at a given location in the sedimentation column. As mentioned earlier in this chapter, the incremental method is based on the measurement of the temporal change of the particle concentration. The particles should be uniformly dispersed throughout the column at the beginning of the experiment. In this case, the initial concentration corresponds to the overall particle concentration at any measurement location. Various methods have been used such as light attenuation or X-ray attenuation for the measurement of the density or concentration of particles in the measurement location.

Lambert-Beer law states that the damping of light is proportional to the cross-sectional area of all particles in the light beam. This has been shown by Eq. 5.1.

$$\frac{I}{I_O} = exp(-kc) \tag{5.1}$$

Where, I and I_0 are the intensities of the attenuated and incident X-rays and k is constant of proportionality.

- Cumulative method

The cumulative method that has been applied in this project, i.e. the amount of the particles which accumulate at the bottom of the sedimentation column, is measured. One can determine the cumulative mass fraction by normalizing the measured concentration value by the initial concentration c_0. This relationship is shown by Eq. 5.2.

$$F_t = 1 - \frac{c(t)}{c_0} \tag{5.2}$$

In the cumulative method, it is required to correlate the sedimentation velocity with the particle size, i.e. Stokes diameter. This is necessary in order to determine

the cumulative mass fraction as a function of particle size. In order to find $F_m(D)$, an expression is needed for D_t, i.e. the particles which have just passed the measuring point at the time t. The particles equation of motion in the Stokes drag regime is given by Eq. 5.3. This equation has been obtained by only considering the drag, the buoyancy and gravity forces.

$$\frac{d_v}{d_t} = -\frac{18\mu}{\rho_d D^2} + \left(1 - \frac{\rho_c}{\rho_d}\right) g \tag{5.3}$$

When the particles have reached terminal velocity, they have no acceleration, and solving Eq. 5.3 for D gives the Stokes diameter D_{St}.

$$D_{St} = \sqrt{\frac{18\mu v_t}{(\rho_d - \rho_c)g}} \tag{5.4}$$

Eq. 5.4 has been used to calculate the Stokes diameter (D_t). It is valid for the Stokes regime, i.e. when $Re_p < 1$ which in general is relevant for sedimentation analysis since the particle dimensions are very small. As mentioned earlier, in this method the amount of particles that are settling on the bottom of the sedimentation column is measured. The particles are measured by an instrument which is called a sedimentation balance. The particles that are collected on the balance pan and the weight of accumulated particles are continuously measured.

According to this method as shown in Fig. 5.1, the weight of the particles will increase gradually over time. The weight of the particles increases at a constant rate during the initial time until all the large particles have accumulated on the balance pan. During the next time interval, the rate of accumulation is reduced since all the large particles have already been precipitated. This will continue for the next time intervals, but the rate of weight increase will be reduced since there is only a portion of the smaller particles in suspension [23].

The mass accumulated on the balance pan at a given time t is given by the following equation:

$$m_t = m_0[1 - F_m(D)] + m_0 \int_0^D \frac{h}{H} f_m(\lambda) d\lambda \tag{5.5}$$

Where, D is the diameter of the particles just settled out during time t, m_0 is the total mass of the sample and h is the distance that the particle size λ has precipitated during time t. The first term represents the mass of the particles

with diameter larger than D, and the second one represents the mass accumulated for all the particles with diameters smaller than D. The distance h is connected to the settling (terminal) velocity and it is shown by Eq. 5.6.

$$h = v_t(\lambda)t \tag{5.6}$$

The last equation has been substituted into Eq. 5.5 and dividing by m_0 gives us the following equation.

$$\frac{m}{m_o} = 1 - F_m(D) + \frac{t}{H}\int_0^D v_t(\lambda)f_m(\lambda)d\lambda \tag{5.7}$$

Equation Eq. 5.8 has been derived with respect to the time, and gives the below equation. Fig. 5.1 gives an illustration of the sedimentation model as well as the temporal change of accumulated mass.

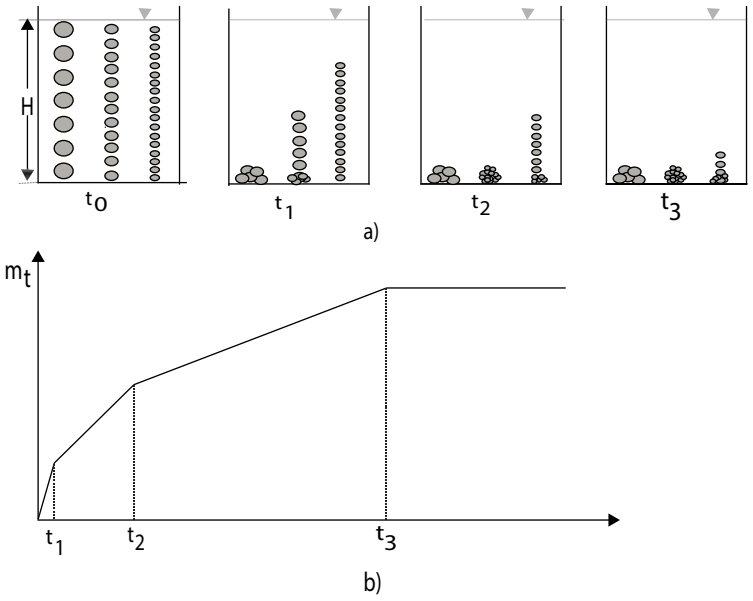

FIGURE 5.1: Sedimentation model to illustrate the incremental model, (a) sedimentation model, (b) temporal change of the accumulated mass. Redrawn from [23].

$$\frac{d}{d_t}(\frac{m}{m_0}) = -\frac{d}{d_t}F_m(D) + \frac{1}{H}\int_0^D v_t(\lambda)f_m(\lambda)d\lambda + \frac{t}{H}v_t(D)f_m(D)\frac{dD}{dt} \tag{5.8}$$

Since at time t, $H = v_t(D)t$, and by definition $F_m(D) = f_m(D)dD$, so the above equation is simplified to Eq. 5.9.

$$\frac{d}{d_t}(\frac{m}{m_0}) = \frac{1}{H}\int_0^D v_t(\lambda) f_m(\lambda) d\lambda \tag{5.9}$$

Equation Eq. 5.10 has been used to relate the integral mass collection and the cumulative mass fraction. We can write the cumulative mass fraction as the following equation, which is called Oden's equation.

$$F_m(D) = t\frac{d}{d_t}(\frac{m}{m_0}) - \frac{m}{m_0} + 1 \tag{5.10}$$

Oden's equation can be used to calculate mass fraction from the slope of the mass accumulation curve as illustrated in Fig. 5.2.

As mentioned, Oden's equation Eq. 5.10 was used to determine the cumulative mass distribution from sedimented mass and the amount of mass change. The Stokes diameter from Eq. 5.4 is used to transform time to particle size. Oden's equation has been used to determine the accumulated mass fraction from the slope of the mass accumulation curve as has been illustrated in Fig. 5.2.

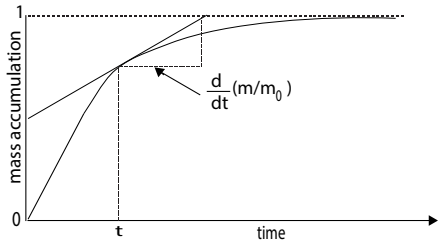

FIGURE 5.2: Graphical determination of mass fraction and slope from data using a sedimentation balance. Redrawn from [23].

An analytical scale from Sartorius with a density determination kit was used for the sedimentation. The equipment was connected to software. Fig. 5.3 shows the set up of instruments which have been used for the sedimentation.

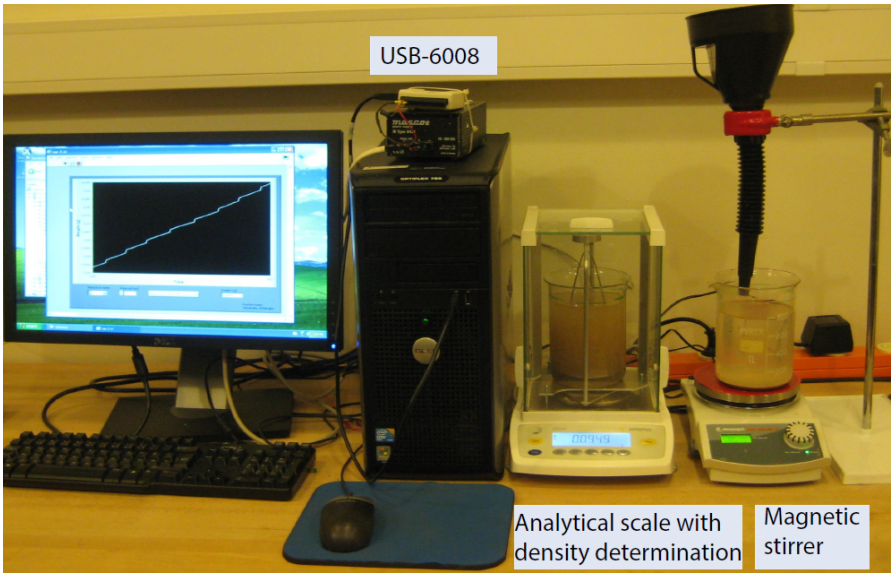

FIGURE 5.3: Photo of magnetic stirrer, analytical scale with density determination which is connected to software.

5.2 Principal component method

One of the most benefits of modelling a data table in form of PCs is to make an easier visualization of the results. By using this method, one can find a pattern in data, and expressing the data to find their similarities and differences. Since the pattern is difficult to obtain when we have a high dimension, then PCA is a good aid for analyzing the data. Depending on examination of variables and objects, the PCs are given as loading and score vectors, as mentioned in section 2.13. Loadings plot and scores plot are used for interpreting relations among variables and objects, respectively. To determine which PCs are more important and relevant, it can be found by measuring variance. Small variance in a PC, i.e. the PC contains little information. In this method, the first component contains the most of the variance, second component contains the second largest amount of variance in the data which is uncorrelated with the first principal component etc. Similarities and differences between objects as well as variables on the PCs can be quantified by two criteria [25]:

• The distances between objects or variables.

• The angle between their object vectors, i.e. the vectors from origin to the objects or variables.

5.3 Viscosity of glycerol-water mixture

The following method was used to calculate the density and viscosity of the glycerol/water mixture to measure the dynamic viscosity of glycerol-water solutions in the temperature of 20°c [35].

The viscosity of the liquid increases when we add glycerol to the volume of the feed tank. We assume that the initial volume fraction glycerol is x_{gl}, and add glycerol to the volume to achieve the new glycerol volume fraction, which is y_{gl}. One can find out the added volume of glycerol if we assume that the initial amounts of fluid are known. The volume of glycerol added to the feed tank is calculated by Eq. 5.13.

$$x_{gl} : \frac{V_{gl,in}}{V_{w,in} + V_{gl,in}} \tag{5.11}$$

$$y_{gl} : \frac{V_{gl,in} + V_{gl,add}}{V_{w,in} + V_{gl,in} + V_{gl,add}} \tag{5.12}$$

$$V_{gl,add} = -\frac{[(V_{w,in} + V_{gl,in})y_{gl}] - V_{gl,in}}{y_{gl} - 1} \tag{5.13}$$

If the rig and tank contain pure water, then the above equation can be simplified to Eq. 5.14 that is used to find out the added glycerol volume.

$$y_{gl} = \frac{V_{gl,add}}{V_{gl,add} + V_{w,in}} \tag{5.14}$$

Where $V_{gl,in}$ and $V_{w,in}$ are the initial volume of glycerol and water, respectively and $V_{gl,add}$ is the volume of glycerol that is added to the feed tank to get a desired liquid viscosity.

5.4 Experimental procedure

In the beginning, several tests were performed to validate the size distributions for the feed and overflow. The tests were based on the particles standard with the same range as the expected size distribution for the experiments. Based on the stabilization of plots for feed and overflow, it was decided to make a suspension by using approximately 38 grams of particles per litre of liquid. The suspension was made by using a bigger glass beaker, and the contents were well stirred by a magnetic stirrer to maintain the suspension before it was transferred to the set-up [23]. The mass of the particles collected on the balance pan of a sedimentation balance was approximately a third of particles' mass beneath the pan, and according to calculations, it should be the opposite. Therefore, a drop of surfactant per four litre liquid was added to the feed tank and additionally the samples were inserted in an ultrasonic bath for 5 minutes to prevent coagulation. Furthermore, in the sedimentation process, a plastic beaker was replaced by a glass beaker to neutralize the charge forces between the liquid, particles and the glass.

The feed tank was filled with measured amounts of water and glycerol. An agitator was used to thoroughly stir the contents of the feed tank and keep its contents uniform throughout. Thus, the exit suspension from the tank's outlet has the same composition as the fluid within the tank. The suspension of particles was made in a bigger glass beaker and then added to the feed tank. Prior to each run, the suspension in the feed tank was mixed manually by using a brush to ensure that a proper suspension was present, then the agitator was started and it ran for 10 minutes before starting the pump. Then, the pump was started for 10 minutes. During that time, the system was set to get a proper total flow rate by checking the Coriolis flow meter, and the volume flow rate of overflow was checked by the Electromagnetic flow meter. The volume flow rates were regulated by three control valves which were connected to the feed piping after the pump and at the end of the hoses.

5.4.1 Measuring process

As mentioned above, the total flow rates were measured directly by the Coriolis flow meter. This device was also used to measure the density, as well as the mass flow rate of liquids. An Electromagnetic flow meter which was connected to software, USB-6008, was utilized to measure the volume flow rate of the overflow

outlet. The underflow outlet flow rates was adjusted to get around 5% of the total flow rate. This was conducted by using two valves which were connected to the ends of the outlets' hosts. As mentioned in section 4.3, the pressures from the inlet and outlets were read from the pressure gauges, and the pressure drop over the hydrocyclone was calculated by subtracting the pressure across the overflow from the total pressure. A pycnometer device was used to find the densities of ρ_f, $\rho_{o,liquid+particle}$ and $\rho_{u,liquid+particle}$. To find each density, three measurements were made and then the average density was calculated as a proper density.

5.4.2 Overall separation efficiency

The total efficiency as mentioned in section 2.8, was calculated by dividing the amounts of particles captured per volume of pycnometer to the total particle mass in the feed ($M_{pyc,u}/M_{pyc,o} + M_{pyc,u}$). Two different methods were used to find the mass of particles in the over and underflow. The one which was using the Eq. 5.15 as is implemented and shown in appendix D, and the second one was conducted by the filtration and drying method. In the second method, the particles were filtrated, heated and then maintained in 70°C. The results from these methods were compared to ensure that a proper separation was present. The results show an extra particle mass around 3% for both the over and underflow by using the filtration and drying method. The computation process for one of the experiments by using the first method is presented in Appendix D, and the total efficiency for the other experiments are calculated in the same way. An overview of the parameters and calculated values for the separation efficiencies are presented in Table 7.2.

$$M_{pyc,liq+p,o} = M_p + M_{liq} = V_p\rho_p + V_{liq}\rho_{liq} \tag{5.15}$$

Chapter 6

Numerical methods and set-up

Computation fluid dynamic is a new approach to examine the problems with fluid dynamics. This method has been used in recent decades, and it has been developed over the years. Nowadays, it is widely used in different industry applications. By CFD, one can easily change different variables, modify the design of the separator and test them efficiently and verify the results. Even if CFD has improved over the last years, it cannot fully replace experiments. The following section gives an introduction to the computation fluid dynamic, which has been used to supplement the experiments and to verify the results.

6.1 Software

In this thesis, the CFD software STAR-CCM+ version 8.06.005 from CD-Adapco was used for the numerical simulations. It is an engineering process which provides models for solving problems related to flow, heat transfer and stress. STAR-CCM+ contains a feature-based parametric, 3D-CAD, that allows geometry to be built from scratch. The program also contains different kinds of meshing abilities to ensure that the calculations that have been made are accurate for different areas in different cases [22].

6.2 Mesh

One can use STAR-CCM+ to generate a quality mesh for different geometries and applications. "The Base Size is a characteristic dimension of the model that you set before using any relative values." [22] By creating the mesh, a base size is specified, and that is the size that the mesh generator works from. How good a result this solution provides, depends on the size of the cells in the mesh. The size of the cells must be fine enough to capture everything that is important, and it has to be coarse enough to make the calculation efficient.

There are two main groups of meshing models in STAR-CCM+, namely the surface meshing and the volume meshing. Both of them have been used to generate the numerical grid for the fluid inside the hydrocyclone [22]. The surface meshing are divided into:

- Surface Wrapper
- Surface Remesher

The surface wrapper can be used when the CAD data is of poor quality. It provides a closed, manifold and non-intersecting surface. The surface remesher is used in the case when the resulting of surface quality from the surface wrapper is not optimal. The volume meshers can obtain a high quality for the starting surface by using the surface remesher. The surface remesher is also used to improve the overall quality of an existing surface and to improve it for the volume mesh models, as well as to re-triangulate the surface.

The surface wrapper is used when imported geometry has:

- Multiple intersecting parts.
- Missing data in the form of holes and gaps.
- Surface mismatches.
- Duplicate and internal surface.
- Overly complex geometry with too much detail.

There are different types of meshing models for STAR-CCM+ that can be used to generate a volume mesh. The different types of meshers get their names from the shape of their cells. The two types of volume meshings are [22]:

- Polyhedral Mesher.
- Prism Layer Mesher.

One obtains a balanced solution for complex mesh generation problems by using polyhedral meshes. The polyhedral meshes are comparatively easy and efficient to make. They contain a fewer number of cells for a given starting surface. This model creates a volume mesh that is composed of cells which are polyhedral shaped. By using the prism layer model one can generate orthogonal prismatic cells next to wall surfaces or boundaries. This layer is important to improve the accuracy of the flow solution. It is defined in terms of its thickness, the number of cell layers that are included, as well as the size distribution of the layers.

6.3 Multiphase flow model

Multiphase flow relates to the flow and interaction of some phases in the same system where there are separate interfaces between the phases. In this thesis, the Eulerian multiphase model has been used to model a multiphase flow. In modeling multiphase flow, it is defined as a quantity of matter within the system which has physical properties, e.g. different density, different size and different shape, to separate it from other phases in the system. Multiphase flows can be divided into two categories:

- Dispersed flows; e.g. droplet, bubbly, and particle flows.
- Stratified flows; e.g. free surface flows or annular film flow in pipes.

There are two options for choosing between flow models for the Eulerian multiphase model in STAR-CCM+. The two options are as following:

- Multiphase Segregated Flow.
- Volume of Fluid (VOF).

The Multiphase Segregated Flow model is generally related to the Eulerian Multiphase Model, but it has a wider importance in STAR-CCM+. The model is used to model Eulerian Multiphase cases. It solves conservation equations for mass, momentum and energy for each phase of the multiphase flow. In this model, the volume fraction is defined as the portion of a volume that a phase has occupied. The pressure is assumed to be equal in all phases, but each phase has its own velocity and physical properties. The amount of volume fraction provides the share of the flow domain that each phase has occupied.

The Volume of Fluid (VOF) is a simple multiphase model which is fitted to simulating flows of some incompatible fluids on numerical grids, which is capable of solving the interface between the phases of the mixture. The physical properties and velocity differ for each phase, but the pressure is assumed to be the same in all of the phases. This model has not been used in this thesis, since the model is suited for simulations of flows where each phase represents a large structure, moreover the method requires a fine mesh. Consequently, the Multiphase Segregated Flow model is used to model the fluid flow inside the hydrocyclone.

6.4 Developed numerical model

Developing the simulation model began by drawing the geometry of the hydrocyclone in the CAD program. The cyclone was drawn in a two dimensional system, and then it was revolved to get in three dimensions. The geometry of the hydrocyclone was completed by extruding and then sketching the inlet, overflow and underflow. The boundary conditions for different boundary phases, namely the walls, inlet and outlets were decided. The velocity and volume fraction for the liquid and particles were specified at the inlet boundary. The wall boundary was selected in no slip and smooth conditions. The particles have the same entrance velocity as the liquid, and it is set to 5 (m/s). The volume fraction of the liquid at the inlet is set to 0.98 and for the particles, is set to 0.02. The outlet boundaries were subjected to the flow-split outlet and the split ratio was selected for physics values. Split ratio is set to 0.95 and 0.05 for overflow and underflow, respectively.

The grid models were selected to build the grid for the simulation. The meshing models that were used to generate the volume mesh are:

- Polyhedral Mesher

- Prism Layer Mesher
- Surface Remesher

A grid dependency test was done to find out the suitable cell size for the grid in the simulation. Different cell sizes were tested, and the cell sizes were varied from 0.5 to 3 millimetres, as they are listed in Table 6.1. Based on the results of the grid dependency test, the base size of the grid is set to 1.5 mm, which also resulted in converting residuals. Fig. 6.1 is an illustration of meshed geometry for a hydrocyclone. Upon choosing the Multiphase Segregated Flow in STAR CCM+, there are two options for time models namely Steady and Implicit Unsteady. The simulations are time-dependent, therefore the Implicit Unsteady model is chosen.

TABLE 6.1: Results from the grid dependency test.The base size of the grid was selected to be 1.5 millimetre.

Test number	Base size[mm]	Cell count
1	0.50	25786236
2	1.00	551214
3	1.50	239191
4	1.75	197379
5	2.00	150333
6	3.00	103389

FIGURE 6.1: Shows an illustration of the grid used for simulation.

The density and the viscosity of the liquid as well as the viscosity of the particles vary due to the fraction of glycerol that was added to the solution, but the particles' density is constant. The Reynolds Stress Model that has been described in section 2.13.2, was used to model the turbulent flow in the hydrocyclone. As mentioned in section 2.13.2, this was used because it is more accurate for the turbulent flow phenomena, and it provides excellent results for swirling flows.

We have to define the physical time-steps and the number of the inner iterations within that instant of time for the solution to be converged. Smaller physical time-steps lead to less solution variation between each time step. On the other hand, a larger physical time provides more inner iterations. Consequently, one should find an optimal balance between the time-steps and the number of inner iterations which are needed for the solution to converge. As mentioned earlier, an implicit unsteady solver with a 2nd-order discretization was utilized to solve the computation domain.

The time-steps and the number of iterations at each time-step for simulations were found to be 0.05 and 5, respectively. The time for each of the simulations differs and it was dependent on the hydrocyclone configuration.

The mass flow rate, velocity, and volume fraction of particles through the inlet and the outlets were calculated by creating a section plane by using the derived parts node. A report was created by selecting the surface average under the reports node for velocity, volume fraction, pressure drop, as well as the mass flow phase for mass flow. Results appear in the outlet window by clicking on the reports node. The volume flow rates of each phase were calculated by multiplying the particle velocity, the volume fraction and the cross section that the particles went through. The pressure drop across the hydrocyclone was calculated by subtracting the pressure loss across the overflow from the pressure drop across the inlet.

Chapter 7

Results and discussion

This chapter starts with some simulations before it moves on to experiments. It ends up with a summary for the results from these two methods by using the principal component analysis (PCA).

The results from this thesis are compiled from both simulations and experiments. In order to get a better understanding of the experimental results, one performs CFD simulations of the hydrocyclone using the same conditions as the experimental part. In the experiments it is easy to make changes in operational parameters and feed compositions. The experimental method can give a better insight into the fluid pattern and one can utilize the results to verify the results from the numerical simulation.

The main objective of this project is to explore potential for using hydrocyclones for the separation of particles from highly viscous liquids. Based on the understanding of development in hydrocyclone performance, one selects a way to modify the hydrocyclone geometry to make it appropriate for highly viscous liquids. The strategy was to increase the viscosity while keeping the flow rate constant. Governing parameters, which are variations in body dimensions, are investigated. These parameters include the overflow diameter and the cone length/cone angle which affect the separation performance as well as the drop in pressure over the cyclone.

A bivariate plot of two variables namely, diameter (D) versus conical part length (CL) has been used to reduce the number of experiments to be performed,

as is shown in Fig.7.1. By taking into account the liquid viscosity, the total number of tests to be performed are seven experiments. Table 7.1 depicts an overview of the experiments that were conducted.

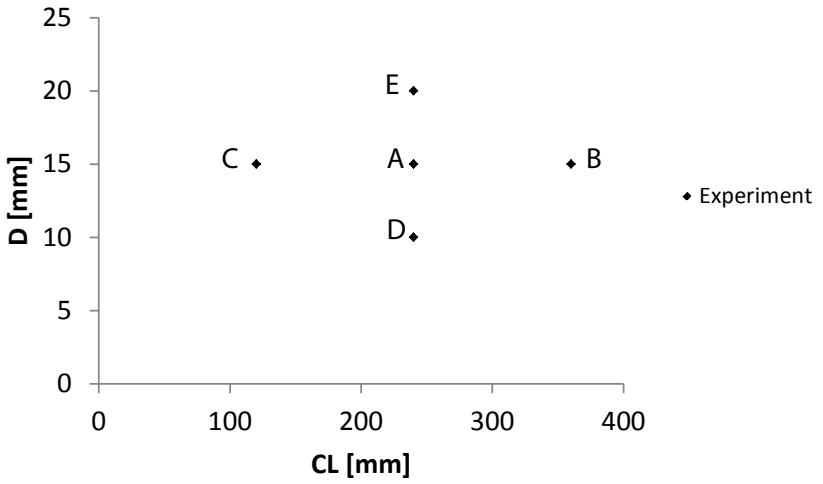

FIGURE 7.1: Bivariate plot of diameter (D) versus conical part length (CL) to determine the number of experiments to be performed.

TABLE 7.1: Overview of the number and grouping of the experiments considering viscosity, conical part length and overflow diameter.

Test No	Hydro-cyclone	μ [cP]	CL [ml]	D [ml]
1	A1	1.0	240	15
2	A2	3.8	240	15
3	A3	15.1	240	15
4	C	3.8	120	15
2	A2	3.8	240	15
5	B	3.8	360	15
6	D	3.8	240	10
2	A2	3.8	240	15
7	E	3.8	240	20

7.1 Numerical results

In this section the numerical simulation of the flow pattern in hydrocyclone with different dimensions is provided. The influence of fluid viscosity as well as the geometrical parameters, namely the overflow diameter and the conical part length on the separation performance and pressure drop have been studied by simulation and through experiments. Different configurations of cyclones are given in section 4.1 and Table 4.1. The numerical raw data obtained for the numerical results are listed in section C and Table C.1 (appendices).

7.1.1 The effect of liquid viscosity on separation efficiency, pressure drop and distributions of particles

The grade-efficiency curves for 1, 3.8 and 15.1 centipoise (cP) viscosity are illustrated in Fig. 7.2. The grade-efficiency curves are based on the particle mass flow, and the underflow rate was found to be 5% of the total volume flow rate. The figure illustrate a comparison of the separation efficiency curves for the viscosities. As can be seen, the sharpness of the curves decreases when we increase the liquid viscosity. Fig. 7.4 shows the distribution of the volume fraction of particles in a hydrocyclone for liquid viscosity from numerical simulations. The figure shows the decrease of the volume fraction of particles in the lower part of the cone section is due to the increase of the liquid viscosity. It can be seen that the higher viscosity has less particle volume fraction at the underflow, which also decreases the grade-efficiency.

As mentioned in section 2.10, the centrifugal force is proportional to the particle mass and then to x^3, while the drag force is proportional to x assuming Stokesian drag. From Eq. 2.15 the drag force being directly acting on particles, is increased with increasing the liquid viscosity proportional to the viscosity. The tangential velocity ($v_{\theta CS}$) reduces when increasing the liquid viscosity and as a consequence, the vortex intensity and the centrifugal force are also affected by the liquid viscosity.

Fig. 7.3 depicts the variations of pressure drop for liquids with different viscosities. It shows that the increase in liquid viscosity leads to a reduction in pressure drop. As mentioned in section 2.6, an increase in viscosity in a hydrocyclone, in contrast to a pipe, leads to a less intensive vortex. As a result, the vortex converts

the static pressure from the outer part to the dynamic pressure in the inner part less efficiently. The dynamic pressure is dissipated in the vortex finder without recover static pressure. So, the pressure drop is larger in a hydrocyclone with a stronger vortex as a result of less liquid viscosity [2].

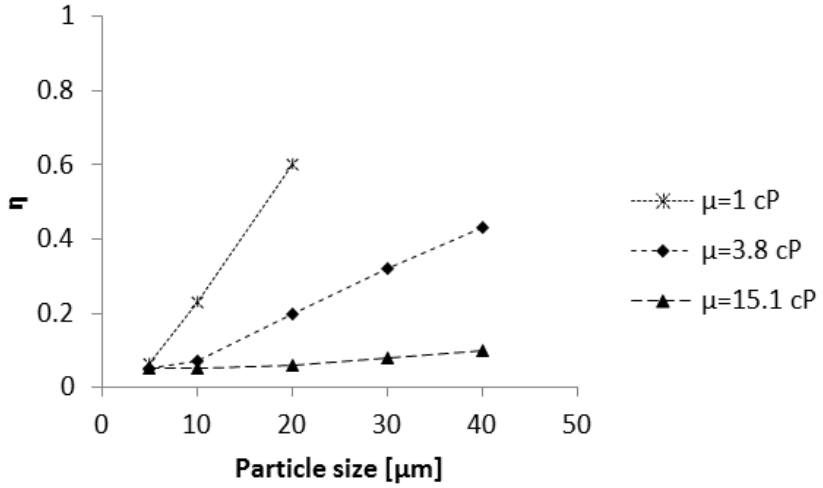

FIGURE 7.2: The effect of viscosity on grade-efficiency.

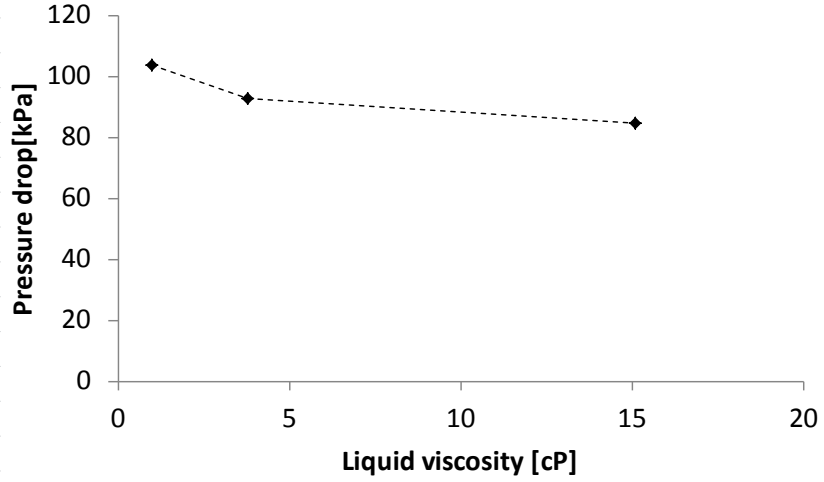

FIGURE 7.3: The effect of viscosity on pressure drop.

Fig. 7.5 shows the influence of the liquid viscosity on the pressure drop for the experiments with different viscosities. From the figure, the pressure loss decreases with the increasing of the viscosity. For the hydrocyclone with the lowest viscosity, a higher intensity of the vortex creates and results in a higher pressure drop in the hydrocyclone. The intense vortex motion in the inner part of the hydrocyclone creates a pressure profile inside of the hydrocyclone with a high static pressure

at the wall and a high dynamic pressure in the inner part of the hydrocyclone. Moreover, the static pressure at the wall reduces from the top to the bottom of the hydrocyclone due to dissipation of static to dynamic pressure as it is shown in Fig. 7.5.

Bradley [7] performed some experiments to investigate the effect of sugar solution on the fluid velocity and the pressure drop. In their work, they found that an increase in liquid viscosity decreases tangential velocity and consequently it will further prevent air core formation. This will further lead to the increase of underflow, i.e. the flow ratio rises by increasing viscosity .

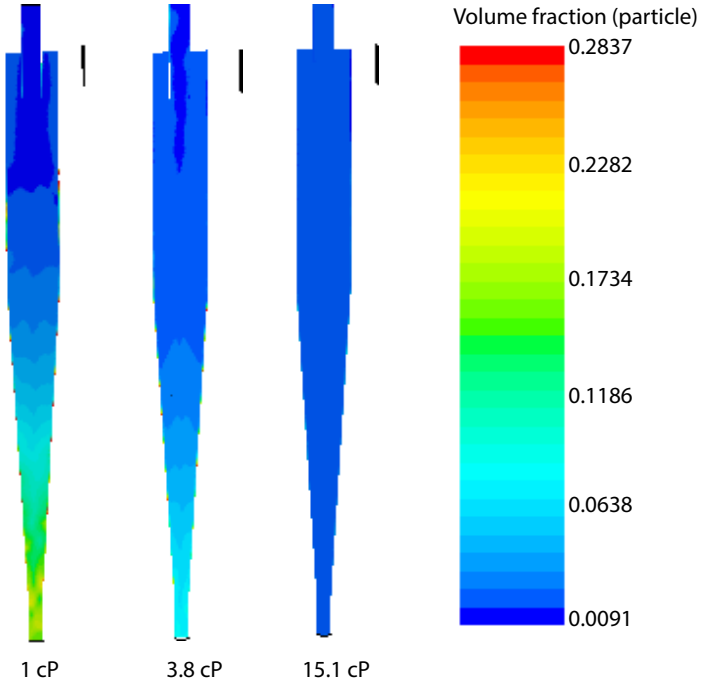

FIGURE 7.4: Distribution of volume faction of particles in the hydrocyclones with different viscosities.

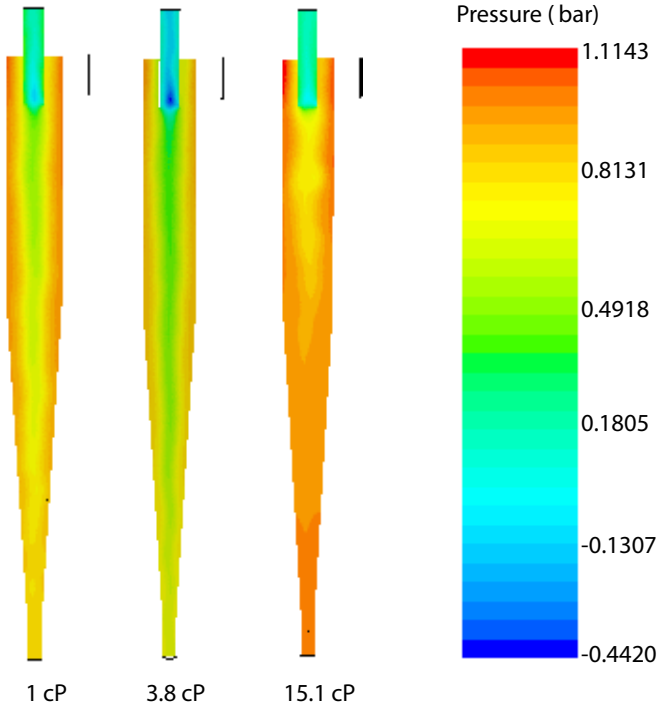

FIGURE 7.5: Distribution of absolute pressure drop in the hydrocyclones with different viscosities.

7.1.2 The effect of different conical part length on separation efficiency and pressure drop

Conical lengths have a significant effect on the hydrocyclone separation efficiency. In this thesis, the effect of three hydrocyclones with different conical part lengths, namely 120, 240 and 360 mm on the hydrocyclone performance and the pressure drop are examined. The grade-efficiency curves are obtained by Eq. 2.8. The grade-efficiency curves for the different conical part length are shown in Fig. 7.6. The figure shows that the hydrocyclone with a 360 mm conical length has a better performance than the other two. The results indicate that a hydrocyclone with a longer conical length has better performance. Furthermore, it shows the grade-efficiency increases for both the fine and the coarse particles when we increase the length of the conical part length.

As can be seen in Fig. 7.8, the volume fraction of particles is the highest for a hydrocyclone with the long cone, namely 360 mm. The volume fraction of the particles is increased for the long cone of 120 to 240 and further to 360 mm. Wang [36] stated that the air core diameter in a hydrocyclone increases by decreasing the cone length. Consequently, this reduces the volume of the underflow.

Mousavian and Najafi [15] investigated four hydrocyclones with different conical angles that range from 15° to 25° and which correspond to a length that varies from 116 to 67 mm. They stated that an increase in the conical leads to a rise in the separation efficiency and a decrease in the pressure drop. For the hydrocyclone with shorter cone, they found that the small particles were aggregated around the air core and there were some large particles in the vortex finder. They concluded that the separation space becomes smaller with a short cone. In the case for cyclone with the short cone length, a much stronger short circuit flow with a higher tangential velocity was created, which resulted in a higher pressure. Furthermore, a decrease in the conical length leads to a decrease the volume of underflow or split ratio and increasing of pressure drop as shown in Fig. 7.7. The figure illustrates that the pressure drop decreases as the conical length is increased.

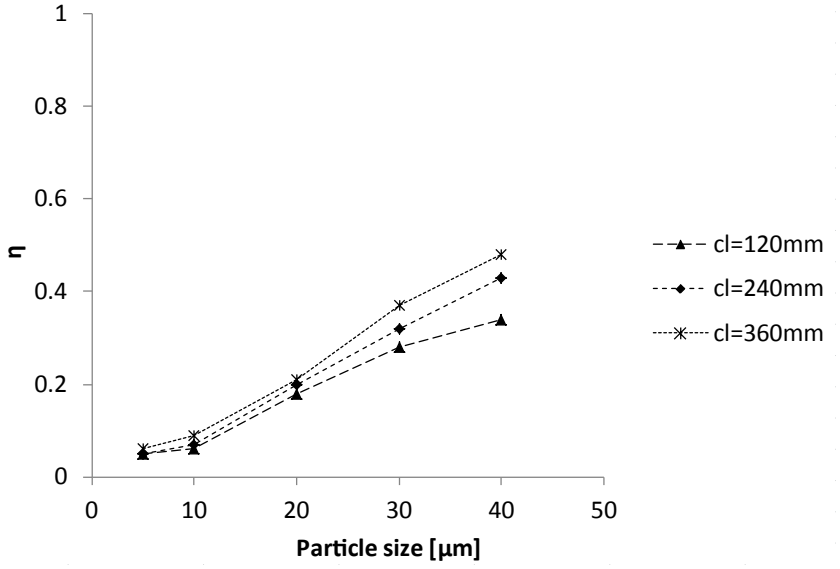

FIGURE 7.6: The effect of conical length on grade-efficiency.

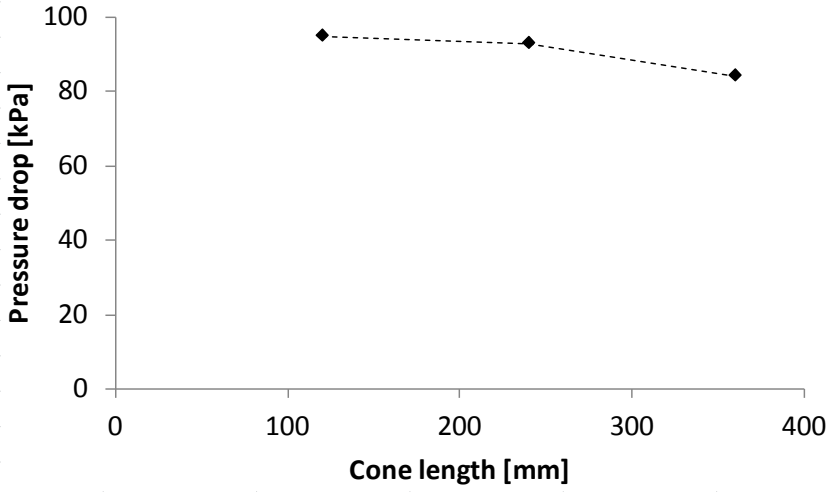

FIGURE 7.7: The effect of conical length on pressure drop.

Yang et al. [5] studied the effect of different cone combinations for solid-liquid on the hydrocyclone performance. In their work, they used Reynolds stress model (RSM) for hydrocyclone simulation, and they operated by using the identical characteristics of feed slurry and operating parameters. They found that the tangential velocity increases with a reduction of radius from wall to axis. The tangential velocity achieves its maximum in the area close to the wall and falls with a reduction of radius until it attains zero on the central axis. Furthermore, they found that the angle change has a significant effect on the value of flow split, separation efficiency, separation sharpness and energy consumption. The grade-efficiency curve became sharper for small angles and this required less energy consumption.

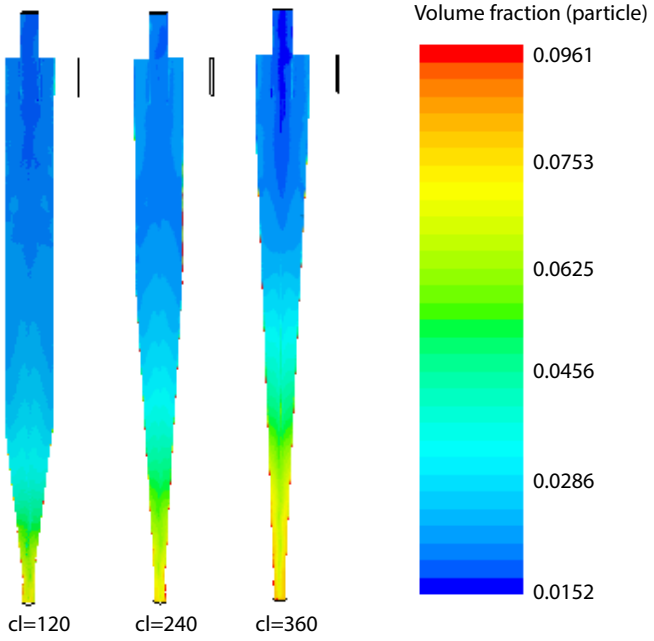

FIGURE 7.8: Distribution of volume fraction in the hydrocyclones with different conical lengths.

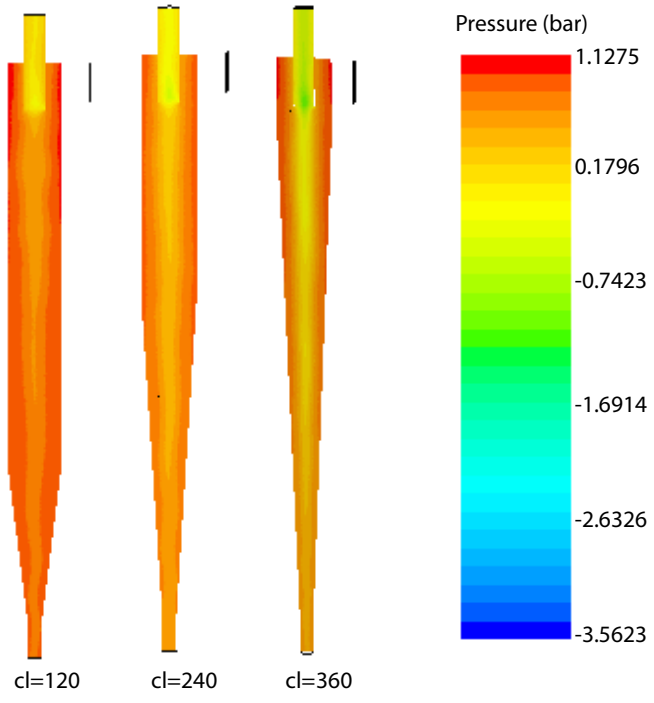

FIGURE 7.9: Distribution of pressure in the hydrocyclones with different conical lengths.

7.1.3 The effect of different overflow diameters on separation efficiency and pressure drop

The grade-efficiency curves for 10, 15 and 20 mm in overflow diameters are shown in Fig. 7.10. From the figure, as we increase the overflow diameter from 10 to 15 diameter, the sharpness of the curve increases which indicates better separation efficiency which was unexpected. Liquid viscosity as previously mentioned, is one of the main factors affecting the hydrocyclone performance. In this thesis, the liquid viscosity was considered to be 3.8 cP, when comparing the effect of a different overflow diameter on the separation efficiency and the pressure drop. As a consequence, the grade-efficiency for 15 mm in the overflow diameter is larger than for 10 mm , as illustrated in Fig. 7.10. The figure illustrates that the increase in the overflow diameter from 10 to 15 mm leads to a rise in the grade-efficiency, but it has an opposite effect when the diameter increases from 10 to 20 mm. This applies particularly for the larger particles, as shown in the figure. The increase of the overflow diameter leads to the increasing of the overflow rate, and this will raise the opportunities of particles to exit into the vortex finder. This will also reduce the centrifugal forces due to the reduction of the underflow vortex. Consequently, the separation efficiency reduces. The influence of the overflow diameter becomes larger as the particle dimensions increases, as shown in Fig. 7.10. In addition, an increase in the overflow diameter leads to more small particles passing through the vortex finder, i.e. the reduction of the flow split ratio in the underflow, which carries less finer particles in the underflow. When the overflow diameter increases, the pressure loss decreases, as illustrated in Fig. 7.11

Fig. 7.12 shows a high volume fraction of the particles in the conical part of the cyclone with D_o=15 mm in comparison with the two others. The difference between the pressure profile which is achieved from simulations of the hydrocyclones with different vortex finder diameters is illustrated in Fig. 7.13. It can be seen in the figure that the pressure drop is the largest in the hydrocyclone with 10 mm in the vortex finder diameter, and the pressure drop decreases by increasing the overflow diameter.

Here, the grade-efficiencies are different in comparison with the results of an investigation which was carried out by Wang and Yu [36]. In their work, they examined a numerical simulation of gas-liquid-solid flow in hydrocyclones with various sizes for the vortex finder. They modelled different components by using the Reynold Stress Model (RSM), and they analysed the flow field, split ratio of

the underflow and the pressure drop. In their study, they worked with the 10, 20, 25 and 50 mm overflow diameters hydrocyclone, and found that the separation efficiency decreases as the overflow diameter increases. As a result, the cyclones with 10 and 50 mm overflow diameter gave the highest and the lowest performance, respectively. The viscosity value which was utilized in their investigation, was unclear. They concluded that the separation efficiency improves by using a hydrocyclone with a narrow vortex finder, and this results in an increase in the pressure drop.

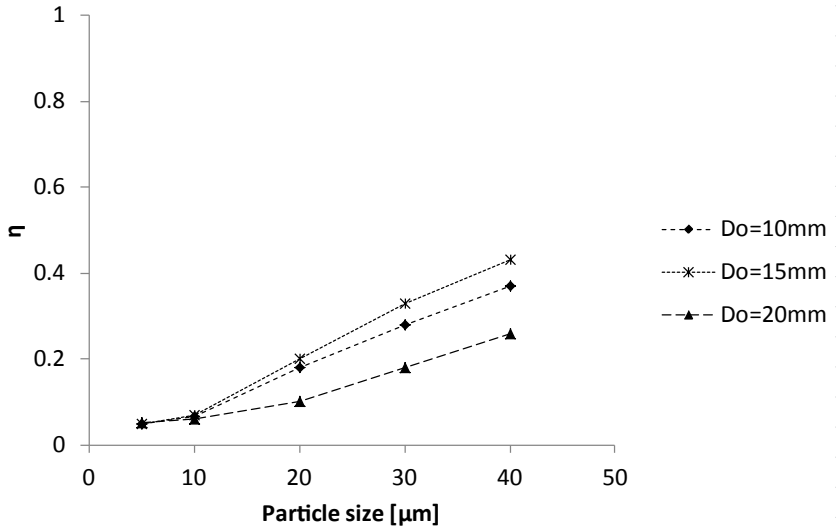

FIGURE 7.10: The effect of overflow diameter on grade-efficiency.

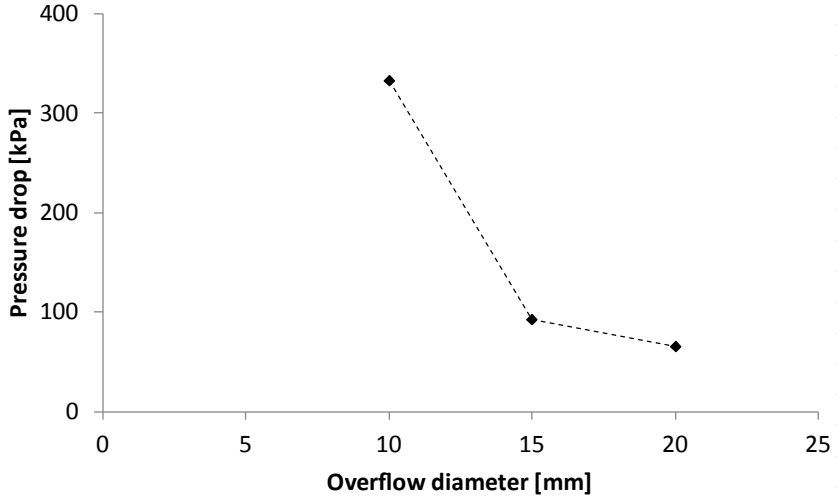

FIGURE 7.11: The effect of overflow diameter on pressure drop.

A study which was performed by Mousavian and Najafi [15] on a hydrocyclone separation efficiency by using 22, 25 and 28 mm in overflow diameters, indicated that the separation efficiency is reduced for both coarse and fine particles with

decreasing the overflow diameter from 25 to 22 mm. The reduction of the overflow diameter leads to transfer of the flow split region to the outlet of coarse particles (spigot). Due to that, the coarse particles gathered close to the conical wall distribute in the spigot region. As a result, the pressure drop increases. Additionally, they found that the increase in the overflow diameter from 25 to 28 mm leads to a decrease in separation efficiency for fine particles. This is due to the reduction of the flow split ratio in the underflow. Consequently, lesser fine particles carries toward underflow outlet.

Hwang et al. [37] modelled and simulated flow pattern and separation effi-

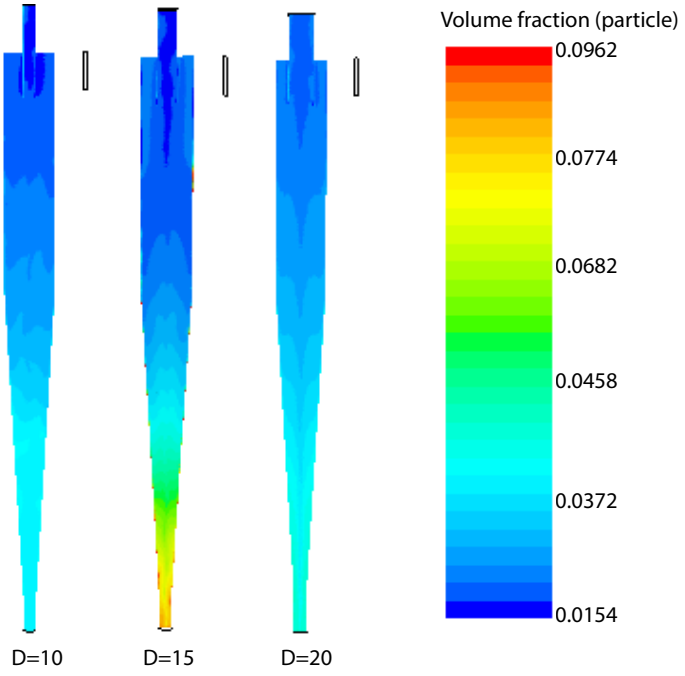

FIGURE 7.12: Distribution of volume fraction of particles with different overflow diameters.

ciency in a 10 mm-diameter hydrocyclone. They studied a particle's separation efficiency by using the computational fluid dynamics (CFD), and the particles' trajectory were simulated by using RFLOW software with a standard $k-\epsilon$ turbulent model. They found that the separation efficiency can be enhanced by reducing the overflow diameter or by enlarging the underflow diameter. They stated that the effect of the underflow diameter is more significant than the overflow diameter. They also found that the separation efficiency decreases for fine particles and increases for the coarse particles by increasing the underflow diameter. This is due to the rise of the water split ratio. Consequently, the most particles of any size are going through the underflow while the underflow diameter is enlarged [15].

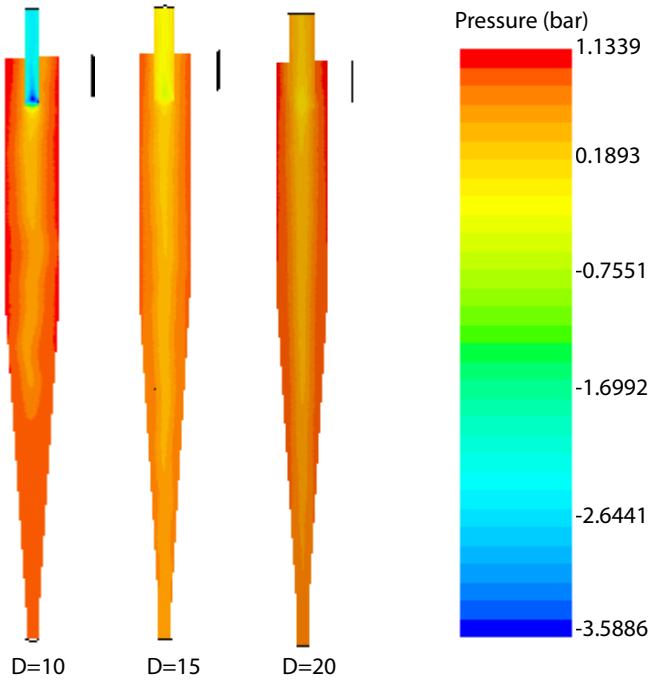

FIGURE 7.13: Distribution of pressure in the hydrocyclones with different overflow diameters.

7.1.4 Distribution of velocities within the hydrocyclone

In this section, the tangential and axial velocity distributions at the axial positions Z=350 and 100 mm of the hydrocyclones are studied. The velocities are measured for the hydrocyclone with a conical length (cl) 240 mm, D_o=15 mm and for the particle dimension of 20 micrometers.

- Tangential velocity

The tangential velocities for the viscosities of 1 cP (centipoise) and 15.1 cP at the position Z=350 mm of the hydrocyclones illustrated in Fig. 7.14. The figure shows the tangential velocity increases with the reduction of the radius from the wall to the centre of the hydrocyclone. It reaches its maximum near the wall of the vortex finder, and then reduces with a reduction of radius until it obtains zero in the centre of the cyclone. Additionally, it depicts that the tangential velocity for 1 cP viscosity is greater than one for 15.1 cP viscosity. As shown in section 2.10, the centrifugal force which is important to the separation in a hydrocyclone, is derived from the tangential velocity. Moreover the tangential velocity is bigger in value than the axial and radial velocities. According to the equilibrium orbit model, Eq. 2.20, the viscosity of liquid impacts the flow pattern inside the hydrocyclone. This

particularly influences the vortex intensity and as a consequence, the tangential velocity reduces. This results in the cut size increasing, according to the equation [2]. From Eq. 2.14, the higher tangential velocity results in greater centrifugal force which leads to a higher separation efficiency. As a result, the grade-efficiency is greater for the tangential velocity with 1 cP in viscosity as is shown in the figure. One can conclude that the liquid viscosity has a big influence on the value of the tangential velocity. The variation of the liquid viscosity influences the tangential velocity such that the tangential velocity decreases with the increasing of viscosity.

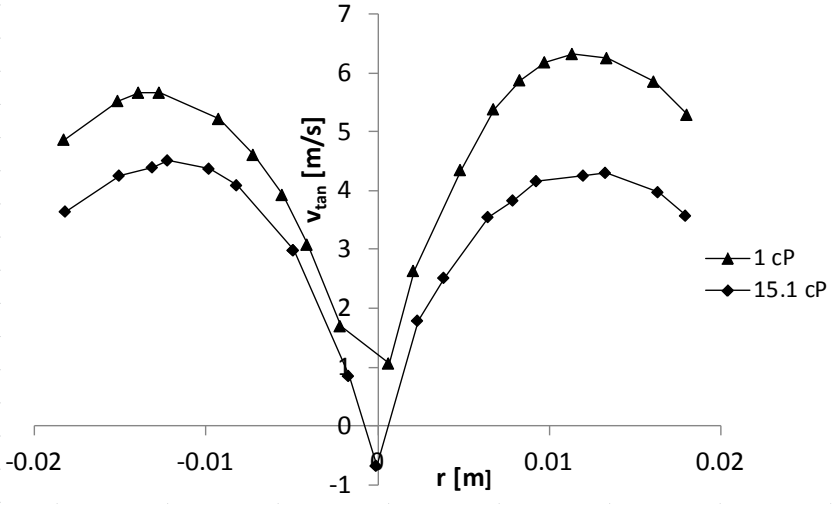

FIGURE 7.14: Tangential velocity profiles for 1 and 15.1 [cP] in viscosity at axial position Z=350 [mm] and the particle dimensions of D_p=20 [μm] within the hydrocyclones.

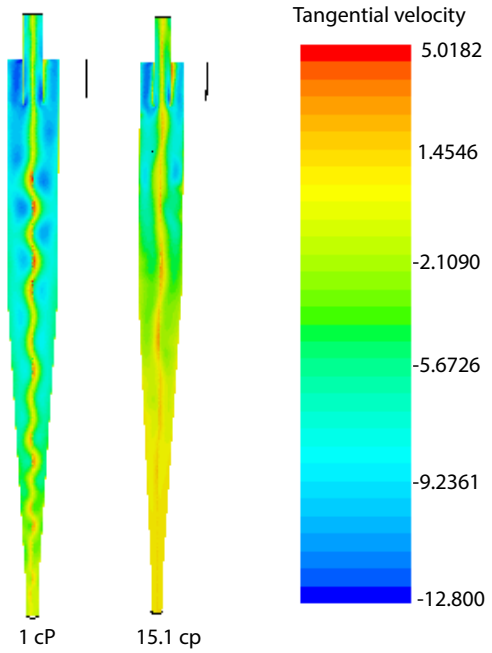

FIGURE 7.15: Tangential velocity distributions of hydrocyclones in the position of Z=350 mm and for particle dimensions of D_p

Fig. 7.16 shows the tangential velocities for the viscosities 1 and 15.1 cP in the position Z=100 mm of the hydrocyclones. Here, the distribution curves are practically identical with the curves in Fig. 7.14, but the distribution of tangential velocities are different in character due to the effect of the feeding. As it can be seen, the maximum value of the tangential velocities at the axial position Z=100 mm is reduced in comparison to the tangential velocities in the position Z=350 mm. This means that the maximum values of the tangential velocities are decreased with decreasing axial distance from the bottom. Additionally, the maximum tangential velocity of the hydrocyclone with 1 cP is significantly higher than that of the hydrocyclone with 15.1 cP.

Nemeth and Verdes [38] studied the distribution of the tangential velocities for pure water and mixture of water and glycerine. The results from their work indicated that an increase in viscosity had no influence onto the tangential velocities, and the distribution curves were practically identical.

As it can be seen from the figure, the minimum tangential velocity for water is reduced to -2 (m/s). This is due to the vortex centre precessing around the centre of the cyclone (and therefore the coordinate system used for the velocities), which leads the tangential velocity to go in the opposite direction in comparison with the previous situation, as is shown in Fig. 7.17. The maximum and minimum tangential velocities are depending on the cross sectional position, the shape of

the tangential velocity as well as the position of tangential velocity through the cyclone.

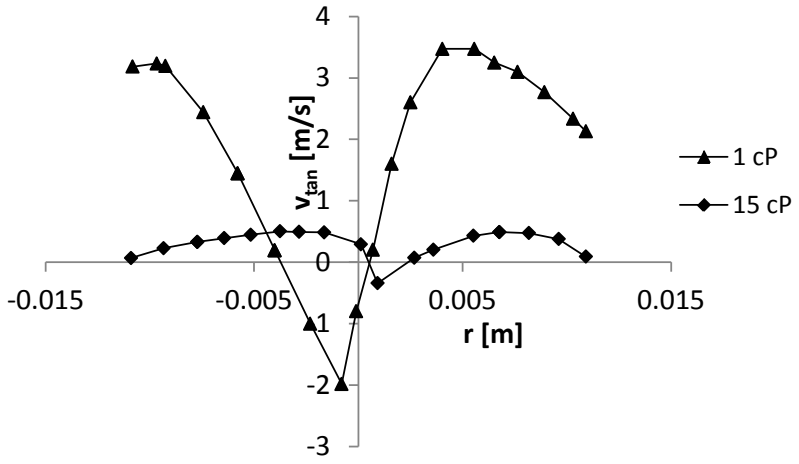

FIGURE 7.16: Tangential liquid velocity profiles for 1 and 15.1 [cP] in viscosity along radius position at Z=100 [mm] and the particle dimensions of D_p=20 [μm] within the hydrocyclones.

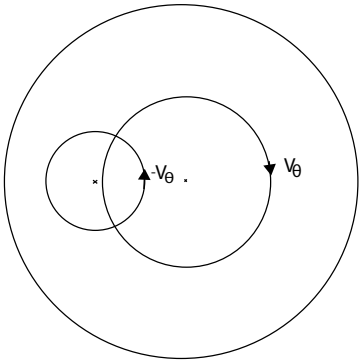

FIGURE 7.17: The circulation tangential velocity on horizontal cross section in the position Z=100 [mm] of the cone part of the hydrocyclone.

• Axial velocity

The axial velocities for the liquid viscosities of 1 cP and 15.1 cP in the position of Z=350 and 100 mm of the hydrocyclone are investigated. Fig. 7.18 shows the axial velocity for the liquid viscosities 1 and 15.1 cP in the position Z=350 mm of the hydrocyclone. The figure illustrates a symmetric distribution that is changing from negative to positive in the direction along the wall of the hydrocyclone towards the centre. It also indicates that the liquid along the wall goes to the underflow outlet, and the liquid around the centre moves to the overflow outlet. The downward velocity increases with the increasing of the radius distance from the centre of the hydrocyclone, and the upward velocity rises with the radial distance form the wall.

For the hydrocyclone with 1 cP viscosity, both the downward and the upward axial velocity is higher than for the one with 15.1 cP viscosity, as shown in Fig. 7.18 and Fig. 7.19. This means that the liquid viscosity has a certain impact on the axial velocity.

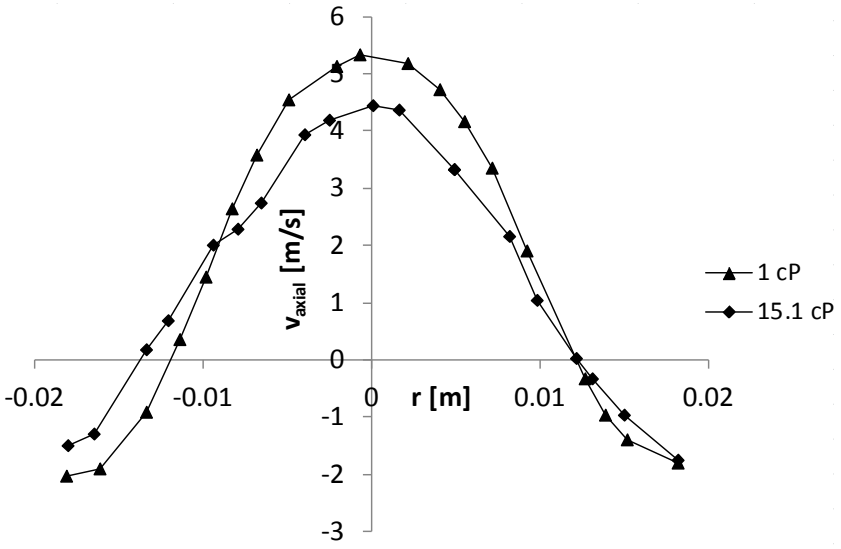

FIGURE 7.18: Axial velocity profiles for 1 and 15.1 [cP] in viscosity at axial position Z=350 [mm] and the particle dimensions of D_p=20 [μm] within the hydrocyclones.

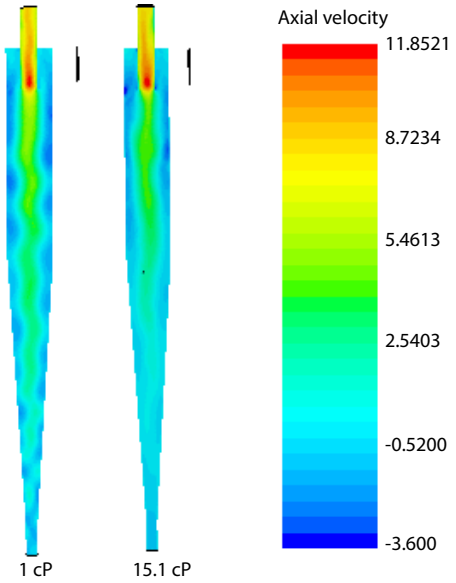

FIGURE 7.19: Axial velocity distributions for 1 and 15.1 [cP] in viscosity at axial position Z=350 [mm] and the particle dimensions of D_p=20 [μm]within the hydrocyclones.

The axial velocity profiles for 1 and 15.1 cP at axial position Z=100 mm are presented by Fig. 7.20. As it can be observed, the maximum axial velocities are reduced and the shape of curves are changed in comparison to the axial velocity profiles in the position Z=350 mm. This is due to the effect of feeding and the position of axial velocity within the hydrocyclone. As can be seen, the values of the maximum axial velocities are decreased with distance from the bottom, i.e. the maximum axial velocity is higher at the axial position Z=350 mm than for Z=100 mm.

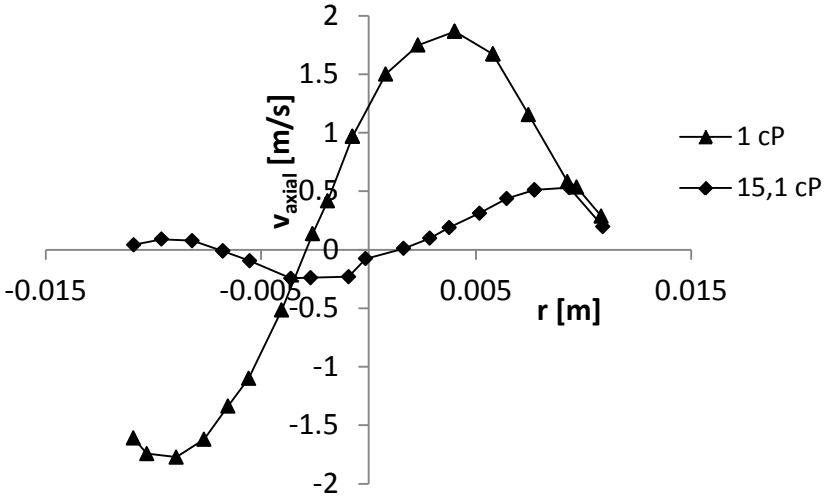

FIGURE 7.20: Axial velocity profiles for 1 and 15.1 [cP] in viscosity at axial position Z=100 [mm] and the particle dimensions of D_p=20 [μm] within the hydrocyclones.

7.2 Experimental results

As previously mentioned, seven experiments were implemented varying the configuration of the hydrocyclone and modifying the liquid viscosity as listed in Table 7.1. The objective of these experiments is studying the grade-efficiency and reduced grade-efficiency curves and the pressure drop of the experiments. The strategy was to keep the flow rate constant, increase the viscosity and modify the configuration of hydrocyclones. The experiments were conducted at 4.6 (m^3/h), which is corresponding to 5 (m/s) inlet liquid viscosity. To increase the viscosity of liquid, the amount of glycerol, which was calculated by using Eq. 5.13, was added to the feed tank.

Table 7.2 presents the parameters which were used for the different experiments. As can be seen, test 6 differs from the others due to the lower inlet velocity. This is because of small diameter of the overflow which leads to a lower inlet liquid velocity. This results in a higher pressure drop across the hydrocyclone.

TABLE 7.2: The measured values of parameters which were used for different experiments. Where subscripts f, o and u denotes the feed, over and underflow fraction, respectively.

Test No	Hydro.	μ [cP]	ρ_f [kg/m^3]	Q_f [m^3/h]	M_f [kg/h]	Q_o [m^3/h]	Q_u [m^3/h]	P_f [bar]	P_o [bar]	P_u [bar]
1	A1	1.0	1011	4.70	4883	4.47	0.23	1.5	0.01	0.18
2	A2	3.8	1120	4.70	5164	4.46	0.24	1.35	0.15	0.38
3	A3	15.1	1165	4.70	5440	4.46	0.24	1.20	0.25	0.60
4	B	3.8	1110	4.70	5152	4.48	0.22	1.33	0.24	0.48
5	C	3.8	1110	4.70	5184	4.46	0.24	1.28	0.02	0.40
6	D	3.8	1110	4.17	4592	3.95	0.22	2.70	0.02	2.00
7	E	3.8	1110	4.70	5173	4.46	0.24	0.97	0.01	0.02

Table 7.3 presents the values of cut size and pressure drop over hydrocyclone for experiments. The cut size determined from analysis of efficiencies from Barth fit, i.e. from Eq. 2.21. In the equation, $\eta = 1/(1 + (x_{50}/x)^n)$, x_{50} is the particle's cut size and n is the slope of the grade-efficiency curves. The values for cumulative cut size, calculated by using the cumulative size distribution of the feed and the overall efficiency.

TABLE 7.3: Overview of efficiencies, cut size and pressure drop across hydrocyclone for the experiments.

Test No	Hydro-cyclone	ΔP [bar]	$x_{50,Barth}$ [μm]	$x_{50,cumulative}$ [μm]	η -	η' -
1	A1	1.49	12.758	25.1	0.353	0.319
2	A2	1.20	20.880	32.2	0.217	0.176
3	A3	0.95	17.647	35.1	0.177	0.135
4	B	1.09	22.622	29.0	0.273	0.238
5	C	1.26	26.791	31.8	0.207	0.164
6	D	2.68	21.094	32.7	0.202	0.163
7	E	0.96	25.816	32.9	0.215	0.172

As previously mentioned in section 5.4, the values of particle mass in the overflow and overflow streams for each experiment were obtained by using Eq. 5.15. Then, the entire and reduced grade-efficiency for different experiments were obtained by using Eq. 2.8 and Eq. 2.9, respectively. Tables 7.4 and 7.5 represent the calculated data for the under and overflow which was used to calculate the total and reduced grade-efficiency of the experiments.

TABLE 7.4: The calculated data for underflow which was used to calculate the overall and reduced grade-efficiency.

Test No	Hydro. cyclone	$M_{pyc,liq+p}$ [g]	$\rho_{liq,f}$ [kg/m^3]	$V_{pyc,liq}$ [ml]	$V_{pyc,p}$ [ml]	$M_{pyc.p}$ [g]	$\dot{M}_{p,u}$ [kg/s]	ρ_u [kg/m^3]
1	A1	51.859	1000.000	47.492	1.671	4.429	0.006	1054.834
2	A2	56.184	1084.889	47.344	1.819	4.821	0.007	1142.805
3	A3	57.977	1152.744	48.292	0.871	2.309	0.003	1179.280
4	B	57.233	1084.889	46.673	2.490	6.598	0.008	1164.157
5	C	56.466	1084.889	47.163	1.999	5.299	0.007	1148.551
6	D	55.957	1084.889	47.488	1.675	4.438	0.006	1138.204
7	E	56.564	1084.889	47.100	2.063	5.466	0.007	1150.553

TABLE 7.5: The calculated data for overflow which was used to calculate the overall and reduced grade-efficiency.

Test No	Hydro.	$M_{pyc,liq+p}$ [g]	$V_{pyc,liq}$ [ml]	$V_{pyc,p}$ [ml]	$M_{pyc.p}$ [g]	$\dot{M}_{p,o}$ [kg/s]	ρ_o [kg/m^3]
1	A1	49.359	49.005	0.158	0.418	0.011	1003.989
2	A2	53.885	48,812	0.351	0.930	0.023	1096.058
3	A3	56.994	48.948	0.215	0.570	0.014	1159.293
4	B	53.845	48.838	0.325	0.861	0.022	1095.229
5	C	53.983	48.750	0.413	1.095	0.028	1098.046
6	D	53.883	48.814	0.350	0.925	0.022	1096.004
7	E	53.885	48.812	0.351	0.930	0.025	1096.058

In order to find the influence of liquid viscosity on the separation efficiency, the effect of three different liquid viscosities on the particle separation in the same hydrocyclone as listed in Table 7.1 are studied. Because it was difficult to draw curves of the best fit to represent the separation efficiency due to the scatter in the data points, therefore we have chosen scatter plots of points to represent the grade-efficiency plots. Furthermore, the separation curves would start from a value of 0 by using these data, which are undesirable. As shown in Fig. 7.21, the separation efficiency percent are plotted against the particle diameters by using scatter plots of the data points to present the separation efficiency.

Fig. 7.22 depicts the reduced grade-efficiency curves for experiments A1, A2 and A3. The curves are starting from the value of 0, as expected. From the figure, it can be seen that the experiment with the highest viscosity (15.1 cP) gave a smaller reduced cut size, i.e. the sharpness of curves increases with increasing of liquid viscosity, which indicate just the opposite of our expectation. However, the values for cut size increase with increasing the viscosity by using the cumulative size distribution, as listed in Table 7.3, i.e. the efficiencies increase with the decreasing the viscosity. As pointed out earlier for the Barth fit, this is because the curves are based on the data points which are scattered in a large variable space. The curves are made by using Barth fit, i.e. using Eq. 2.21 and using the equation for reduced grade-efficiency (Eq. 2.9). The pressure drop across the hydrocyclone decreases with increasing of the fluid viscosity as tabulated in Table

7.2.

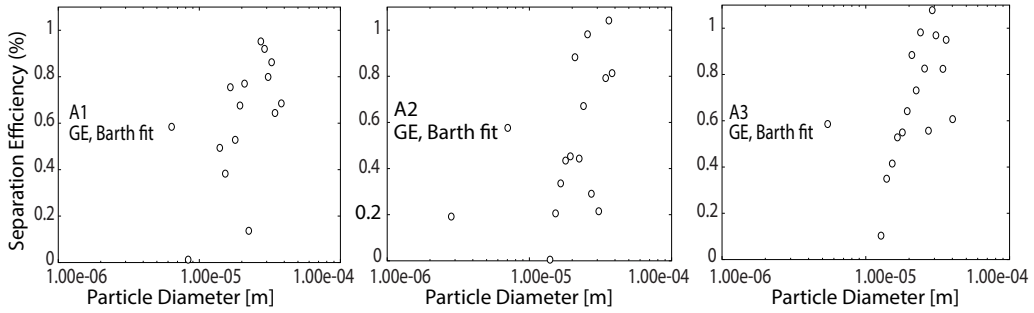

FIGURE 7.21: The effect of viscosity on the separation efficiency for experiments A1, A2 and A3, which are listed in Table 7.2.

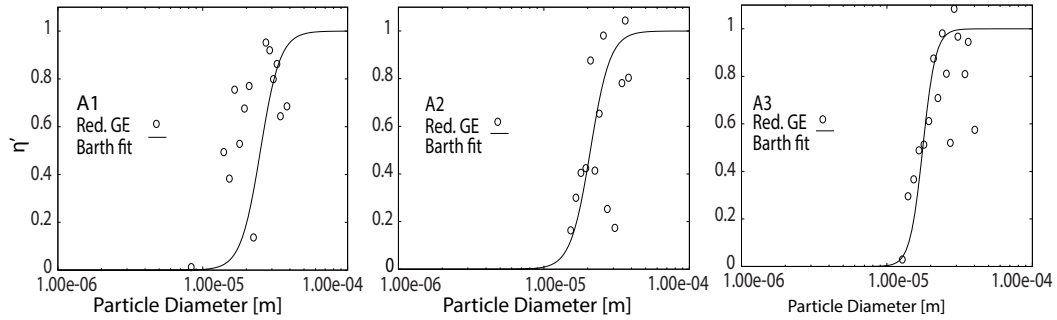

FIGURE 7.22: The reduced grade-efficiency curves for experiments A1, A2 and A3, which are listed in Table 7.2. The curves are drawn by using Barth fit, Eq. 2.21.

In this work, three hydrocyclones with different lengths of the cone part as listed in Table 7.1 are studied. Since there was difficulty with making curves of best fit to represent the separation efficiency, hence scatter plots of points are selected to depict the grade-efficiency plots. The grade-efficiency plots for experiments A2, B and C are presented by Fig. 7.23.

As it can be seen from the figure, the data points scattered in a large variable space, then it will be difficult to make curves to represent the grade-efficiency by using Barth fit.

Fig. 7.24 depicts the comparison of the reduced grade-efficiency for experiments C, A2 and B. The sharpness of cut is slightly increased from experiment C to A2 and further to B. This means that the cut size decreases with the extension of conical part length of a hydrocyclone. From Table 7.2, we can see that the hydrocyclone pressure drop is decreased with increasing the conical part length.

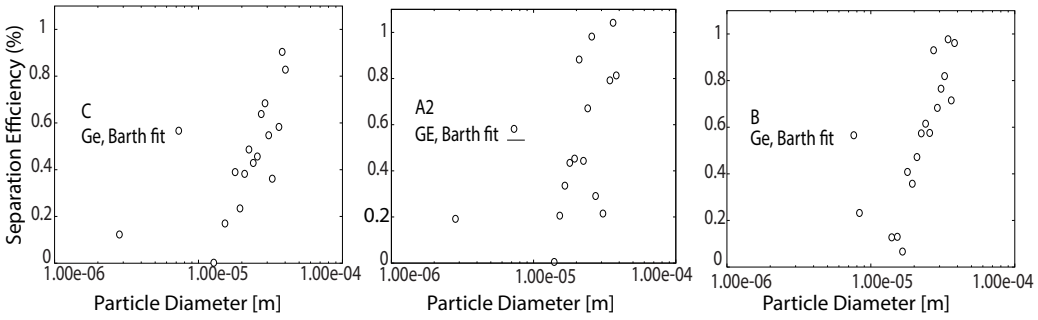

FIGURE 7.23: The effect of conical par length on the separation efficiency for experiments C, A2, and B, which are listed in Table 7.2.

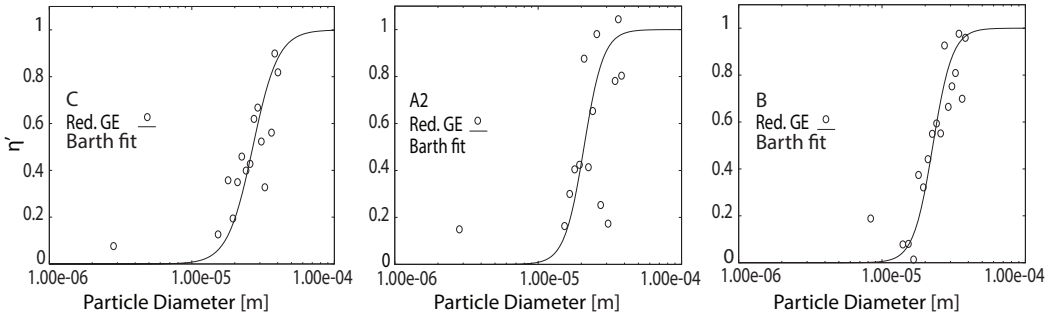

FIGURE 7.24: The reduced grade-efficiency curves for experiments C, A2, and B, which are listed in Table 7.2. The curves are drawn by using Barth fit, Eq. 2.21.

Fig. 7.25 illustrates the scatter plots for experiments D, A2 and E, i.e. for vortex finder diameter as listed in Table 7.1. There are scatter plots of data points of curves used to represent the grade-efficiency plots, due to the reasons mentioned

above.

Fig. 7.26 presents the reduced grade-efficiency curves for experiments A2, D and E. From the figure, the sharpness of the curves is slightly decreased with increasing of the overflow diameter from experiment D to A2 and further to E. As mentioned earlier in this section, experiment D with 10 mm in overflow diameter had a lower inlet flow rate which leads to poor reduced grade-efficiency. The flow rate as well as the efficiency can be increased by using a more powerful pump, as mentioned earlier. Horsley [39] performed some experiments to investigate the effect of rheology on the performance of hydrocyclones. He carried out the experimental work on a range of spigot diameters. The results from his work indicate that the reduced cut size decreases as the spigot diameter increases. This means that the separation efficiency improves with the enlarging of D_u, and this slightly increased the sharpness of the cut.

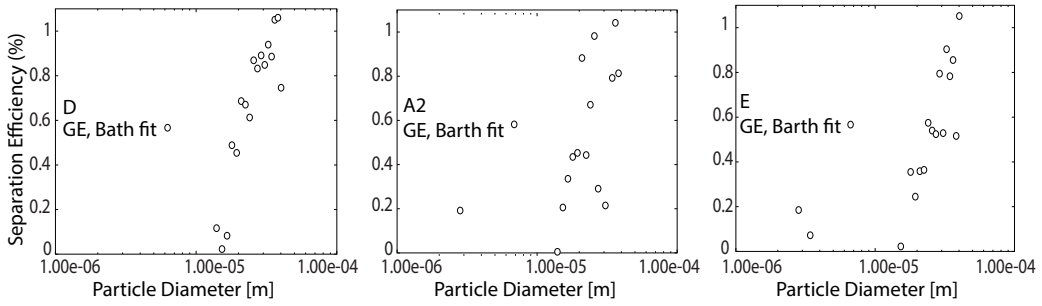

FIGURE 7.25: The effect of vortex finder diameter on the separation efficiency for experiments D, A2, and E, which are listed in Table 7.2.

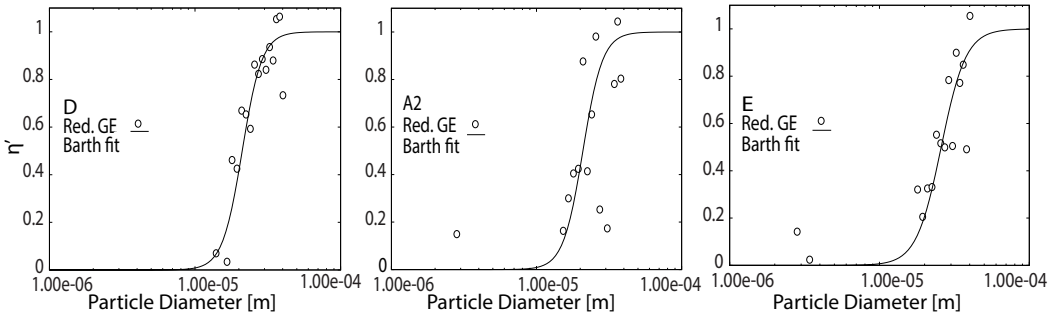

FIGURE 7.26: The reduced grade-efficiency curves for experiments D, A2, and E, which are listed in Table 7.2. The curves are drawn by using Barth fit, Eq. 2.21.

The reduced grade-efficiency curves for the experiments are achieved by using Eq. 2.9. The reduced grade-efficiency can be obtained from the overflow and feed size distribution by using Eq. 2.11 and substituting η with η' in this equation

Marthinussen et al. [6]. Fig. 7.22 illustrates the reduced grade-efficiency for test A1, A2 and A3.

7.3 Further discussion

7.3.1 Principal components analysis (PCA)

In this section, principal component analysis (PCA) has been used to interpret the data. The PCs are used to study variables and experiments in a dataset. Hence, the PCs are provided as loadings and scores plot for interpreting the relations among variables and experiments, respectively [40]. From the dataset, one has taken two PCs to analyse and interpret the data. One used correlations between the principal components (PCs) to interpret the variables and experiments.

As can be seen from Fig. 7.27, PC1 and PC2 contain 48.2% and 29.1% in variance, respectively. This means that the PC1 carries more information of the dataset in comparison with the PC2 and therefore it is more important.

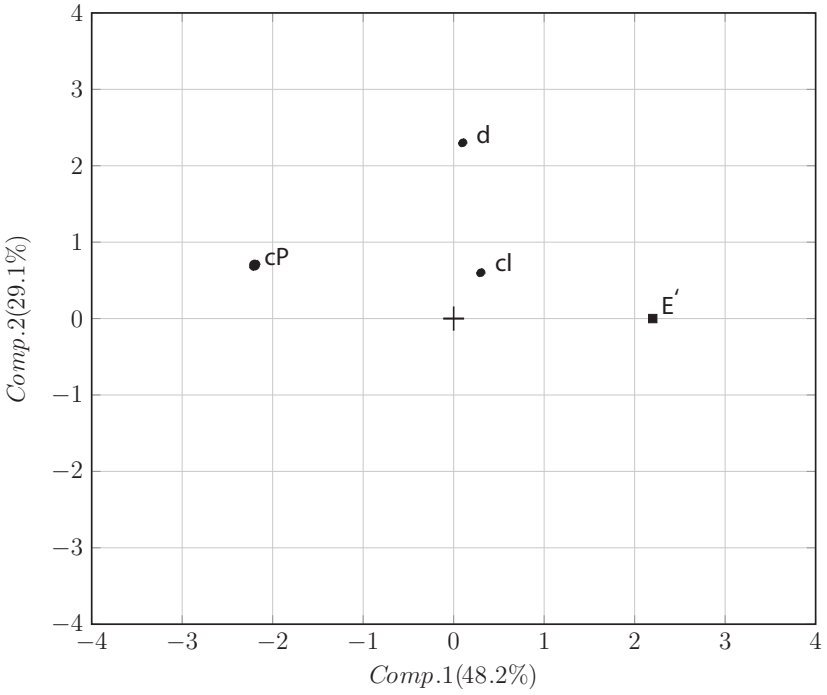

FIGURE 7.27: Loadings plot of PC2 versus PC1, which illustrates the location of the variables and efficiency as well as the relationship between the variables and efficiency.

In the scatter plot of the loadings plot Fig. 7.28, the efficiency is located somewhere which has a very high value for the PC1, and the viscosity (cP) is important to the

PC1. Since the cone length (cl) is located closer to the spectrum, therefore it has smaller influence on the PC1 and PC2. The efficiency (E') is located at the right side of the origin, while the viscosity is located at the left of the origin. An increase in efficiency will increase the value of PC1, while an increase in viscosity will reduce the value of PC1. This means that the first component is more correlated with the efficiency and negatively correlated with the viscosity.

The second principal component (PC2) is mostly influenced by the overflow diameter (d), since the cone length (cl) is located closer to the origin. This means that the PC2 increases with the increasing of the diameter.

From Fig. 7.28, experiments A1 and A3 are important to the PC1, while experiments E and D are valuable to the PC2. Therefore PC1 is correlated with experiments A1 and A3 and PC2 is correlated with E and D. Experiments C, B and particularly A2 are localized closer to the spectrum, therefore they have small impacts in both PC1 and PC2.

7.3.2 Interpreting the principal component model

The viscosity has the longest distance and the largest angle with the efficiency, i.e. the efficiency and the viscosity localized in the opposite direction with opposite signs. Consequently, an increase in the viscosity will lead to a strong decrease in efficiency. As a result, the efficiency has a strong, negative correlation among the variables with the viscosity.

The overflow diameter is forming approximately a 90% angle with the efficiency, therefore it has a small influence on efficiency. The cone length (cl) has small distance, moreover it has formed a smaller angle with the efficiency. Therefore, cl is the second variable which has the most impact on the efficiency.

As can be seen from Fig. 7.28, A1 positively and A3 negatively correlated with the principal component 1. Furthermore, A1 has smaller distance and angle with the efficiency, therefore it has the highest efficiency of all of the experiments. A1 with the lowest viscosity and cP have opposite signs, and they are negatively correlated. A3 and viscosity (cP) are localized in the same direction with negative signs. This means an increase in viscosity will result in a rise in viscosity for object A3, and this leads to a further reduction in efficiency for this experiment. Since the experiments E and D have formed a 90% angle with the efficiency, they have small influence on the efficiency. It can be concluded that a change in the diameter of the overflow has little impact on the efficiency in comparison with

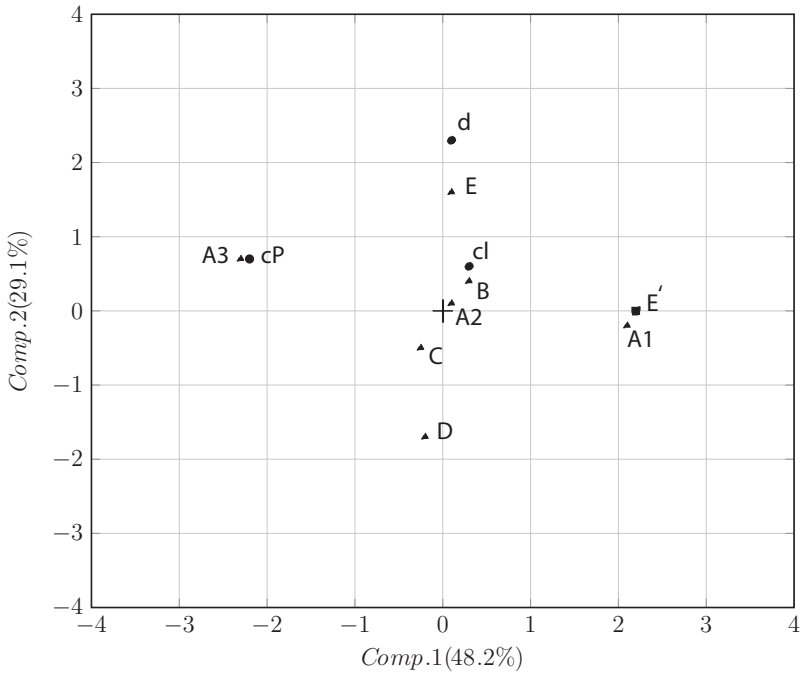

FIGURE 7.28: Biplot, represents the location and relationship between the variables and objects (experiments) as well as the efficiency.

other variables e.g. the *cP* and *cl*. Experiment B which has the longest cone length, is positively correlated with the *cl*. B located in 180% with C, then they are negative correlated. As it can be seen from the biplot, experiments A2 and B are localized in the same direction as variable cl, i.e. they are positively correlated. An increase in the cone length to some extent, led to an increase in efficiency for these experiments. As mentioned earlier, *cl* has formed a little angle and has a shorter distance with the efficiency, hence it is positively correlated with efficiency. Experiment C is negatively correlated with the efficiency, and an increase in *cl* will increase the efficiency of C since C and *cl* are negatively correlated.

Chapter 8

Conclusions

In this work, separation efficiency and pressure drop across hydrocyclones with different dimensions of body construction, which include the vortex finder diameter and conical part length for the separation of particles from highly viscous liquids are investigated. The influence of the liquid viscosity and variations in body dimensions are examined by using Computational Fluid Dynamics (CFD) and through experiments.

To investigate the new geometry of the suggested solid-liquid hydrocyclone, an experimental design which took into account three different dimensions of vortex finders and also conical part lengths, listed in Table 4.1 was conducted. The experimental rig was designed with some modifications during assembly, which made it suitable for solid-liquid separation of viscous liquids as well as measuring the pressure drop over the cyclone (see Fig. 4.3). Additionally, an experimental setup for particle size distribution was implemented by using a cumulative method. An experimental procedure combined with this method was utilized to obtain the volume flow rate, the pressure drop across the hydrocyclones and reduced grade-efficiency curves for different experiments.

In order to understand the effect of the governing parameters on the hydrocyclone performance and pressure drop, CFD simulations utilizing the Reynolds Stress Model (RSM) was used to study the influences. The results from the simulations indicate that an increase in the liquid viscosity increases the value for the cut size x_{50}, while the hydrocyclone efficiency and pressure drop are decreased. The hydrocyclone separation efficiency increases with increasing the length of the conical part, whereas the pressure drop across the cyclone decreases. Moreover,

the results show that the separation efficiency increases when the vortex finder diameter increased from 10 to 15 mm, while the increase in overflow diameter from 15 to 20 mm leads to a reduction in the separation efficiency (see Fig. 7.2). The pressure loss increases with a drop in the overflow diameter.

The tangential and axial velocity profiles for the viscosity of 1 and 15.1 cP at axial position Z= 350 and Z= 100 mm are obtained, this indicates that both the tangential and axial velocities for the liquid viscosity 1 cP are greater than they are for 15.1 cP. The results obviously illustrate that the maximum of the tangential and axial velocities decreases with decreasing axial position over the bottom. These velocity profiles provide valuable information about the influence of fluid viscosity on liquid velocity, as well as the stream of fluid inside of the hydrocyclones.

The separation efficiency of the experimental tests are presented as scatter plots of data points, while the reduced grade-efficiency curves are a functional form due to using Barth. The grade-efficiency and pressure drop across the hydrocyclone were influenced by the governing parameters studied, which are the overflow diameter, conical part length/cone angle, and the liquid viscosity. The results from the reduced grade-efficiency curves (see Fig. 7.24 and Fig. 7.26) show that the sharpness of the curves slightly increases with increasing the conical part length and decreasing overflow diameter. It emerges from the reduced grade-efficiency curves for the liquid viscosity (see Fig. 7.22) that an increase of the liquid viscosity led to a slightly increased sharpness of the curves.

Chapter 9

Suggestions for further work

9.1 Simulations

As previous mentioned, in this thesis the influence of liquid viscosity as well as the geometry of a hydrocyclone on separation efficiency is studied. The results from this work, have given significant information regarding the effect of liquid viscosity and alternate geometries design of hydrocyclones on the hydrocyclone separation efficiency.

The simulation was carried out by using the Eulerian-Eulerian method and Reynolds Stress Model (RSM) as a model. The results show that this is a good model for studying liquid viscosity and the variation of geometry of hydrocyclone on separation efficiency. But the results from the simulations are different from the experimental results, i.e. the sharpness of the grade-efficiency curves for the experimental method were increased which led to better separation efficiency for this method. A Large Eddy Simulation model (LES) is closer in predicting the experimental results, so the Reynolds Stress Model (RSM) which is used in this thesis could be replaced by a Large Eddy Simulation to increase the values.

9.2 Improving the experimental set-up

During the execution of the experiments and sampling, the Electromagnetic magnetic flow meter which was connected to the overflow, showed a lower value for

volume flow rate for overflow. This is due to small air bubbles being formed in the feed tank during the sampling the over and underflow. Further tuning of experimental set-up can improve the results. The two ball valves which are connected to the end of the over and underflow hoses, should be replaced by three-way valves so that the flow can be rerouted during the sampling. The air bubbles will be removed by using this technique.

As mentioned in section 7.2, test 6 (hydrocyclone:D) is different from the other tests. This is due to the lower dimension of the vortex finder which results in the lower inlet liquid velocity. A further investigation should look at the execution of experiments over a range of 12 to 20 mm of vortex finder, or by using a more powerful pump than a Centrifugal pump (Q_{max}= 6.8 m^3/h), in order to improve the results for this test.

9.3 Analyzing the new geometry of hydrocyclone

In this work, viscosity is one of the important variables, and we want to have high viscosity so that in reality is used. Therefore, we have to find an optimal method to make the cyclone suitable for highly viscous liquids. Consequently, a further investigation should look at experimental design of hydrocyclone by using factorial design as a method. To study the design of hydrocyclone, the geometry of cyclone is considered by taking into account the vortex finder diameters ($X1$), length of the conical parts ($X2$) and the different viscosities of liquid ($X3$). Table 9.1 gives an overview of experiments, and coding of data is shown by Table 9.2.

TABLE 9.1: Experimental design at two levels with three variables.

Experiment	$X1$	$X2$	$X3$
1	-1	-1	-1
2	1	-1	-1
3	- 1	1	-1
4	1	1	-1
5	0	0	0
6	-1	1	0
7	0	1	1
8	-1	0	1
9	-1	-1	1
10	1	-1	1
11	-1	1	1
12	1	1	1

TABLE 9.2: Coding of data.

Experiment	-1	0	+1
$X1$	10	15	20
$X2$	120	240	360
$X3$	3.8	17	30.2

Appendix A

An estimate of errors

Experimental results always contains some kinds of error since there is not a complete measurement of the physical measurement. Therefore, the measured value will likely deviate from the correct value of the quantity. The sum of these deviations is called error analysis.

There are several methods one can use to estimate the error in a particular measurement. One of the best ways one can use to estimate the error is to make a series of measurements and calculate the mean value and standard deviation from these measurements. The mean, i.e. which measures the central value, and the standard deviation, i.e give a description of the spread of the measured values about the mean.

The mean value of N measurements is defined by Eq.

$$\bar{y} = \frac{1}{N}\sum_{i=1}^{N} y_i \tag{A.1}$$

Where y_i is the value of experiments number i-th of the measurement.

The variance is given by the following equation:

$$s^2 = \frac{1}{N-1}\sum_{i=1}^{N}(y_i - \bar{y})^2 \tag{A.2}$$

The standard deviation (s) equals the square root of the variance, and it is given by formula:

$$s = \left[\frac{1}{N-1} \sum_{i=1}^{N} (y_i - \bar{y})^2 \right]^{\frac{1}{2}} \tag{A.3}$$

Where the quantity (n-1) is called degrees of freedom which is related to the sample standard deviation.

For experimental measurements, we are more interested in calculating the mean value of a series of measurements than in the individual observations. Then, we should find the standard deviation for each of the average values. The value of standard deviation of individual results will be larger than the standard deviation of the average values. The standard deviation is then expressed by the following equation:

$$s_{mean} = \frac{s}{\sqrt{N}} \tag{A.4}$$

Appendix B

Calculation of flow meters

B.1 The Coriolis flow meter

The Coriolis flow meter was calibrated manually by measuring the flow rate from the outlets. The calibration was performed by using water as a fluid. The pump had a constant speed during calibration and it corresponded to a volume flow rate which was 5,0241 m^3/h. The calibration was carried out by measuring the time required to fill a bucket with water discharging from the outlets, weighing it, and compared with the one from the Coriolis flow meter. Table B.1 gives the results from calibration. The standard deviation from the manually measured mass flow has been calculated, and the percent difference between $Q_{Coriolis}$ and Q_{calib} is calculated by:

$$\% \text{ difference} = \frac{Q_{Coriolis} - Q_{calib}}{0.5(Q_{Coriolis} + Q_{calib})} 100 \tag{B.1}$$

TABLE B.1: Calibration of the Coriolis flow meter versus manual measured outlet flow.

Test NO	t s	m_{fluid} [kg]	$\dot{M}_{calib}$ [kg/h]
1	6.8	9.605	5085.000
2	6.9	9.94	5186.087
3	7.2	9.892	4946.000
4	7.7	10.372	4849.247
5	7.4	10.278	5000.108
6	7.2	10.026	5013.000
7	6.9	10.14	5290.435
8	7.5	10.145	4869.600
9	7.1	10.051	5096.282
10	7.6	10.577	5010.158

Where t is the time required to fill up the bucket, m_{fluid} is the manually measured mass for each test and $\dot{M}_{calib}$ is the manually measured mass flow of water. The mean manually measured mass flow($\bar{\dot{M}}_{calib}$) is 5034 kg/h, the calculated standard deviation (s) is 136 kg/h. The measured ($\dot{Q}_{calib}$) and Coriolis ($Q_{coriolis}$) volume flow rate are 5.044 and 4.019 m^3/h, respectively. The percentage difference is calculated by the percent difference between $\dot{Q}_{Coriolis}$ and $\dot{Q}_{calib}$, is -22.6.

B.2 The electromagnetic flow meter

As mentioned in section 4, the electromagnetic flow meter was installed at the overflow to measure the volumetric flow rate. The flow meter was programmed, and connected to software before it could be used. Since the flow meter had a minimum flow rate of 0.4 (m^3/h), it was decided to connect it to overflow. The flow meter was calibrated solely by running water through the pipes. Table B.2 gives the results from the calibration.

TABLE B.2: Calibration of the Electromagnetic flow meter versus manual measured outlet flow.

Test NO	t [s]	m_{fluid} [kg]	$\dot{M}_{calib}$ [kg/h]
1	5.6	6.956	4471.714
2	6.9	8.948	4668.522
3	6.5	8.371	4636.246
4	7.2	9.13	4565.000
5	6.9	8.91	4648.696
6	7.1	9.08	4603.944
7	6.7	8.715	4682.687
8	6.8	8.823	4671.000

Here, the mean manually measured mass flow ($\bar{\dot{M}}_{calib}$) is 4618 kg/h, the calculated standard deviation (s) is 71 kg/h. The measured ($\dot{Q}_{calib}$) and Coriolis ($Q_{coriolis}$) volume flow rate are 4.7 and 5 m^3/h, respectively. The percentage difference is calculated by the percent difference between $\dot{Q}_{Coriolis}$ and $\dot{Q}_{calib}$, is 7.64.

Appendix C

Processing of simulation raw data

The raw data obtained under each simulation are processed and given in Table C.1. Parameters which are used during of simulations and experiments are given in Table 7.2.

TABLE C.1: Raw and processed data for different geometric structures of five experiments; A1, A2, A3, B, C, D and E with different viscosity; 1, 3.8 and 15.1 cP used in simulations. x is different particle dimensions in Ax. The pressure loss across the hydrocyclone is calculated by subtracting the pressure of overflow from the pressure across the inlet, and the efficiency is the ratio of the particle mass flow in the underflow to the particle mass flow in the feed.

Hydrocyc.	μ [cP]	M_f [kg/s]	M_u [kg/s]	P_f [kPa]	P_o [kPa]	ΔP [kPa]	$\Delta\ \bar{P}$ [kPa]	η -
A1,5	1	0.07	0.005	17.929	-95.179	113.108		0.065
A1,10	1	0.07	0.016	14.375	-92.103	106.478	103.447	0.232
A1,20	1	0.07	0.042	13.692	-77.064	90.755		0.599
A2,5	3.8	0.07	0.004	13.297	-96.340	109.637		0.05
A2,10	3.8	0.07	0.005	10.078	-91.038	101.116		0.065
A2,20	3.8	0.07	0.014	7.200	-86.965	94.165	92.994	0.205
A2,30	3.8	0.07	0.019	5.052	-78.060	83.112		0.271
A2,40	3.8	0.07	0.032	7.011	-73.929	80.940		0.466

Hydrocyc.	μ [cP]	M_f [kg/s]	M_u [kg/s]	P_f [kPa]	P_o [kPa]	ΔP [kPa]	$\Delta\ \bar{P}$ [kPa]	η -
A3,5	15.1	0.07	0.004	12.297	-110.350	122.647		0.050
A3,10	15.1	0.07	0.004	20.042	-89.470	110.512		0.051
A3,20	15.1	0.07	0.004	19.077	-77.013	96.090	85.343	0.058
A3,30	15.1	0.07	0.005	15.714	-75.866	91.580		0.077
A3,40	15.1	0.07	0.006	15.921	-74.015	89.936		0.093
B5	3.8	0.07	0.004	105.930	55.524	50.406		0.052
B10	3.8	0.07	0.006	107.080	20.551	86.529		0.087
B20	3.8	0.07	0.014	106.970	18.417	88.553	83.982	0.194
B30	3.8	0.07	0.025	103.180	13.242	89.938		0.355
B40	3.8	0.07	0.034	106.190	1.704	104.486		0.485
C5	3.8	0.07	0.005	128.080	15.220	112.86		0.072
C10	3.8	0.07	0.005	113.240	20.951	92.289		0.067
C20	3.8	0.07	0.013	112.130	18.933	93.197	95.200	0.187
C30	3.8	0.07	0.018	112.700	21.204	91.496		0.254
C40	3.8	0.07	0.024	110.410	24.248	86.162		0.340
D5	3.8	0.07	0.004	99.428	-267.60	367.028		0.052
D10	3.8	0.07	0.004	97.914	-231.880	329.794		0.063
D20	3.8	0.07	0.013	98.657	-233.200	331.857	333.157	0.180
D30	3.8	0.07	0.018	97.689	-219.330	317.019		0.261
D40	3.8	0.07	0.025	97.756	-222.330	320.086		0.372
E5	3.8	0.07	0.004	126.490	50.399	76.091		0.051
E10	3.8	0.07	0.004	115.990	41.869	74.121		0.06
E20	3.8	0.07	0.006	116.190	53.607	62.583	66.050	0.091
E30	3.8	0.07	0.010	115.340	58.610	56.73		0.144
E40	3.8	0.07	0.018	115.760	55.058	60.702		0.259

Appendix D

Efficiency calculations from experiments

In this section, the mass flow as well as the efficiency of hydrocyclone B is calculated. The efficiency for the other hydrocyclones is calculated in the same way.

TABLE D.1: Raw and processed data from experiment for experiment B. The mass ,$\bar{M}_{pyc+liq}$, is the calculated average mass for the overflow and underflow and the liquid density is the calculated average density for overflow and underflow by using pycnometer as measuring device.

	$\bar{M}_{pyc+liq}$ [g]	M_{pyc} [g]	$\bar{M}_{pyc,liq+p}$ [g]	$\bar{M}_{liq,feed}$ [g]	V_{pyc} [ml]	ρ_{liq} $[\frac{kg}{m^3}]$
Overflow	82.616	28.772	53.845	53.336	49.163	1084.889
Underflow	86.005	28.772	57.233	53.336	49.163	1084.890

• Calculation of the mass flow of particles in overflow for hydrocyclone B.

$M_{pyc,liq+p,o}$= M_p+M_{liq}= V_p ρ_p+ V_{liq} ρ_{liq}

53.8445×10^{-3}(kg) = $[(49.1628\times10^{-6})-V_{liq,o}](m^3)\times2650(\frac{kg}{m^3})+[V_{liq,o}\times1084.8894(\frac{kg}{m^3})]$

53.8445×10^{-3}(kg)= 0.1303 (kg) - 1565.1106(kg)$\times$ $V_{liq,o}$

$V_{liq,o}$ = 48.8380(ml)

$V_{p,o}$ = $V_{liq+p,o}$ - $V_{liq,o}$

$V_{p,o}$ = (49.1628- 48.8499)(ml)

$V_{p,o}$ = 0.3248 (ml)

$M_{p,o}$= ρ_p $V_{p,o}$

$M_{p,o}$ = 2650×10^{-3} ($\frac{g}{ml}$) × 0.3248 (ml)

$M_{p,o}$ = 0.8610 (g)

$\dot{M}_{p,o}$ = $\frac{M_{pyc,p,o}}{V_{pyc}}$ × $\dot{Q}$

$\dot{M}_{p,o}$ = $\frac{0.861\times10^{-3}(kg)}{49.1628\times10^{-6}(m^3)}$ × $\frac{4.48}{3600}$ ($\frac{m^3}{s}$)

$\dot{M}_{p,o}$ = 0.0218 ($\frac{kg}{s}$)

• Calculation of the mass flow of particles in underflow for hydrocyclone B.

The mass flow of particles in the underflow is calculated as the same way as for mass flow in overflow.

$M_{pyc,liq+p,u}$= M_p+M_{liq}= V_p ρ_p+ V_{liq} ρ_{liq}

57.2332×10^{-3}(kg) = [(49.1628×10^{-6})−$V_{liq,u}$](m^3)×2650($\frac{kg}{m^3}$)+[$V_{liq,u}$×1084.8894($\frac{kg}{m^3}$)]

57.2332 × 10^{-3}(kg)= 0.1303 (kg) - 1565.1106(kg)× $V_{liq,u}$

$V_{liq,u}$ = 46.6729(ml)

$V_{p,u}$ = $V_{liq+p,u}$ - $V_{liq,u}$

$V_{p,u}$ = (49.1628- 46.6729)(ml)

$V_{p,u}$ = 2.4899 (ml)

$M_{p,u}$= ρ_p $V_{p,u}$

$M_{p,u}$ = 2650×10^{-3} ($\frac{g}{ml}$) × 2.4899 (ml)

$M_{p,u}$ = 6.5982 (g)

$\dot{M}_{p,u}$ = $\frac{M_{pyc,p,u}}{V_{pyc}}$ × $\dot{Q}$

$\dot{M}_{p,u}$ = $\frac{2.4899\times10^{-3}(kg)}{49.1628\times10^{-6}(m^3)}$ × $\frac{o.22}{3600}$ ($\frac{m^3}{s}$)

$\dot{M}_{p,u}$ = 0.0082 ($\frac{kg}{s}$)

• Calculation of the grade-efficiency.

$\eta = \frac{\dot{M}_{p,u}}{\dot{M}_{p,o}+\dot{M}_{p,u}}$

$\eta = \frac{0.0082(\frac{kg}{s})}{0.0218+0.0082(\frac{kg}{s})}$

$\eta = 0.2733$

Bibliography

[1] M. B. Ray, P. E. Luning, A. C. Hoffmann, A. Plomp, and M. I. Beumer. Improving the removal efficiency of industrial-scale cyclones for particles smaller than five micrometre. *International journal of mineral processing*, 53(1):39–47, 1998.

[2] A. C. Hoffmann and L. E. Stein. *Gas Cyclones and Swirl Tubes: Principles, Design, and Operation*. Springer, 2007. ISBN 354074696X.

[3] L. Svarovsky. *Solid-liquid separation*. Butterworth-heinemann, 2000.

[4] E. Bretney. Water purifier, May 26 1891. URL `https://www.google.com/patents/US453105`. US Patent 453,105.

[5] Q. Yang, H. L. Wang, Y. Liu, and Z. M. Li. Solid/liquid separation performance of hydrocyclones with different cone combinations. *Separation and purification Technology*, 74(3):271–279, 2010.

[6] S. A. Marthinussen, Y. F. Chang, B. Balakin, and A. C. Hoffmann. Removal of particles from highly viscous liquids with hydrocyclones. *Chemical Engineering Science*, 2011.

[7] D. Bradley. *The hydrocyclone*, volume 64. Pergamon Press London, 1965.

[8] Y. F. Chang, G. I. Pisarev, A. C. Hoffmann, T. E. Simos, G. Psihoyios, C. Tsitouras, and Z. Anastassi. Numerical study of the "end of the vortex" phenomenon in a hydrocyclone separator.

[9] R. B. Bird, W. E. Stewart, and E. N. Lightfoot. *Transport phenomena*. John Wiley & Sons, 2007.

[10] K. Rietema and C. G. Verver. *Cyclones in industry*. Elsevier, 1961.

[11] R. M. Alexander. Fundamentals of cyclone design and operation. In *Proc. Aust. Inst. Min. Met*, volume 152, page 202, 1949.

[12] L. Svarovsky and M. T. Thew. *Hydrocyclones: analysis and applications*, volume 12. Springer, 1992.

[13] A. J. Hoekstra, J. J. Derksen, and H. E. A. Van Den Akker. An experimental and numerical study of turbulent swirling flow in gas cyclones. *Chemical Engineering Science*, 54(13):2055–2065, 1999.

[14] A. L. Mular, D. N. Halbe, and D. J. Barratt. *Mineral processing plant design, practice, and control proceedings*, volume 1. SME, 2002.

[15] S. M. Mousavian A. F. and Najafi. Influence of geometry on separation efficiency in a hydrocyclone. *Archive of applied mechanics*, 79(11):1033–1050, 2009.

[16] A. C. Hoffmann, R. De Jonge, H. Arends, and C. Hanrats. Evidence of the natural vortex lengthand its effect on the separation efficiency of gas cyclones. *Filtration & Separation*, 32(8):799–804, 1995.

[17] S. Obermair, J. Woisetschläger, and G. Staudinger. Investigation of the flow pattern in different dust outlet geometries of a gas cyclone by laser doppler anemometry. *Powder Technology*, 138(2):239–251, 2003.

[18] R. Chang. *General chemistry: the essential concepts*. Mc Graw Hill, 2000.

[19] W. L. McCabe, J. C. Smith, and P. Harriott. *Unit operations of chemical engineering*, volume 5. McGraw-Hill New York, 1993.

[20] J. H. Ferziger and M. Perić. *Computational methods for fluid dynamics*, volume 3. Springer Berlin, 1996.

[21] M. Breuer. Large eddy simulation of the subcritical flow past a circular cylinder: numerical and modeling aspects. *International Journal for Numerical Methods in Fluids*, 28(9):1281–1302, 1998.

[22] CD-adapco. User guide star-ccm+ versjon 8.06.007, 2014.

[23] C. T. Crowe, J. D. Schwarzkopf, M. Sommerfeld, and Y. Tsuji. *Multiphase flows with droplets and particles*. CRC press, 2011.

[24] C. Huang, J. A. McDonald, and W. Stuetzle. Variable resolution bivariate plots. *Journal of Computational and Graphical Statistics*, 6(4):383–396, 1997.

[25] R. G. Brereton. *Chemometrics: data analysis for the laboratory and chemical plant*. John Wiley & Sons, 2003.

[26] J. J. Van Rossum. Separation of emulsions in a cyclone. *Rietema, K., Verver, CG Elsevier, Amsterdam*, page 110, 1961.

[27] J. Guo, D. T. Gong, J. Zhang, L. Y. Wang, Z. C. Zheng, and K. M. Li. Studies on mechanism of sand removal from crude oil. *Journal of Hydrodynamics, Ser. B*, 18(3):394–399, 2006.

[28] S. K. Kawatra, A. K. Bakshi, and M. T. Rusesky. Effect of viscosity on the cut (d¡ sub¿ 50¡/sub¿) size of hydrocyclone classifiers. *Minerals Engineering*, 9(8):881–891, 1996.

[29] G. E. Agar and J. A. Herbst. The effect of fluid viscosity on cyclone classification. *Trans. AIME*, 235:145–149, 1966.

[30] M. Jiang, L. X. Zhao, and Z. C. Wang. Effects of geometric and operating parameters on pressure drop and oil-water separation performance for hydrocyclones. In *Proceeding of The Twelfth International Offshore and Polar Engineering Conference, Kitakyushu, Japan, May*, pages 26–31, 2002.

[31] S. Swain and S. Mohanty. A 3-dimensional eulerian–eulerian cfd simulation of a hydrocyclone. *Applied Mathematical Modelling*, 37(5):2921–2932, 2013.

[32] Endress+Hauser. Techincal information: Proline Promass 80F, 83F. `http://www.kengen.co.ke/userfiles/TI101DEN_0210%20Mass%20flowmeters.pdf`. [Online; accessed 14-April-2014].

[33] Autotrk AS. The MC608 A/B concerter, EUROMARG INTERNATIONAL sensors. `http://www.autek.no/default.asp?artid=58/fromwww.euromag.com/brochure608a-b-rengrev2.pdf`. [Online; accessed 12-Jul-2014].

[34] Sartorius AG. Electronic Micro-,Analytical and Precision Balance and Precious Metal Scales with Density Determination Kit. `http://sartorius.com/http://www.sartorius.com/en/search/?tx_solr%5Bq%5D=Electronic+and+precision+balance&id=65&L=0&x=0&y=0`. [Online; accessed 20-August-2014].

[35] N. S. Cheng. Formula for the viscosity of a glycerol-water mixture. *Industrial & engineering chemistry research*, 47:3285–3288, 2008.

[36] B. Wang and A. B. Yu. Numerical study of the gas–liquid–solid flow in hydrocyclones with different configuration of vortex finder. *Chemical Engineering Journal*, 135(1):33–42, 2008.

[37] K. J. Hwang, W. H. Wu, S. Qian, and Y. Nagase. Cfd study on the effect of hydrocyclone structure on the separation efficiency of fine particles. *Separation Science and Technology*, 43(15):3777–3797, 2008.

[38] J. NÉmeth and S. Verdes. Flow pattern within hydrocyclone. *Hungarian Journal of Industry and Chemistry*, 39:437–445, 2011.

[39] R. R. Horsley, Q. K. Tran, and J. A. Reizes. The effect of rheology on the performance of hydrocyclones. In *Hydrocyclones*, pages 215–227. Springer, 1992.

[40] R. Nortvedt. *Anvendelse av kjemometri innen forskning og industri*. Tidskriftsforl. Kjemi, 1996.